ARMY RESEARCH LABORATORY

Hydrocode Simulation of the Formation and Penetration of a Linear Shaped Demolition Charge Into an RHA Plate

G. A. Gazonas
S. B. Segletes
S. R. Stegall
C. V. Paxton

ARL-TR-788

July 1995

APPROVED FOR PUBLIC RELEASE; DISTRIBUTION IS UNLIMITED.

NOTICES

REPORT DOCUMENTATION PAGE

Form Approved
OMB No. 0704-0188

1. AGENCY USE ONLY *(Leave blank)*	2. REPORT DATE	3. REPORT TYPE AND DATES COVERED
	July 1995	Final, Jan–Dec 1994

4. TITLE AND SUBTITLE

Hydrocode Simulation of the Formation and Penetration of a Linear Shaped Demolition Charge Into an RHA Plate

5. FUNDING NUMBERS

PR: 4G015-402-P4

6. AUTHOR(S)

G. A. Gazonas, S. B. Segletes, S. R. Stegall, and C. V. Paxton

7. PERFORMING ORGANIZATION NAME(S) AND ADDRESS(ES)

U.S. Army Research Laboratory
ATTN: AMSRL-WT-PD
Aberdeen Proving Ground, MD 21005-5066

8. PERFORMING ORGANIZATION REPORT NUMBER

ARL-TR-788

9. SPONSORING/MONITORING AGENCY NAME(S) AND ADDRESS(ES)

10. SPONSORING/MONITORING AGENCY REPORT NUMBER

11. SUPPLEMENTARY NOTES

12a. DISTRIBUTION/AVAILABILITY STATEMENT

Approved for public release; distribution is unlimited.

12b. DISTRIBUTION CODE

13. ABSTRACT *(Maximum 200 words)*

This report presents the results of a combined experimental and numerical investigation of the formation and penetration of a linear shaped demolition charge into a rolled homogeneous armor (RHA) plate. The demolition charge is composed of a mild steel liner, filled with castable Composition-B high explosive. The numerical computations were conducted before the experiments using the Lagrangian hydrocode EPIC92 and predict a jet tip free flight velocity of about 5.2 km/s at 12 μs. However, observed jet tip free flight velocities of the linear shaped charge (LSC) range from 3.3 to 3.5 km/s as determined from flash radiography, and 3.5 km/s using a special electrical makewire circuit test fixture. The reason for the large discrepancy between the predicted and observed jet tip free flight velocities appears to be related to computational inaccuracies resulting from the highly distorted computational mesh in the collapsing liner. Using the automatic rezone feature in the EPIC94 version of the hydrocode results in the reduction of the jet tip velocity from 4.7 km/s to 3.8 km/s at 4 μs. However, computations beyond 4 μs were not possible due to numerical instabilities associated with requiring a vanishingly small integration time increment resulting from an equation-of-state instability. Penetration depths into two rectangular, 2-in-thick (50.8 mm) RHA plates measure 17 and 18 mm respectively, whereas the hydrocode simulation predicts a greater penetration depth of 22.9 mm. The work attests to the importance of conducting experiments in order to verify baseline hydrocode simulations.

14. SUBJECT TERMS

linear shaped charge; hydrocode; demolition charge; rolled homogeneous armor (RHA)

15. NUMBER OF PAGES

85

16. PRICE CODE

17. SECURITY CLASSIFICATION OF REPORT	18. SECURITY CLASSIFICATION OF THIS PAGE	19. SECURITY CLASSIFICATION OF ABSTRACT	20. LIMITATION OF ABSTRACT
UNCLASSIFIED	UNCLASSIFIED	UNCLASSIFIED	UL

INTENTIONALLY LEFT BLANK.

ACKNOWLEDGMENTS

This work was supported by the Naval Explosive Ordnance Disposal (NAVEOD) Technology Center, Indian Head, MD, under U.S. Army Research Laboratory (ARL) Work Order No. 4G015-402-P4. The authors would like to acknowledge the overall assistance of Mr. Atul Patel and Mr. Richard Gold of NAVEOD with regards to the linear shaped charge demolition problem. Thanks also go to Mr. Todd Bjerke and Mr. Richard Gold for their constructive reviews.

INTENTIONALLY LEFT BLANK.

TABLE OF CONTENTS

INTENTIONALLY LEFT BLANK.

LIST OF FIGURES

LIST OF FIGURES (continued)

1. INTRODUCTION

Military demolition operations use a variety of shaped charge geometries (e.g., cylindrical, linear, curvilinear, and flexilinear) for the clearance of obstacles and barriers, the destruction of facilities and materiel, the construction of roads and trenches, and in land clearance and quarrying. The linear shaped charge (LSC) is commonly used in explosive ordnance disposal (EOD) as a means to initially cut open cases containing explosive-filled ordnance. The Mk-7 Mod 8 demolition charge (Figure 1) consists of an inert mild steel container (liner) filled with plastic explosive (e.g., C-4). A blasting cap is placed on the top surface of the explosive to prime the charge.

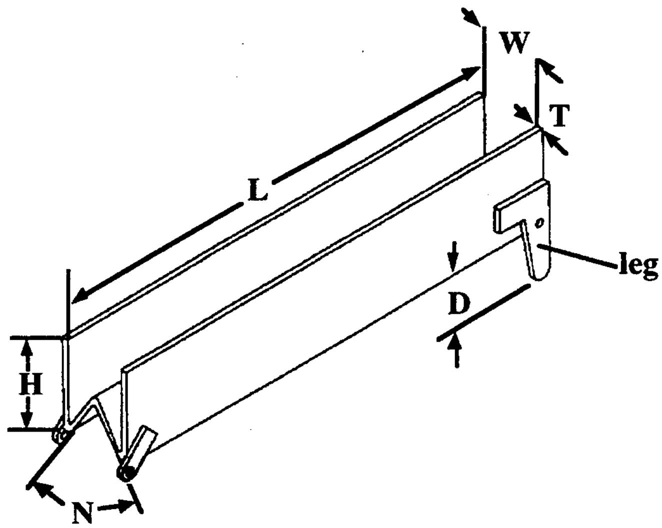

Figure 1. Critical dimensions of the Mk-7 Mod 8 demolition charge (Department of the Navy EODB/Department of the Army TM/U.S. Air Force TO 60A-2-1-51 1992).

The charges may be used individually or linked together in a continuous series if a long cut is desired. Linking several individual charges together in series is achieved by connecting the short leg of one charge to the long leg of an adjacent charge; in this configuration, the charge has a uniformly short standoff distance on the order of 28 mm (1.1 in), in the series arrangement (the dimensions of the Mk-7 Mod 8 charge are: N = 80^{o}, W = 1.00 in [25.4 mm], T = 0.053 in [1.35 mm], H = 1.12 in [28.45 mm], L = 6.0 in [152.4 mm], and D = 1.06 in [26.92 mm]).

The experimental determination of optimal jet cutting properties for a particular EOD application requires parametric variation of design variables such as the liner material, liner geometry, standoff distance, and explosive properties. Since experiments can be costly and hazardous to conduct, there is a strong motivation to develop numerical methods using hydrocodes to assist in the development of EOD procedures. Even though the Mk-7 series of demolition charges have a well-defined penetration depth

into steel and aluminum, these LSCs are known to produce low-order or high-order detonations (see Department of the Navy EODB/Department of the Army TM/U.S. Air Force TO 60A-2-1-51 1992). In this study, we use the Lagrangian-based hydrocode EPIC92 (Elastic Plastic Impact Calculations) (Johnson et al. 1992a, 1992b) to model the formation of an LSC (Mk-7 Mod 8 demolition charge), and its subsequent penetration into a 2-in (51 mm)-thick rolled-homogeneous-armor (RHA) plate. The incorporation of slideline erosion algorithms has permitted Lagrangian computations in large-scale penetration problems (Johnson 1984); nonetheless, Raftenberg (1994) points out that there are a paucity of shaped charge jet (SCJ) penetration studies using EPIC in the open literature. The Raftenberg (1994) study primarily concentrates on failure modeling of a thin RHA target perforated by a shaped charge of relatively long standoff distance; in that work, a 7.73 km/s particulated-copper jet tip is simulated by a 5-parameter geometric model using flash radiographic data. In this study, however, the jet is continuous and has a short standoff distance. Since the jet tip begins interacting with the RHA target almost immediately after it is formed, it is difficult to characterize the jet geometry using radiographic methods. For this reason, in this study, we model *both* the formation and penetration of the LSC using the EPIC92 hydrocode.

Experiments were performed for which the jet tip free flight velocity data are obtained from flash radiographs, and from a test fixture that is specially designed to measure the free flight velocity of the jet using a makewire circuit. These data are compared with the hydrocode velocity predictions in order to assess EPIC92 computational accuracy for the jet *formation* problem. The hydrocode computations were performed first, followed by the experiments, in order to avoid the bias inherent in studies which "tweak" the simulation parameters so as to exactly fit the experiment. Indeed, one of the motivations of the current study is to assess the accuracy of the hydrocode in instances where experimental data are lacking, such as in demolition work where data can be hazardous or costly to obtain. In addition, we compare the depth of penetration into the RHA target with the penetration depth predicted by the hydrocode. Finally, the accuracy in predicting the penetration depth will be shown to be a direct function of our ability to accurately model the formation of the jet.

2. COMPUTATIONS

Computations were performed using the Lagrangian-based explicit EPIC92 hydrocode (Johnson 1977; Johnson et al. 1992a, 1992b) that has been primarily used in the analysis of terminal ballistic or hypervelocity impact problems.

In the current case, we are trying to idealize the jet from an Mk-7 LSC, so that a rezoned version of the problem, without the difficulties associated with the distorted grid, may be employed to simulate the jet penetration. Our problem is further complicated by the fact that the jet must be idealized at a relatively late point in the jet formation process (chosen at 12 μs), so that the rear of the jet is formed,

and is thus characterizable; yet the penetration simulation to follow is at such a short standoff that the resultant idealization must be backed up in time (to 7.2 μs) to the onset of penetration. The initial grid for the jet formation problem appears in Figure 2. It consists of 1,485 nodes and 2,732 finite elements. The initial finite element grid was generated from the charge geometry given in the Introduction. The input deck and computational results out to 20 μs appear in Appendix A.

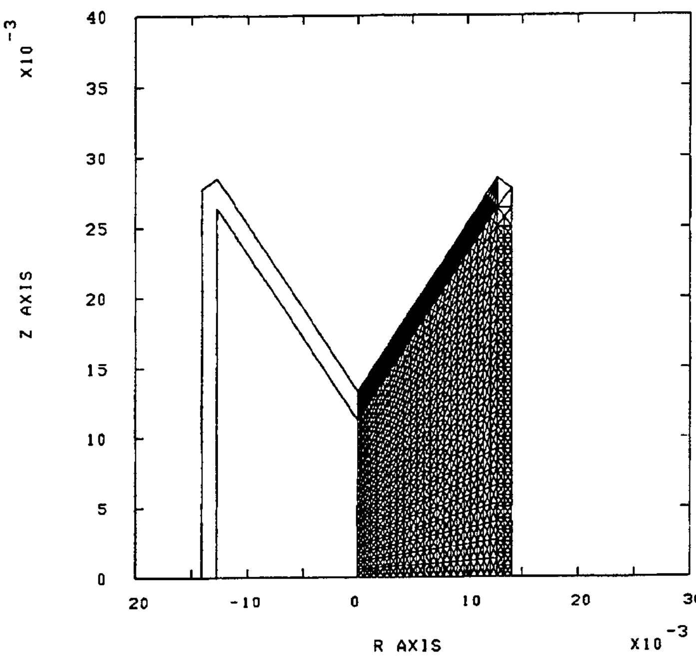

Figure 2. Computational mesh for jet formation problem (in meters).

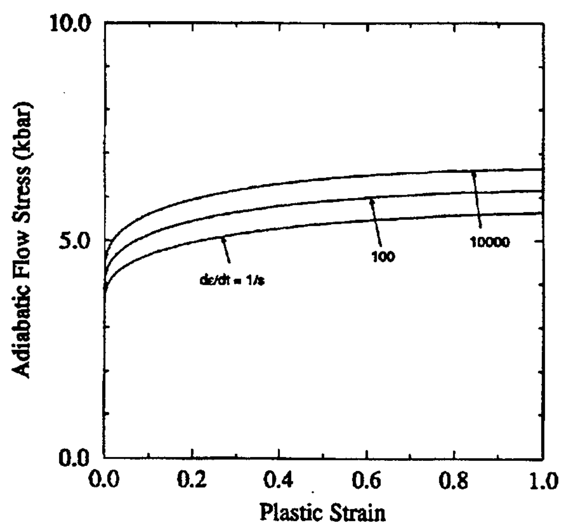

Figure 3. Adiabatic flow stress versus equivalent plastic strain for 1006 mild steel as a function of strain rate.

The distortional behavior of the mild steel liner material is modeled using the Johnson-Cook viscoplastic constitutive model (Johnson and Cook 1985) together with a von Mises initial yield condition (EPIC92 material model 6, 1006 steel, Figure 3). An isotropic hardening rule governs subsequent yield surface behavior together with a radial-return algorithm (Johnson 1984; Cook, Rajendran, and Grove 1992). Because of the high strain rates encountered in impact problems, the temperature fields in bodies modeled using EPIC92 are adiabatic ($dQ = 0$, i.e., there is no heat flow within the body) and thermal softening of a material element is directly proportional to the amount of accumulated plastic work. The dilatational behavior of the Comp-B high explosive is modeled using the Jones-Wilkins-Lee (JWL) equation of state (EPIC92 material model 43, Figure 4). The entire cross section of the finite element charge is simultaneously detonated in order to approximate a 2-D plane detonation wave traveling along the length of the charge.

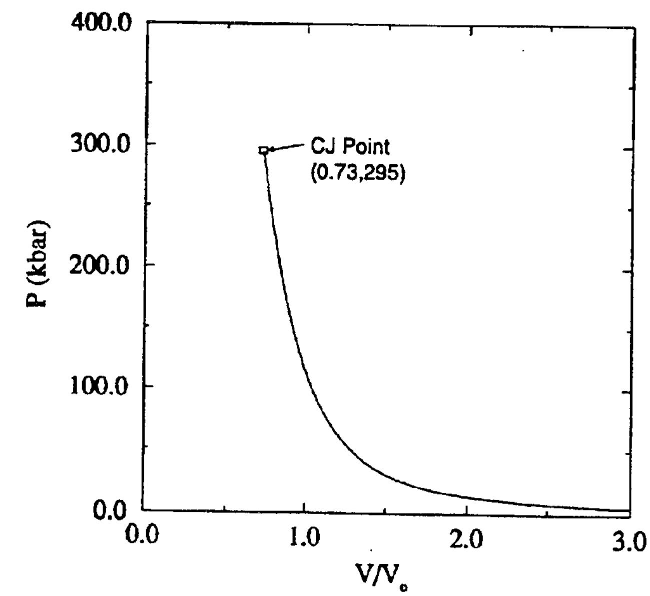

Figure 4. JWL equation-of-state isentrope for Comp-B.

The damage criterion in EPIC92 is assumed to be a scalar function of the incremental (cumulative) equivalent plastic strain, normalized with respect to the fracture strain (Johnson et al. 1992a, 1992b). If the damage threshold is exceeded in a particular finite element, the element behaves as a fluid, and cannot sustain shear or tensile stresses. EPIC92 has the capability of handling severe distortions encountered in SCJ penetration problems using an element erosion algorithm that eliminates

element volume, but retains element mass (e.g., when a critical value of the equivalent plastic strain is exceeded).

The initial mesh geometry for the penetration computations is illustrated in Figure 5. The initial geometry was derived based on the results of the jet formation simulation to be subsequently described. At the start of the computation, both the tip of the LSC jet and RHA target are in normal contact.

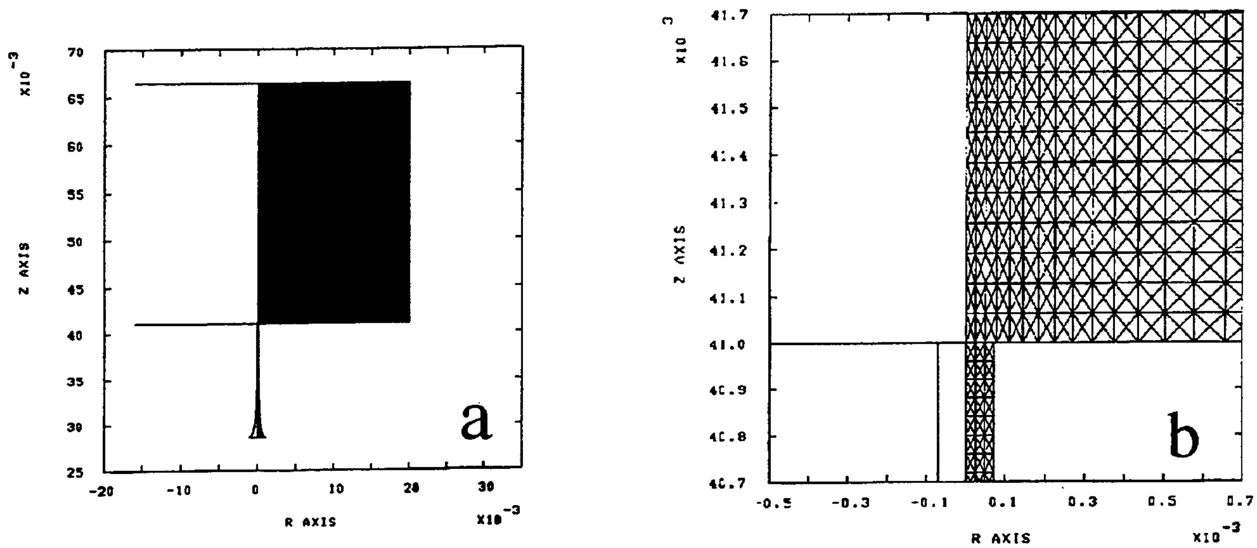

Figure 5. <u>a) Computational mesh, b) Magnified computational mesh in the vicinity of the shaped charge jet tip (in meters).</u>

The linear contact region between jet tip and target describes a locus of slideline points wherein both the jet tip and the target have been alternately defined as master and slave erosional surfaces. This procedure permits both the jet and the target to erode during the penetration process. The entire jet penetration simulation consists of 37,224 finite elements and 19,300 nodes; however, 3,720 elements and 2,170 nodes comprise the jet geometry, while the remainder are in the target. The finite elements are 2-D plane strain constant strain triangles (CSTs), with an assumed displacement field which varies linearly within each finite element. The jet *penetration* computations are described in detail in Section 2.2. In the next section, we more fully describe the details and difficulties encountered in modeling the jet *formation* problem.

2.1 <u>LSC Jet Formation</u>. When simulating the collapse and jet formation of a shaped charge, the resultant velocity distribution in the simulated jet is a function not only of axial location (which the idealized theories assume), but also of radial distance (Walters and Zukas 1989). Similarly, the discretized nature of Lagrangian simulations is such that additional velocity scatter along the simulated

jet occurs. This scattered velocity distribution poses problems when trying to idealize the jet in one dimension for subsequent modeling and/or analysis. The problem is modeled in 2-D plane strain, and therefore, to simulate a plane detonation wave traveling normal to the cross section of the LSC, all of the Comp-B is assumed to simultaneously detonate at the start of the simulation.

We first fit a curve directly to the cumulative mass distribution as a function of jet velocity, thus obtaining $M(v)$. Unfortunately, the velocity scatter inherent in the jet formation simulation caused the poor resultant fit, when viewed in terms of mass versus position (i.e., jet geometry). An enlarged view of this poor fit is shown in Figure 6, where the curve predicting the outer contour of the jet is compared to the liner's node points of the computer simulation at 12 μs.

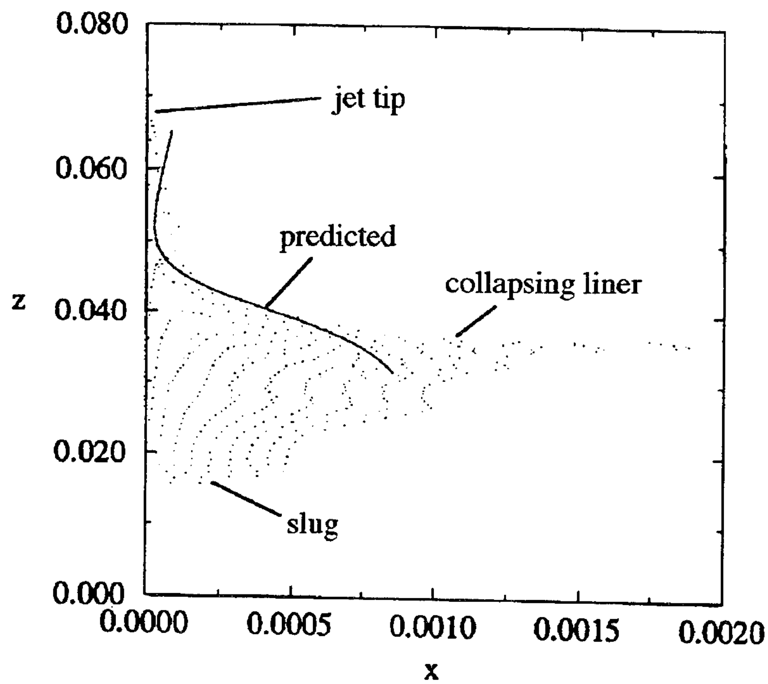

Figure 6. Prediction of jet contour at 12 μs (solid line) versus hydrocode simulation (dots) (length dimensions in meters, not to scale).

The full grid of the jet formation simulation at 12 μs is shown in Figure 7. The original inner steel liner consists of 446 nodes and 800 elements. In light of this unacceptable fit, a second approach was taken, whereby cumulative jet mass was fit as a function of axial jet coordinate at the selected fitting time, $\bar{t} = 12$ μs, giving $M(\bar{z})$ (see Figure 8). Use of this fit to axial location should guarantee a good fit to the jet geometry. If a reasonable fit can be made to the scattered data of axial position versus jet velocity, $\bar{z} = \bar{z}(v)$ (see Figure 9), then the fit to cumulative mass versus velocity may be derived by combining

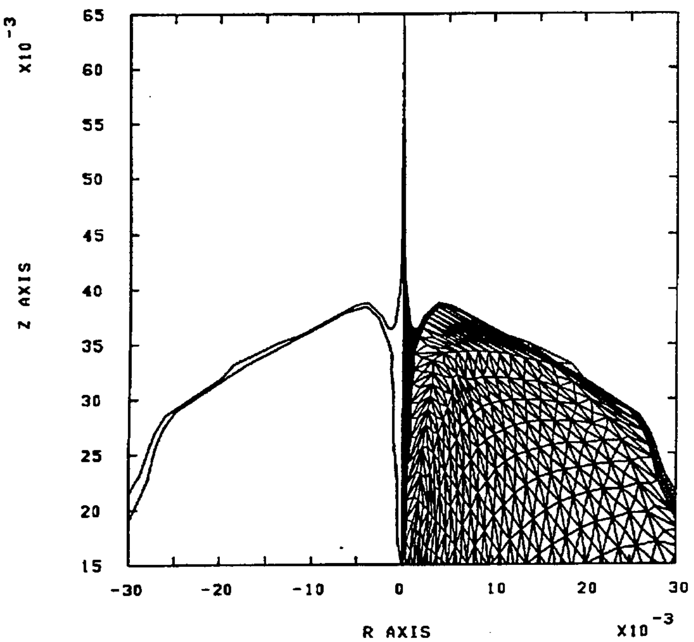

Figure 7. LSC jet geometry at 12 μs (in meters).

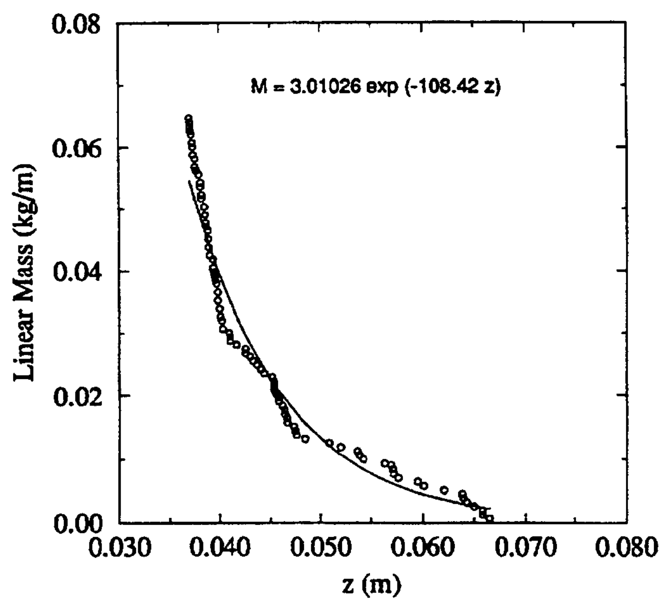

Figure 8. Cumulative jet mass versus position at 12 μs.

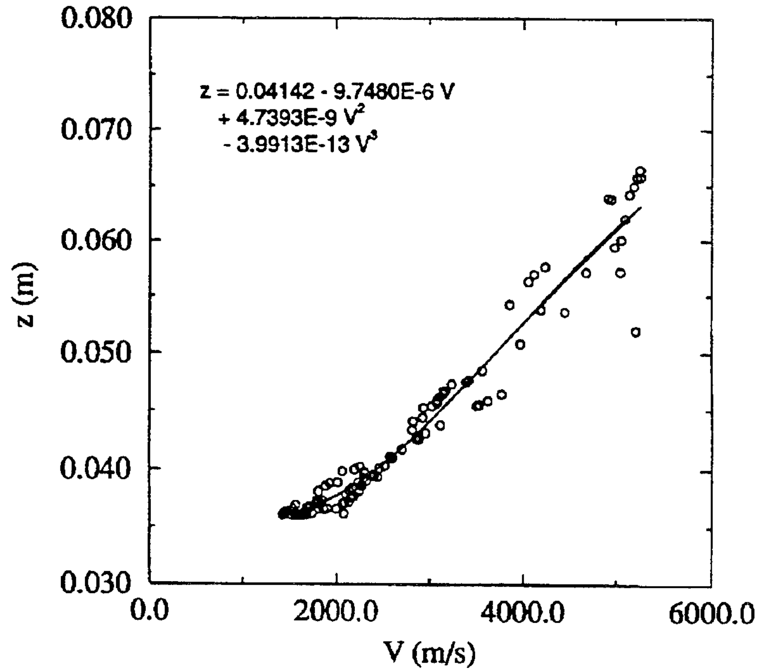

Figure 9. Axial velocity versus position at 12 μs.

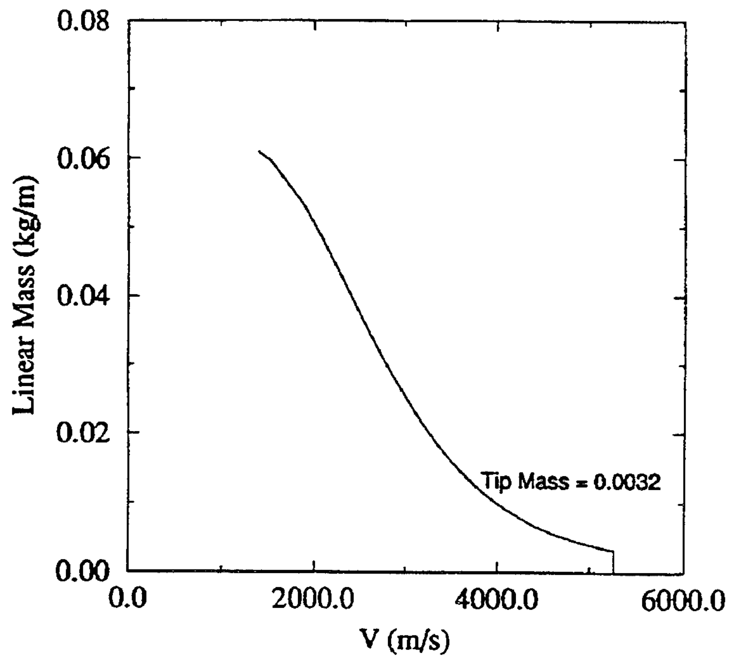

Figure 10. Cumulative mass versus velocity at 12 μs.

the two fits; thus, $M(v) = M(\bar{z}(v))$ (see Figure 10). The following fitting forms have been employed for this particular data set in question:

$$M(\bar{z}) = Ke^{-B\bar{z}} \tag{1}$$

$$\bar{z}(v) = C_0 + C_1 v + C_2 v^2 + C_3 v^3 \quad , \tag{2}$$

where K, B and the C terms are fitting constants. Thus, cumulative mass is obtainable in terms of jet velocity, and its derivative also, given by

$$\frac{dM}{dv} = -KB\frac{d\bar{z}}{dv}e^{-B\bar{z}} \tag{3}$$

for the fitting forms proposed.

For a linear shaped charge jet of unit depth, density ρ, and half-thickness d, the derivative of the cumulative mass curve is described by

$$\frac{dM}{dz} = -2\rho d \quad . \tag{4}$$

If the cumulative mass distribution is known, and it is the jet half thickness to be determined, simple algebraic manipulation and the use of the chain rule provide that

$$d = \frac{-dM/dv}{2\rho\, dz/dv} \quad . \tag{5}$$

The cumulative mass derivative is given above in Equation 3, using parameters from the fits, while the position derivative will now be described.

The axial coordinate, $\bar{z}$, applies specifically at the fitting time of 12 μs. By assuming that the jet particles do not accelerate after the jet is formed (i.e., constant velocity jet particles), the axial coordinate of a jet particle at any time may be directly obtained from

$$z = \bar{z} + v(t - \bar{t}) \quad . \tag{6}$$

With this equation, the derivative of position versus velocity is simply

$$\frac{dz}{dv} = \frac{d\bar{z}}{dv} + (t - \bar{t}) \quad . \tag{7}$$

Again, the $\bar{z}$ derivative is obtainable from the data fit in Equation 2. Combining and substituting these terms gives the fit to the jet half thickness as

$$d(v,t) = \frac{KB(d\bar{z} / dv)e^{-B\bar{z}}}{2\rho(d\bar{z} / dv + t - \bar{t})} \quad . \tag{8}$$

For the jet tip of given mass, M_0, a half diameter $d_0 = d(v_0)$ is assumed and length L_0 is computed via

$$L_0 = \frac{M_0}{2\rho d_0} \quad . \tag{9}$$

The geometric fit, using the current technique, is shown at 12 μs (Figure 11). The fit is good from the jet tip back to the location $\bar{z} = 0.041$ m, corresponding to a jet velocity of approximately 2.5 km/s. It is believed that the relative jet thickness is large enough at this jet location so that the "effective" tail of the jet will lie ahead of this location. Thus, the divergent fit behind this location should not affect the penetration capability of the jet. Figure 12 depicts the jet fit, backed up in time to 8 μs, and compares it to the hydrocode results at that time. As can be seen, the fit to the jet contour, and thus the technique for backing up the idealization in time, properly accounts for mass continuity over time. Figure 13 provides a not-to-scale geometrical representation of the idealized jet contour impinging upon the monolithic target at 7.2 μs in time. The target location was chosen 12.7 mm (0.5 in) from the original Mk-7 liner base, which is a representative standoff at which the device is employed. Again, Figure 5b shows the computational grid in a closeup at the jet/target interface, depicting the grid resolution. In the current configuration, the jet penetration simulation has 26,444 elements and 13,855 nodes (Figure 5a).

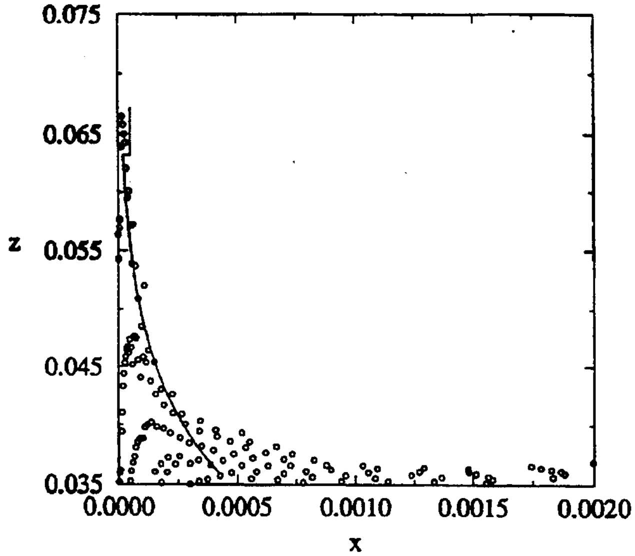

Figure 11. Nodal mass points in simulated jet compared to fit using (v,z) and dM/dz data at 12 μs (length dimensions in meters, not to scale).

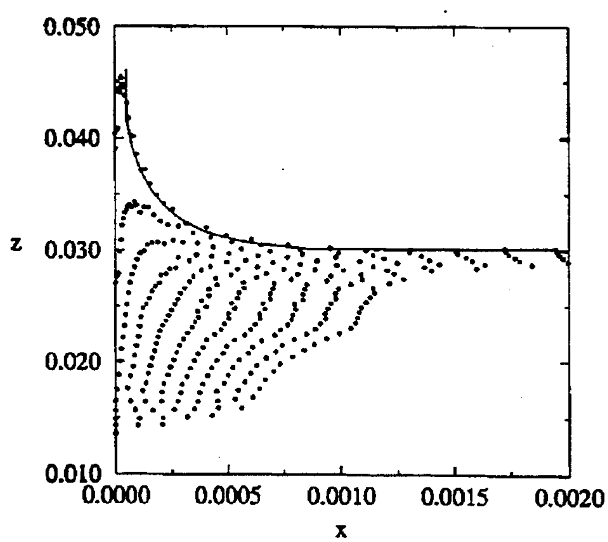

Figure 12. Nodal mass points in simulated jet compared to fit using (v,z) and dM/dz data interpolated back to 8 μs (length dimensions in meters, not to scale).

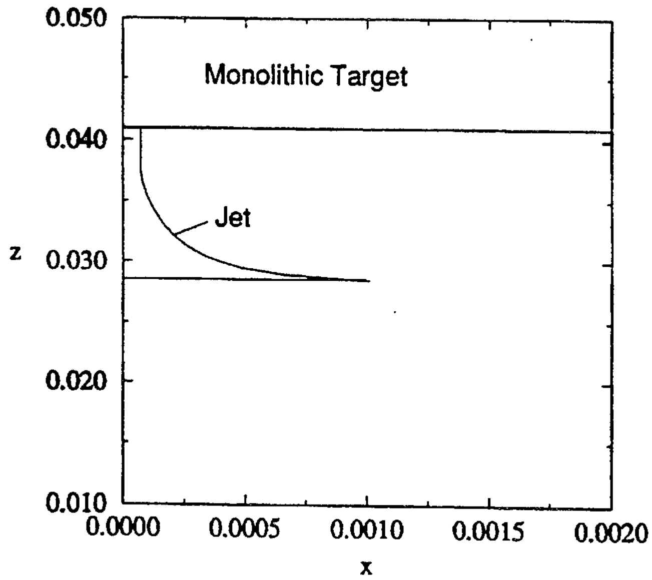

Figure 13. Idealized jet contour impinging upon monolithic target at 7.2 μs (length dimensions in meters, not to scale).

2.2 LSC Jet Penetration. Having fully characterized the LSC jet geometry and initial velocity, we proceed to solve the *penetration* problem. The complete LSC penetration simulation is illustrated at 4 μs time intervals in Appendix B. Although the RHA plate used in the experiment was 2-in (50.8 mm)-thick, we chose to reduce the size of the total problem by modeling a plate of only half the actual plate thickness (i.e., a 1-in [25.4 mm]-thick plate). We felt justified in using a reduced plate thickness in our simulation since the documented cutting depth for the Mk-7 Mod 8 LSC is only 18 mm (0.70 in) (see Department of the Navy EODB/Department of the Army TM/U.S. Air Force TO 60A-2-1-51 1992). The EPIC92 input deck for the LSC jet penetration problem can also be found in Appendix B. The penetration depth of the jet is 24.5 mm when measured from the front plane of the target. If one accounts for target bulge as unpenetrated material, then penetrated thickness = original thickness - unpenetrated thickness = 25.4 mm - 2.5 mm = 22.9 mm.

3. EXPERIMENTS

3.1 Free Flight LSC Jet Tip Velocity (*Makewire Circuit*). The free flight velocity of the LSC was determined at ARL Range 17 by measuring the travel time of the jet as it consecutively severed three parallel double-lead wires, fastened to a plexiglas test fixture (Figure 14). As each wire is impinged by the electrically conductive jet, a circuit is completed sending a signal to an oscilloscope from which the travel time and velocity of the jet can be deduced. A breakwire circuit was not used because it might interact with the electrically conductive jet. A uniform standoff distance is assured by elevating the short legs of the liner with wooden spacers. The charge is detonated at one end by hotwire initiation

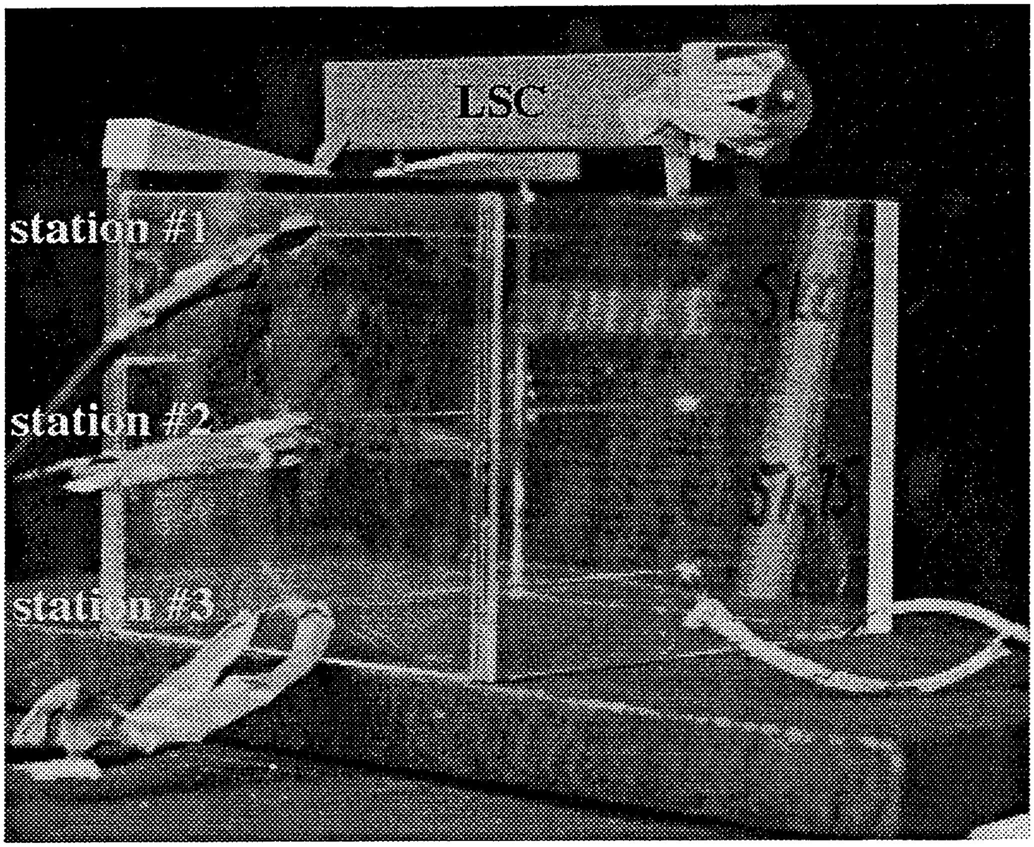

Figure 14. Plexiglas makewire test fixture for free flight velocity measurement (RHA witness plate is 1-in [25.4 mm]-thick).

of two layers of C-6 Detasheet explosive that are press fit onto the Comp-B; each layer of Detasheet is about 6-mm thick. Detasheet is manufactured by Dupont and is composed of 68% PETN, 28% acetyl tributyl citrate, and 8 % nitrocellulose (Asay et al. 1994). The test fixture stands on a 1-in (25.4 mm)-thick rectangular witness plate composed of RHA. As the jet tip cuts through each double-lead, the wires are bridged, which completes the electrical *makewire* circuit. When the circuit is completed, a 67.5-volt signal is simultaneously discharged from a battery to a Nicolet model 2090 oscilloscope. Prior to detonating the charge, the oscilloscopes are triggered and begin to collect data at a sampling rate of 50 ns/pt. Two separate experiments were conducted to estimate the free-flight velocity of the jet. For Shot #1, the jet tip severs the first wire at station 1 (Figure 13), and oscilloscopes #1 and #3 record signals after 23.2 μs and 22.8 μs respectively (Figure 14). The jet tip severs the second wire at station 2, and oscilloscopes #1 and #2 record signals after 38.0 μs respectively. Finally, the jet tip severs the third wire

at station 3, and oscilloscopes # 2 and #3 record signals at 52.95 μs and 52.5 μs respectively. A similar sequence of events occurs for Shot # 2 but with slightly different interstation distances and travel times (Figure 15). Jet velocities are deduced from these data. The test results are compiled in Table 1. The free flight jet tip velocity is found to average 3.52 ± 0.10 km/sec and is relatively constant over a total flight distance of about 4 in (100 mm).

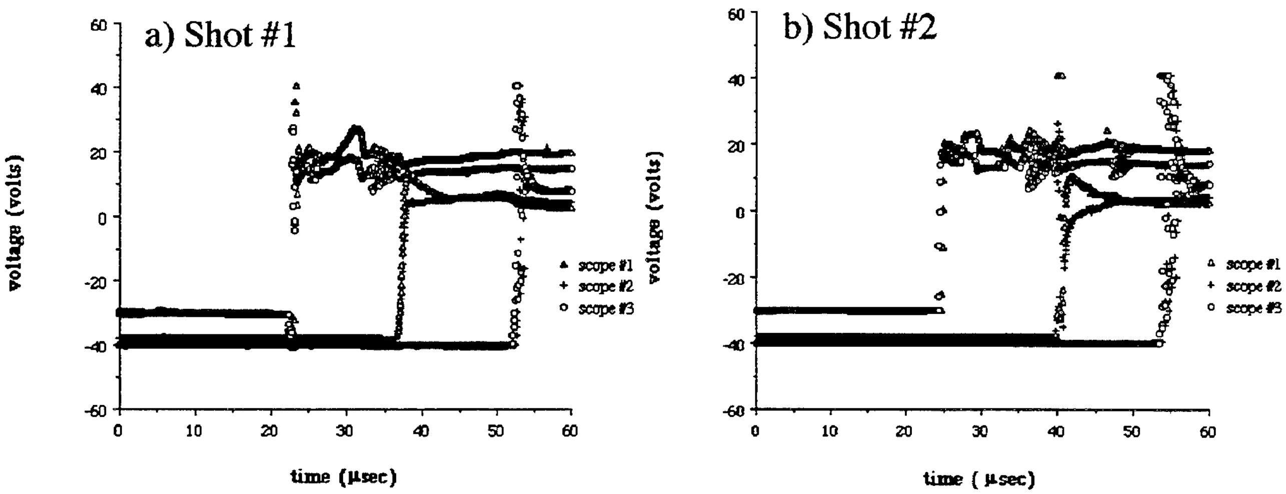

Figure 15. Oscilloscope traces.

Table 1. Free Flight Velocity Measurements

Shot #	Stations	Interstation Distance (mm)	Travel Time (μs)	Jet Tip Velocity (km/s)
1	1 to 2	51.0	14.8	3.445
	2 to 3	51.75	14.95	3.46
	1 to 3	102.75	29.7	3.46
2	1 to 2	51.5	14.9	3.456
	2 to 3	51.5	13.9	3.7
	1 to 3	103.0	28.85	3.57
			average:	3.52

3.2 Free Flight LSC Jet Tip Velocity *(Orthogonal X-rays)*. The free flight velocity of the LSC was also determined at ARL Range 16 by an orthogonal x-ray measurement method so that a direct comparison could be made to the electrical makewire measurement method. The experimental test configuration is illustrated in Figure 16. The LSC is shown suspended by two nylon ropes with radiographic film cassettes oriented at right angles relative to the charge. Our attempts to obtain orthogonal radiographs of the jet as it formed were unsuccessful because the radiographic film cassettes were damaged by laterally projected fragments of the steel liner (Figure 17). In one test, such a fragment remained relatively intact and created a rectangular imprint on the interior wall of the test facility (Figure 18). A shield was then constructed by cutting a rectangular hole in a 2-in (50.8 mm)-thick RHA plate. The LSC was suspended within the hole in an attempt to prevent the side fragments of the liner from puncturing the photographic plate; this test configuration was also relatively ineffectual in preventing photographic plate damage, so jet tip velocity had to be estimated from a single radiograph (Figure 19). Knowing the distance from the base of the LSC to the tip of the jet, one can determine the jet tip velocity from information about the test system time delays. Test system time delays were estimated at 3 μs for predetonation electrical delay, 3 μs for Detasheet burn delay, 3 μs to 6 μs for Comp-B burn delay, and 5 μs for jet formation delay. The jet formation delay is the time required for the jet to emerge from the base of the LSC at a given cross section, once the detonation wave reaches that cross section, and is included in the delay times since all distance measures were made from the base of the LSC. The jet formation delay was determined from the hydrocode computations (see Appendix A).

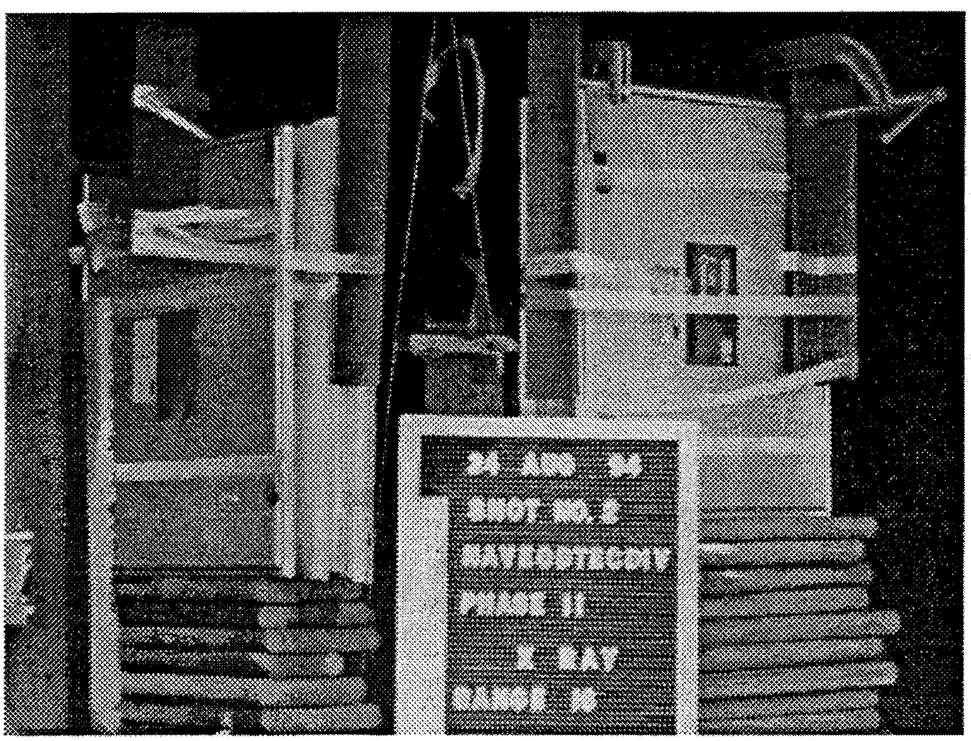

Figure 16. Test configuration for free flight velocity measurement.

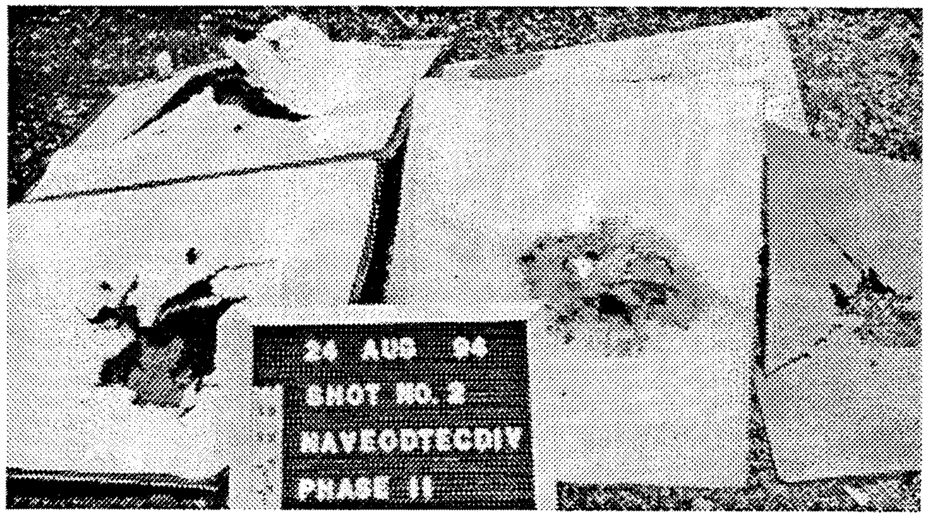

Figure 17. Radiographic film cassette damaged by LSC liner fragment.

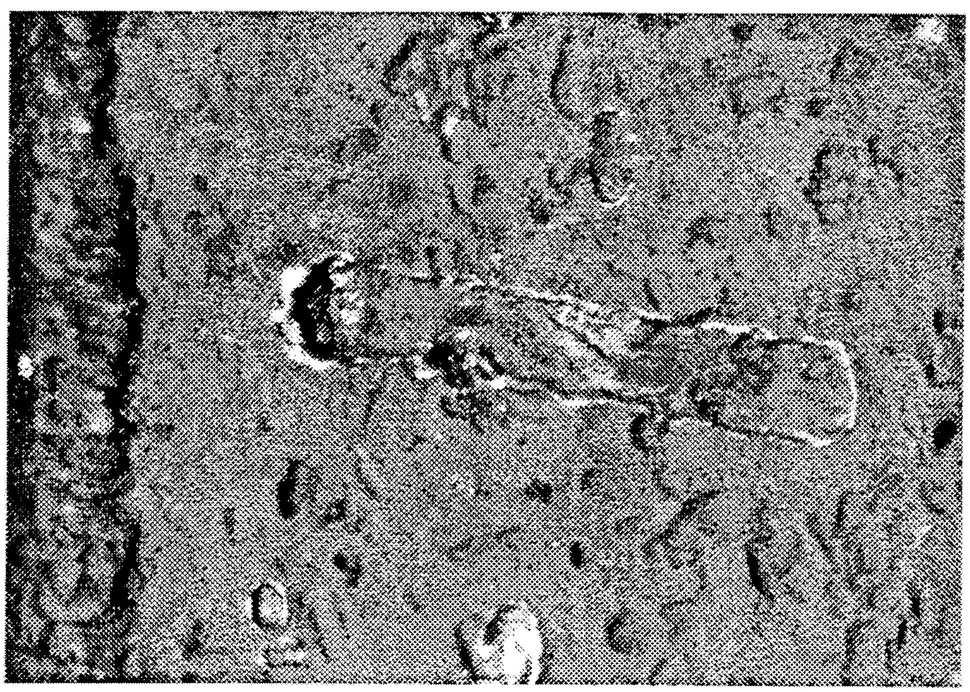

Figure 18. Liner imprint on wall of test facility

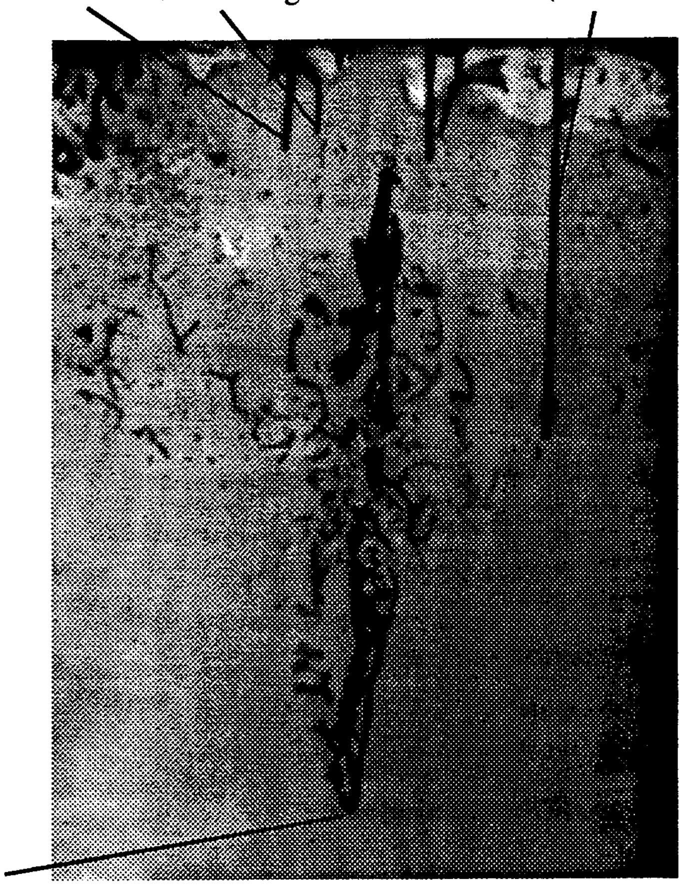

Figure 19. X-ray radiograph of LSC (axial view) at 73.5 μs.

The total time delay thus ranges from 14 μs to 17 μs. The radiograph flash time occurred at 73.5 μs so that the total travel time ranged from 56.5 μs to 59.5 μs. The distance traveled by the jet is estimated at 197.9 mm from the radiograph so that jet tip velocity is estimated to range from 3.3 km/s to 3.5 km/s.

3.3 LSC Jet Penetration Measurements. The penetration performance of the LSC into RHA plates that measure 450x200x51 mm is characterized using two test configurations. In the first test configuration (Figure 20a), the LSC has a nonuniform standoff distance in which the liner base makes an angle of about 8.6^{0} with the surface of the RHA plate. In the second test configuration, shortening the long legs, and elevating the short legs of the LSC with wooden spacers (Figure 20b) creates a uniform standoff distance on the order of 12.7 mm. The Comp-B within the liner is detonated normal to its long axis by precursively detonating two, 5-mm thick Detasheet explosive wafers at one end of the charge; this same explosive initiation procedure was used in the free flight experiments. Figure 21 shows a plan view of the damaged RHA plate experiments from the nonuniform standoff test. A relatively straight narrow cut is seen, 10-mm wide at the center, and about 170-mm long. The cut in the RHA is

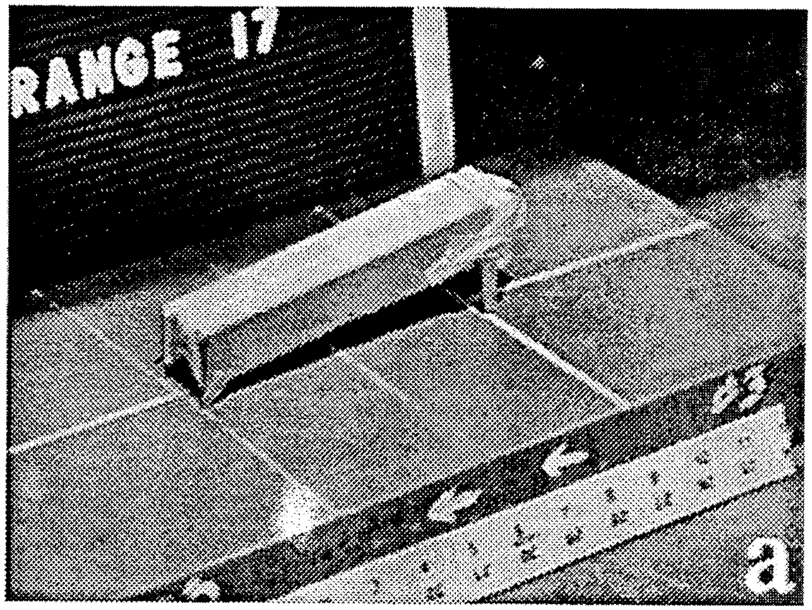

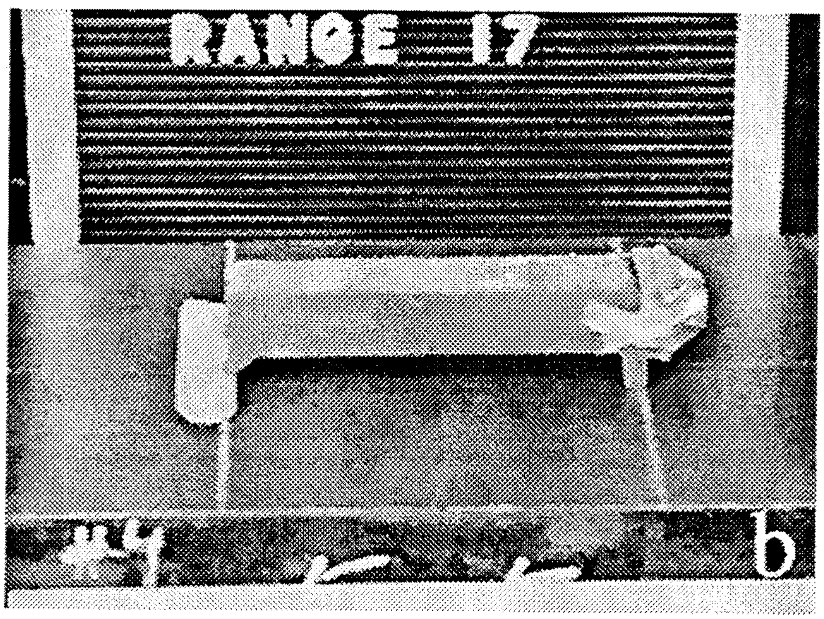

Figure 20. LSC test configurations, a) nonuniform, and b) uniform.

virtually the same in both the uniform and the nonuniform standoff test. A relatively straight narrow cut is seen, 10-mm wide at the center, and about 170-mm long. The cut in the RHA is virtually the same in both the uniform and nonuniform charge configurations. However, the jet penetrated to a depth of 18 mm in the nonuniform charge configuration, and to a depth of only 17 mm for the uniform charge configuration; the penetration measurements were made by sectioning the RHA plates normal to the long axis of symmetry of the cut, and then measuring the distance from the bottom surface of the plate to the

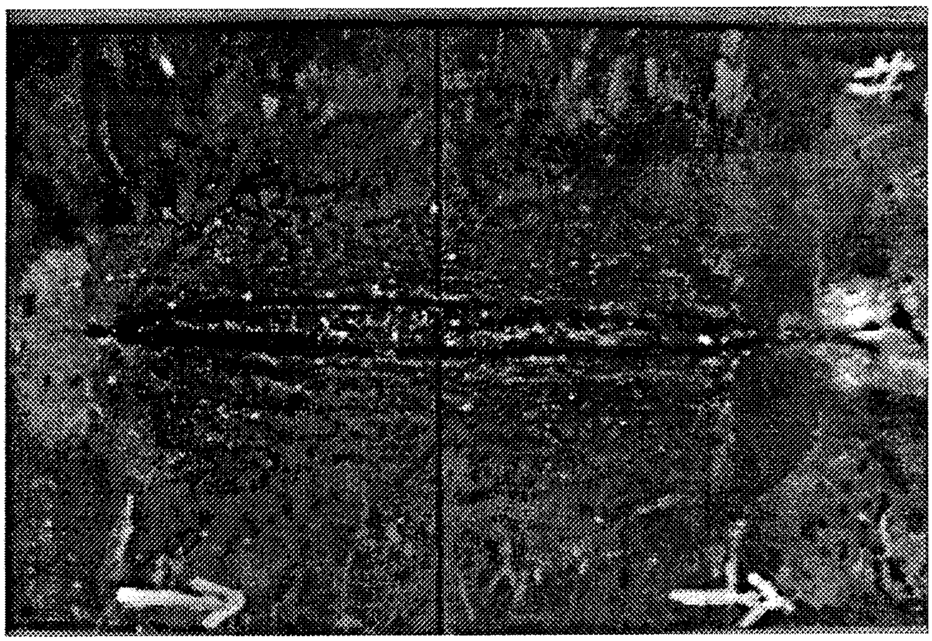

Figure 21. Damaged RHA plate (plan view) for nonuniform standoff test. Detonation wave traveled from left to right (indicated by arrows).

bottom of the cut and subtracting this distance from the initial plate thickness of 51 mm. Figure 22a shows a closeup view of the sectioned plate for the nonuniform standoff test; residual liner material is visible at the base of each of the cuts. An experiment was also conducted using a 25.4-mm-thick mild steel target. The cut is wider (15 mm) in the mild steel plate than in the RHA plate. In addition, the jet nearly penetrated through the mild steel plate and caused it to bulge and crack longitudinally along the lower surface (Figure 22b). The 152-mm-long LSC creates a cut in the mild steel that is about the same length as the cut in the RHA (i.e., about 170 mm).

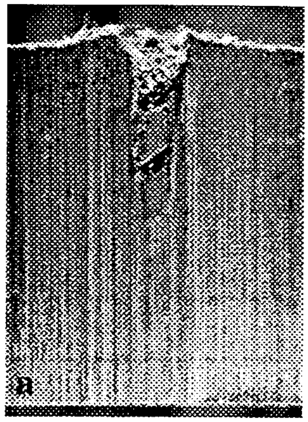

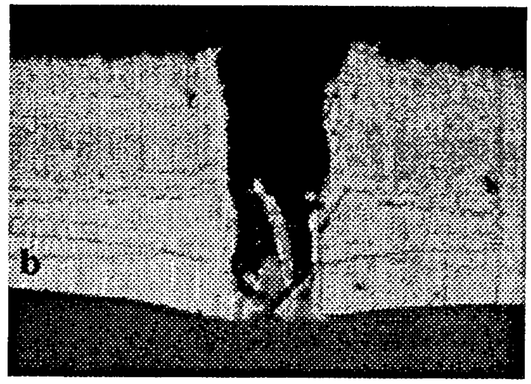

Figure 22. Cross sections through a) RHA plate 2-in (50.8 mm)-thick, and b) Mild steel plate 1-in (25.4 mm)-thick.

4. COMPARISON OF COMPUTATIONS AND EXPERIMENTS

The hydrocode simulations predict a jet tip free flight velocity of about 5.2 km/s. However, observed jet tip free flight velocities of the LSC range from 3.3 to 3.5 km/s as determined from flash radiography, and 3.52 km/s using a special makewire circuit test fixture. Furthermore, the simulations predict a greater penetration depth of 22.9 mm, whereas penetration depths into two rectangular, 2-in-thick RHA plates measure about 17 and 18 mm respectively. The greater predicted plate penetration depth is expected since the predicted jet tip velocities were greater than those observed. We decided to rerun the jet *formation* problem by varying certain input parameters in an attempt to reduce the predicted jet tip velocity. The following additional simulations were conducted, yet all were relatively unsuccessful in significantly decreasing the jet velocity; a synopsis of these results appears as snapshots of the jet velocity versus axial position at 4 μs and 12 μs for each of the following conditions:

(1) Original liner mesh density with element erosion = 0.0 (Figure 23a).

(2) A mesh density increase through the liner thickness by a factor of two (dense mesh) (Figure 23b).

(3) A dense mesh with a flat inner liner mesh geometry (Figure 23c).

(4) A modified dense mesh with a flat inner liner mesh geometry and apex angle = 82° (Figure 23d).

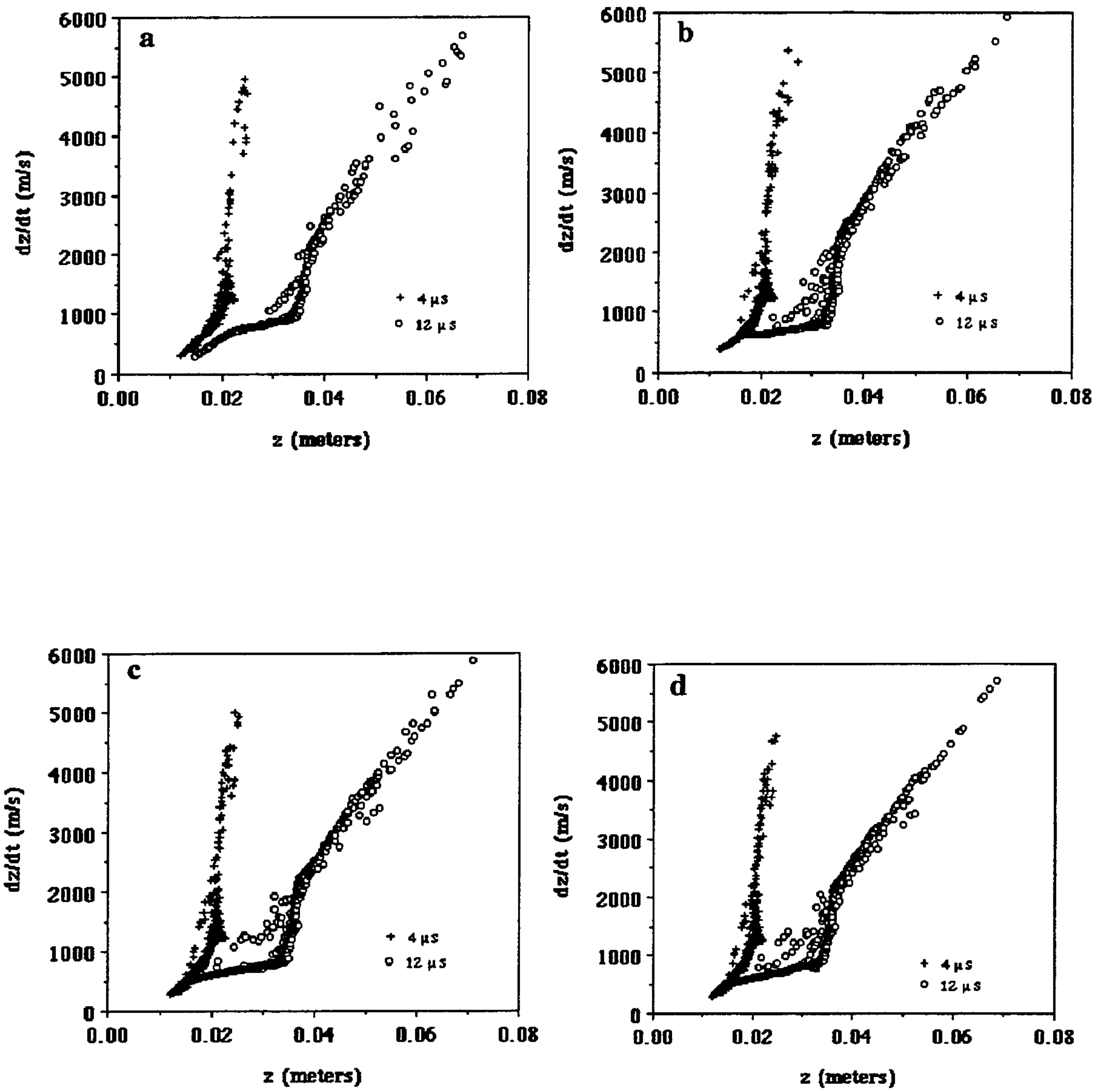

Figure 23. Jet velocity versus axial position at 4 μs and 12 μs. a) Original liner with element erosion = 0.0. b) Dense mesh. c) Dense mesh with flat liner. d) Modified dense mesh, flat inner liner with apex angle = 82^{0}.

Magnified views in the vicinity of the liner apex of both the dense mesh, and the modified dense mesh at 0 μs and 4 μs appear in Figures 24 and 25, respectively. The effect of increasing the finite element density in the liner is to increase the jet velocity (e.g., compare maximum jet tip velocity in Figures 23b, c, and d with that in Figure 23a) rather than to decrease jet velocity; similar spatial resolution effects are reported in Walters and Zukas (1989) in some EPIC lead hemispherical liner computations. The Walters and Zukas (1989) computations predict jet tip velocities to within 5.3% of the experimentally measured velocities, yet our computations overpredict the jet tip velocity by 33%. The good agreement between the predicted and experimental results of Walters and Zukas (1989) could be a result of the smoothly varying surface geometry of the hemispherical liner. Altering the LSC liner geometry from v-notch to flat, however, only slightly reduced the maximum jet tip velocity (e.g., compare maximum jet tip velocity in Figure 23b with that in Figure 23c).

We also attempted to rezone the liner at 2 μs, since the triangular elements in the jet tip become highly distorted and may artificially affect mesh stiffness and hence nodal displacements and velocities. We were unsuccessful in using the EPIC92 rezoner. We also hypothesized that in the fully 3-D problem, a pressure-release wave might closely follow the detonation wave as it travels along the axis of the LSC; the pressure-release wave would have the effect of reducing the total momentum transferred to the liner and thus decrease the jet tip velocity. The pressure-release phenomenon might affect the computational results for our 2-D plane strain model, so several simulations were also conducted, whereby the explosive material was dropped from the analysis at 4 μs, 6 μs, and 8 μs (effectively modeling the pressure release phenomenon); dropping the explosive material at these times did not appreciably decrease the jet tip velocities. Finally, we reran the problem using the EPIC94 version of the hydrocode which has an automatic mesh rezone feature. This attempt provided successful computations to 4 μs with the original mesh density. The jet tip velocity was reduced from 4.7 km/s at 4 μs in the original problem (see Figure 23a) to 3.8 km/s in the rezoned problem at 4 μs (Figure 26b). We were unable to obtain results beyond 4 μs because of numerical instabilities associated with requiring a vanishingly small integration time increment as a result of an equation-of-state instability. It is interesting to note that these numerical instabilities were not encountered when the problem was initially run without rezoning. Unstable numerical behavior was also encountered when we doubled the mesh density and used the EPIC94 automatic rezoner.

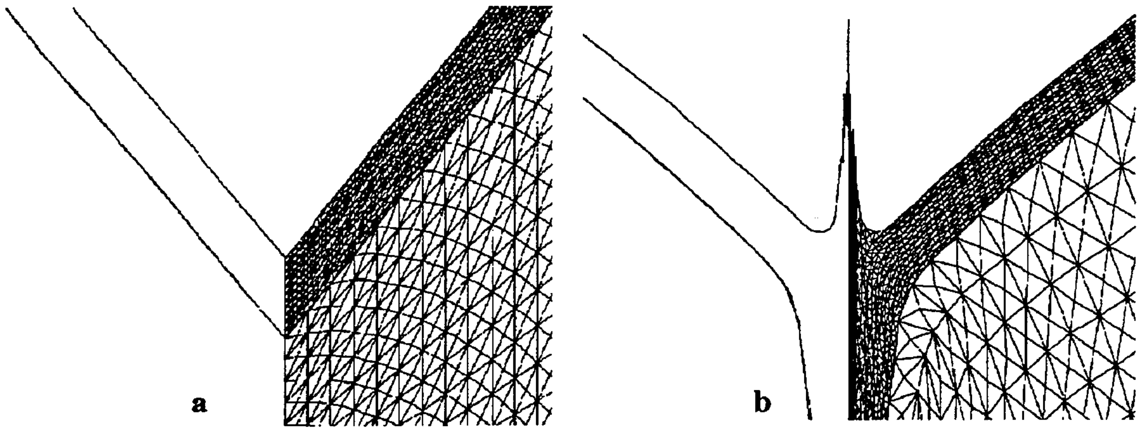

Figure 24. Computational mesh (magnified) for the dense liner in the vicinity of the liner apex at: a) t = 0 μs, and b) t = 4 μs.

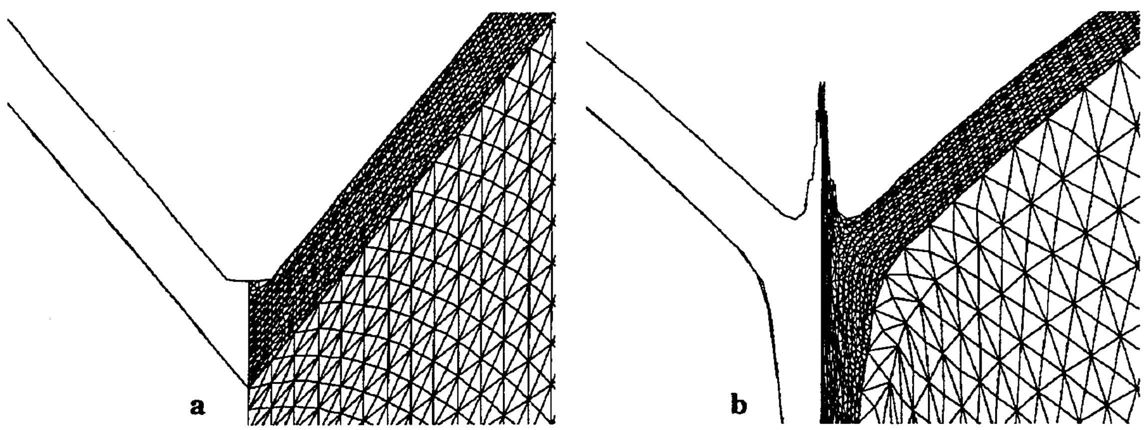

Figure 25. Computational mesh (magnified) for the modified dense mesh in the vicinity of the liner apex at: a) t = 0 μs, and b) t = 4 μs.

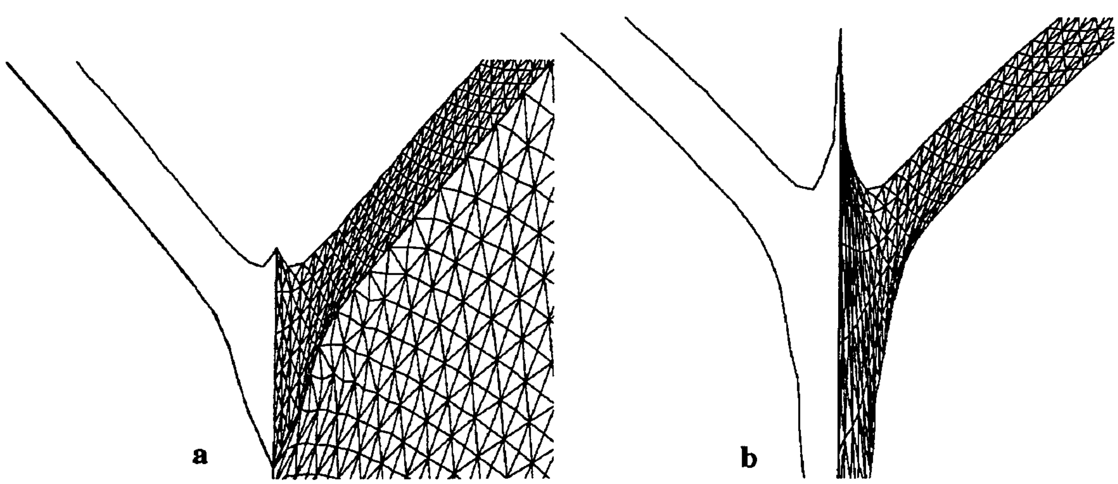

Figure 26. Computational mesh (magnified) rezoned at: a) t = 2 μs, and b) t = 4 μs.

5. CONCLUSIONS

(1) Lagrangian hydrocode computations in 2-D plane strain using EPIC92 predict an early time jet tip velocity of 5.2 km/s at 12 μs for the Mk-7 Mod 8 demolition charge; this result greatly overpredicts the observed later time jet tip free flight velocities which range from 3.3 to 3.5 km/s at nearly 60 μs using flash radiography, and 3.52 km/s averaged from 20 μs to 60 μs using an electrical makewire circuit.

(2) Jet tip velocity was not constant in the simulation, rising from 4.7 km/s at 4 μs to 5.2 km/s at 12 μs. After the jet has formed, such accelerations are nonphysical, based upon our understanding of the jet formation process, and likely result from the overly stiff nature of the constant strain triangles used to simulate the jet formation process.

(3) Parametric attempts to reduce the jet tip velocity prediction by: a) eliminating jet erosion (i.e., setting the element erosion feature = 0.0), b) doubling liner mesh density, c) flattening the liner apex angle, and d) increasing the liner apex angle from 80^{o} to 82^{o}, were unsuccessful.

(4) Use of the automatic rezone feature in the EPIC94 version of the hydrocode resulted in a reduction of the jet tip velocity from 4.7 km/s to 3.8 km/s at 4 μs in the coarse mesh. The computations thus overpredict the observed jet tip velocity by 8 % if one assumes a constant velocity jet. Computations beyond 4 μs were not possible due to numerical instabilities associated with requiring a vanishingly small integration time increment resulting from an equation-of-state instability. This behavior was also observed in the denser mesh. We were unscuccessful in utilizing the *manual* EPIC92 rezoner.

(5) Penetration depths into two rectangular, 2-in (50.8 mm)-thick RHA plates measured 17 and 18 mm respectively, whereas the hydrocode simulation predicted a greater penetration depth of 22.9 mm. The overprediction in the computed penetration depth is expected since jet tip velocities were also overpredicted by the hydrocode. The work attests to the importance of conducting experiments in order to verify baseline hydrocode simulations.

6. REFERENCES

Asay, B. W., J. B. Ramsay, M. U. Anderson, and R. A. Graham. "Shock Response of the Commercial High Explosive Detasheet." Shock Waves, vol. 3, pp. 267-271, 1994.

Cook, W. H., A. M. Rajendran, and D. J. Grove. "An Efficient Numerical Implementation of the Bodner-Partom Model in the EPIC-1 Code." Engineering Fracture Mechanics, vol. 41, no. 5, pp. 607-623, 1992.

Department of theNavy EODB/Department of the Army TM/U.S. Air Force TO 60A-2-1-51. Explosive Ordnance Disposal Procedures, Shaped Charges: General Information , September 1992.

Johnson, G. R. "High Velocity Impact Calculations in Three Dimensions." Journal of Applied Mechanics, vol. 99, no. 1, pp. 95-100, 1977.

Johnson, G. R. "Short Presentation by G. R. Johnson." Theoretical Foundation for Large-Scale Computations of Nonlinear Material Behavior. Edited by S. Nemat Nasser et al. Boston: Martinus Nijhoff Publishers, 1984.

Johnson, G. R., and W. H. Cook. "Fracture Characteristics of Three Metals Subjected to Various Strains, Strain Rates, Temperatures, and Pressures." Engineering Fracture Mechanics, vol. 21, no. 1, pp. 31-48, 1985.

Johnson, G. R., R. A. Stryk, D. E. Pratt, and J. A. Schonhardt. EPIC Hydrocode User's Workshop. Alliant Techsystems, Inc., Brooklyn Park, MN, October 1992a.

Johnson, G. R., R. A. Stryk, D. E. Pratt, and J. A. Schonhardt. User Instructions for the 1992 Version of the EPIC Code. Alliant Techsystems, Inc., Brooklyn Park, MN, October 1992b.

Raftenberg, M. N. "Lagrangian Hydrocode Simulations of Rolled-Homogeneous-Armor Plate Perforation by a Shaped Charge Jet." International Journal of Impact Engineering, vol. 15, no. 5, pp. 619-643, 1994.

Walters, W. P., and J. A. Zukas. Fundamentals of Shaped Charges. New York: John Wiley and Sons, 1989.

INTENTIONALLY LEFT BLANK.

APPENDIX A:

SHAPED CHARGE JET FORMATION
INPUT DECK AND COMPUTATIONAL RESULTS

INTENTIONALLY LEFT BLANK.

```
   3    1 NEOD Linear Shaped Charge - S. Segletes & George Gazonas - NOV 1993
$
$ This restart run will start at 0 us and continue to 12 microseconds
$
$$ main run data    **************************************************************
$
$cycl.ncpu......time.....dtmax.....dtmin.......ssf......tmax.....cpmax......emax
    0    0 0000.0e-6       1.0     0.1e-9      0.80   12.0e-6  10800.00
$tplt.drop..add.pres.push..hrg....vfract.....vnref...nabfact...sphdist//////////
    1    0    0    0    0    0
$.sys.nplt.lplt.dplt.....dtsys......tsys....dtnode.....tnode.....dtdyn......tdyn
    1    0              1.0e-6       0.0   0.25e-6       0.0
$.....time....echeck....ncheck.....rdamp.save.burn.yprt.ndat.slpr.proj..pat.rzne
  02.0E-06    1001.0       999       0.0    3    0    1  500    2    0    0    0
  04.0E-06    1001.0       999       0.0    3    0    1  500    2    0    0    0
  06.0E-06    1001.0       999       0.0    3    0    1  500    2    0    0    0
  08.0E-06    1001.0       999       0.0    3    0    1  500    2    0    0    0
  10.0E-06    1001.0       999       0.0    3    0    1  500    2    0    0    0
 999.0E-06    1001.0       999       0.0    3    0    1  500    2    0    0    0

$$ preprocessor data  ***********************************************************
$       Target is: UNCLASSIFIED, Linear Shaped Charge Detonation
$       Mk-7 is:
$                - Mild Steel Liner ASTM-A569
$                - Explosive C-4
$
$type.case...........problem description.......................................]
    1    1 NEOD TARGET - S. Segletes & George Gazonas - NOV 1993
$geom.prnt.save.nsld.nmas.nrst.nrig.nchk.load.nzonPCrtz.splt..dp3.unit/////..per
    5    1    3    2    0    1    0    0    0    0 1100    0    0    1         0
$ material data
$ solids from library
$matl....0..dam.fail.dfrc.efal.SOLIDS FROM LIBRARY
    6    0    1    0        999. 1006 Steel (Mild Steel Simulant)
$MATL    0   DAM FAIL       EFAL solids
   43    0    1    0        999. JWL Comp B (C-4 Simulant)
         $ end of material
$//\\//\\//\\//\\//\\//\\//\\//\\//\\//\\//\\//\\//\\//\\//\\//\\//\\//\\//\\//\\//
$ projectile nodes (Liner/Case)
$.x/rscale....yscale....zscale..x/rshift....zshift....rotate.....slant.x/r0...z0
    0.0254    0.0254    0.0254   0.00000      0.00     000.0        0.0    0    0
$ Rod nodes
$...2..nor..nir.npln..rad...ax.cros.join...n1.ntop......ztop......zbot....expand
    2    6    1   41    2    2    1    0 5001    0   1.03755    .44167        1.
$......RT1.......RT2.......RT3.......RT4.......RT5.......RT6 (FOR rad=2)
     .4594   .467526    .47564   .483763    .49188      .500
$......RB1.......RB2.......RB3.......RB4.......RB5.......RB6 (FOR rad=2)
      .000      .000      .000     0.000      .000      .000
$......ZT1.......ZT2.......ZT3.......ZT4.......ZT5.......ZT6 (FOR ax=2)
    1.0716  1.064798  1.057986  1.051174  1.044362   1.03755
$......ZB1.......ZB2.......ZB3.......ZB4.......ZB5.......ZB6 (FOR ax=2)
     .5241   .507614   .491128   .474642   .458156    .44167
$...1.nnod..rtzxxxxxxxxxxxxxxxxxxxxxxxxx...n1..inc.......exp
    1    1  000                          5447    0        1.
```

```
$......r1........y1........z1........rn........yn........zn
     .5000              1.1200
$...1.nnod..rtzxxxxxxxxxxxxxxxxxxxxxxxxxx...n1..inc.......exp
    1    1  000                          5448    0        1.
$......r1........y1........z1........rn........yn........zn
     .5530              1.0906
$...1.nnod..rtzxxxxxxxxxxxxxxxxxxxxxxxxxx...n1..inc.......exp
    1    1  000                          5449    0        1.
$......r1........y1........z1........rn........yn........zn
     .5530              1.0376
$...1.nnod..rtzxxxxxxxxxxxxxxxxxxxxxxxxxx...n1..inc.......exp
    1    1  000                          5450    0        1.
$......r1........y1........z1........rn........yn........zn
     .5265              1.0110
$...2..nor..nir.npln..rad...ax.cros.join...n1.ntop......ztop......zbot....expand
    2    3    1   31    1    0    1    0 6001    0    .98400   0.00000        1.
$....ROTOP.....RITOP.....ROBOT.....RIBOT (FOR rad=1)
      .553      .500      .553     0.500
         $ end of target nodes
$ target nodes (Explosive)
$.x/rscale....yscale....zscale..x/rshift....zshift....rotate.....slant.x/r0...z0
   0.0254    0.0254    0.0254   0.00000      0.00     000.0        0.0    0    0
$ Rod nodes
$...2..nor..nir.npln..rad...ax.cros.join...n1.ntop......ztop......zbot....expand
    2   21    0   21    1    1    1    0 7001    0     0.000     0.000        1.
$....ROTOP.....RITOP.....ROBOT.....RIBOT (FOR rad=1)
      .500      .000      .500     0.000
$......A0........A1........A2........A3 (FOR ax=1)
   0.44167   1.19176      .000   0.00000
$......B0........B1........B2........B3 (FOR ax=1)
   0.00000   0.00000      .000   0.00000
         $ end of projectile nodes
$//\\//\\//\\//\\//\\//\\//\\//\\//\\//\\//\\//\\//\\//\\//\\//\\//\\//\\//\\//
$ projectile element data (Liner/Case)
$...2.matl...n1.diag.noer.nier.nlay......shel.plac//////////.....thick
    2    6 5001    5    6    2   40         0    0
    1    6    1 5447 5001 5002
    1    6    1 5447 5002 5003
    1    6    1 5447 5003 5004
    1    6    1 5447 5004 5005
    1    6    1 5447 5005 5006
    1    6    1 5447 5006 5448
    1    6    1 5448 5006 5449
    1    6    1 5450 5449 5006
    1    6    1 5450 6003 5449
    1    6    1 5450 6002 6003
    1    6    1 5450 6001 6002
    1    6    1 5450 5006 6001
    2    6 6001    5    3    2   30         0    0
         $ end of target elements
$ target element data (Explosive)
$ rod elements
```

```
$...2.matl...nl.diag.noer.nier.nlay......shel.plac//////////.....thick

    2   43 7001    5   21    1   20          0    0
         $ end of projectile elements
$//\\//\\//\\//\\//\\//\\//\\//\\//\\//\\//\\//\\//\\//\\//\\//\\//\\//\\//
$ begin slide line data
$
$ slide #1
$ master: target (liner/case) inner surface
$ slave : projectile (explosive) surface
$.nmg..nmn..nsg..nsn..nsr.type.mbot..isr..it1..it2...ref vel.....erode..friction
    2    0    2    0    0    1 0000    0    1    0                  999.
$.m1g..mng..inc
 6151 6001   -5               $ inside of case
$.m1g..mng..inc
 5006 5446   11               $ inside of liner
$.s1g..sng..inc
 7001 7022    1               $ explosive next to liner
$.s1g..sng..inc
 7065 7882   43               $ explosive next to case
$
$ slide #2
$ master: projectile (explosive) surface
$ slave : target (liner/case) inner surface
$.nmg..nmn..nsg..nsn..nsr.type.mbot..isr..it1..it2...ref vel.....erode..friction
    2    0    2    0    0    1 0000    0    1    0                  999.
$.m1g..mng..inc
 7001 7022    1               $ explosive next to liner
$.m1g..mng..inc
 7065 7882   43               $ explosive next to case
$.s1g..sng..inc
 6151 6001   -5               $ inside of case
$.s1g..sng..inc
 5006 5446   11               $ inside of liner
$
$//\\//\\//\\//\\//\\//\\//\\//\\//\\//\\//\\//\\//\\//\\//\\//\\//\\//\\//
$ Restraints (Ties liner nodes to axis of symmetry)
    6    1  100
 5441 5446    1
$ detonation (By detonating at t=-1, all explosive will simultaneously
$ detonate at t=0, at the start of the simulation)
$...x/rdet......ydet......zdet.....tburn.shad.npnt
       0.0       0.0       0.0      -1.0
$ initial velocity data
$..px/rdot...py/tdot.....pzdot...tx/rdot...ty/tdot.....tzdot.......dt1.vfld/////
   -000.00       0.0       0.0       0.0       0.0       0.0
$$ preprocessor data  *************************************************************
$
$type.case...........problem description........................................]
$    3    1 NEOD Linear Shaped Charge - S. Segletes & George Gazonas - NOV 1993
$
$$ main run data    *************************************************************
$
$cycl.ncpu......time.....dtmax.....dtmin.......ssf......tmax.....cpmax......emax
    0    0 0000.0e-6       1.0    0.1e-9      0.80   20.0e-6  10800.00
$tplt.drop..add.pres.push..hrg....vfract.....vnref...nabfact...sphdist//////////
    1    0    0    0    0    0
```

```
$.sys.nplt.lplt.dplt.....dtsys......tsys....dtnode.....tnode.....dtdyn......tdyn
    1    0              1.0e-6       0.0   0.25e-6       0.0


$type.case...........problem description......................................]
    3    1 NEOD Linear Shaped Charge - S. Segletes & George Gazonas - NOV 1993
$
$ This restart run will start at 0 us and continue to 12 microseconds
$
$$ main run data    ************************************************************
$
$cycl.ncpu......time.....dtmax.....dtmin.......ssf......tmax.....cpmax......emax
    0    0 0000.0e-6       1.0    0.1e-9      0.80   12.0e-6  10800.00
$tplt.drop..add.pres.push..hrg....vfract.....vnref...nabfact...sphdist//////////
    1    0    0    0    0    0
$.sys.nplt.lplt.dplt.....dtsys......tsys....dtnode.....tnode.....dtdyn......tdyn
    1    0              1.0e-6       0.0   0.25e-6       0.0
$.....time....echeck....ncheck.....rdamp.save.burn.yprt.ndat.slpr.proj..pat.rzne
  02.0E-06    1001.0       999       0.0    3    0    1  500    2    0    0    0
  04.0E-06    1001.0       999       0.0    3    0    1  500    2    0    0    0
  06.0E-06    1001.0       999       0.0    3    0    1  500    2    0    0    0
  08.0E-06    1001.0       999       0.0    3    0    1  500    2    0    0    0
  10.0E-06    1001.0       999       0.0    3    0    1  500    2    0    0    0
 999.0E-06    1001.0       999       0.0    3    0    1  500    2    0    0    0


$type.case...........problem description......................................]
    3    1 NEOD Linear Shaped Charge - S. Segletes & George Gazonas - NOV 1993
$
$ This restart run will restart at 12 us and then drop the explosive and
$ casing at 12.1 microseconds, continuing on until 20 microseconds.
$
$$ main run data    ************************************************************
$
$cycl.ncpu......time.....dtmax.....dtmin.......ssf......tmax.....cpmax......emax
    0    0 0012.0e-6       1.0    0.1e-9      0.80   20.0e-6  10800.00
$tplt.drop..add.pres.push..hrg....vfract.....vnref...nabfact...sphdist//////////
    1    1    0    0    0    0
$.sys.nplt.lplt.dplt.....dtsys......tsys....dtnode.....tnode.....dtdyn......tdyn
    1    0              1.0e-6       0.0   0.25e-6       0.0
$....tdrop.nnod.nnab.nele.nsld.nrig.nchk.load.nzon.nplt.lplt**RYZ.nfal*****..per
 0012.1e-6  446    0  800    0    0    0    0    0    0    0  100   20        0
$.ef1..ef2..ef3..ef4..ef5..ef6..ef7..ef8..ef9.ef10.ef11.ef12.ef13.ef14.ef15.ef16
    1    2    3    4    5    6    7    8    9   10   11   12   13   14   15   16
$ef17.ef18.ef19.ef20
   17   18   19   20
$.....time....echeck....ncheck.....rdamp.save.burn.yprt.ndat.slpr.proj..pat.rzne
  14.0E-06    1001.0       999       0.0    3    0    1  500    2    0    0    0
  16.0E-06    1001.0       999       0.0    3    0    1  500    2    0    0    0
  18.0E-06    1001.0       999       0.0    3    0    1  500    2    0    0    0
  21.0E-06    1001.0       999       0.0    3    0    1  500    2    0    0    0
```

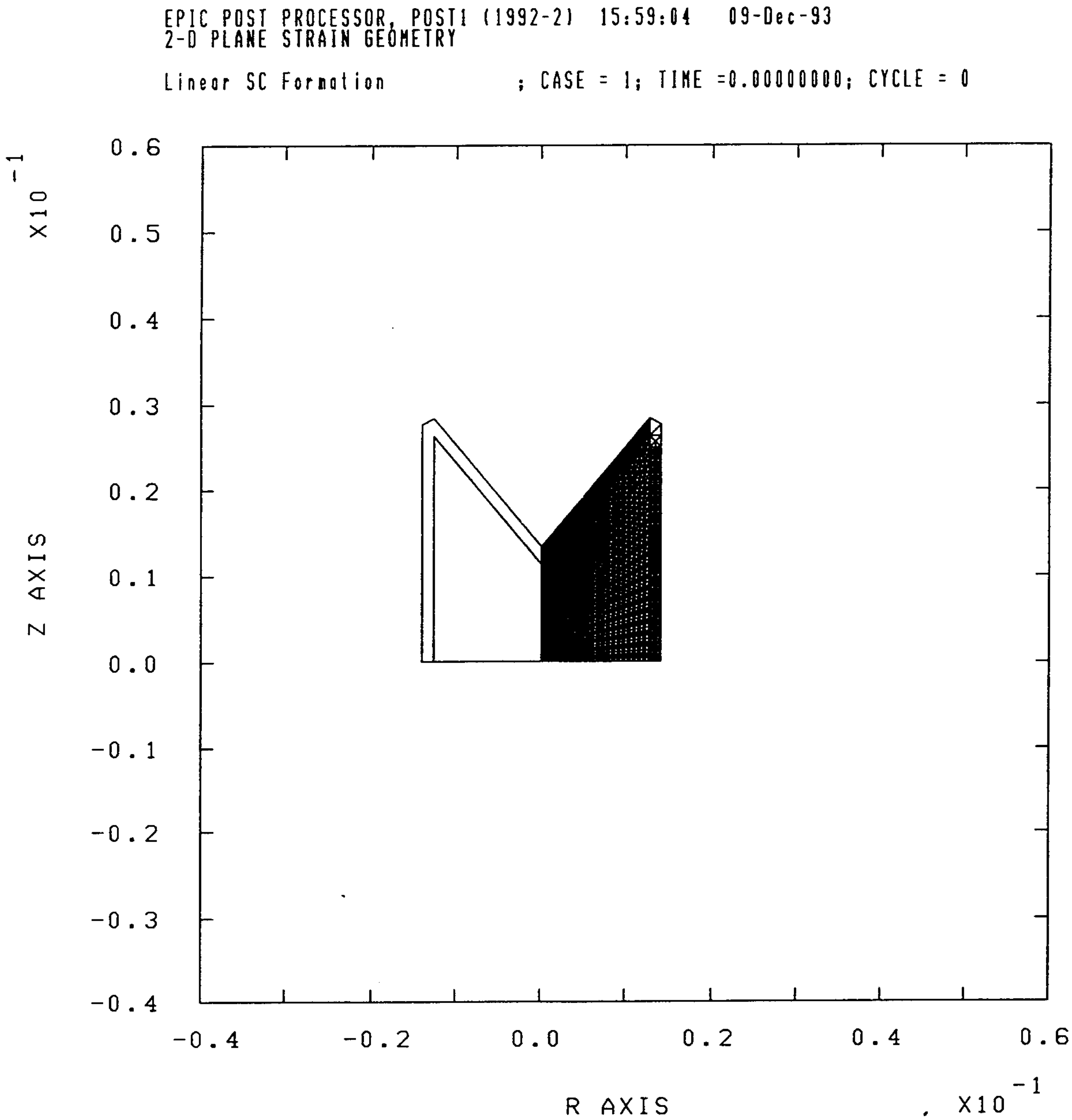
EPIC POST PROCESSOR, POST1 (1992-2) 15:59:04 09-Dec-93
2-D PLANE STRAIN GEOMETRY
Linear SC Formation ; CASE = 1; TIME =0.00000000; CYCLE = 0
Z AXIS
X10 -1
R AXIS
, X10 -1
0.6
0.5
0.4
0.3
0.2
0.1
0.0
-0.1
-0.2
-0.3
-0.4
-0.4
-0.2
0.0
0.2
0.4
0.6

EPIC POST PROCESSOR, POST1 (1992-2) 16:00:17 09-Dec-93
2-D PLANE STRAIN GEOMETRY

Linear SC Formation ; CASE = 1; TIME =0.00000200; CYCLE = 374

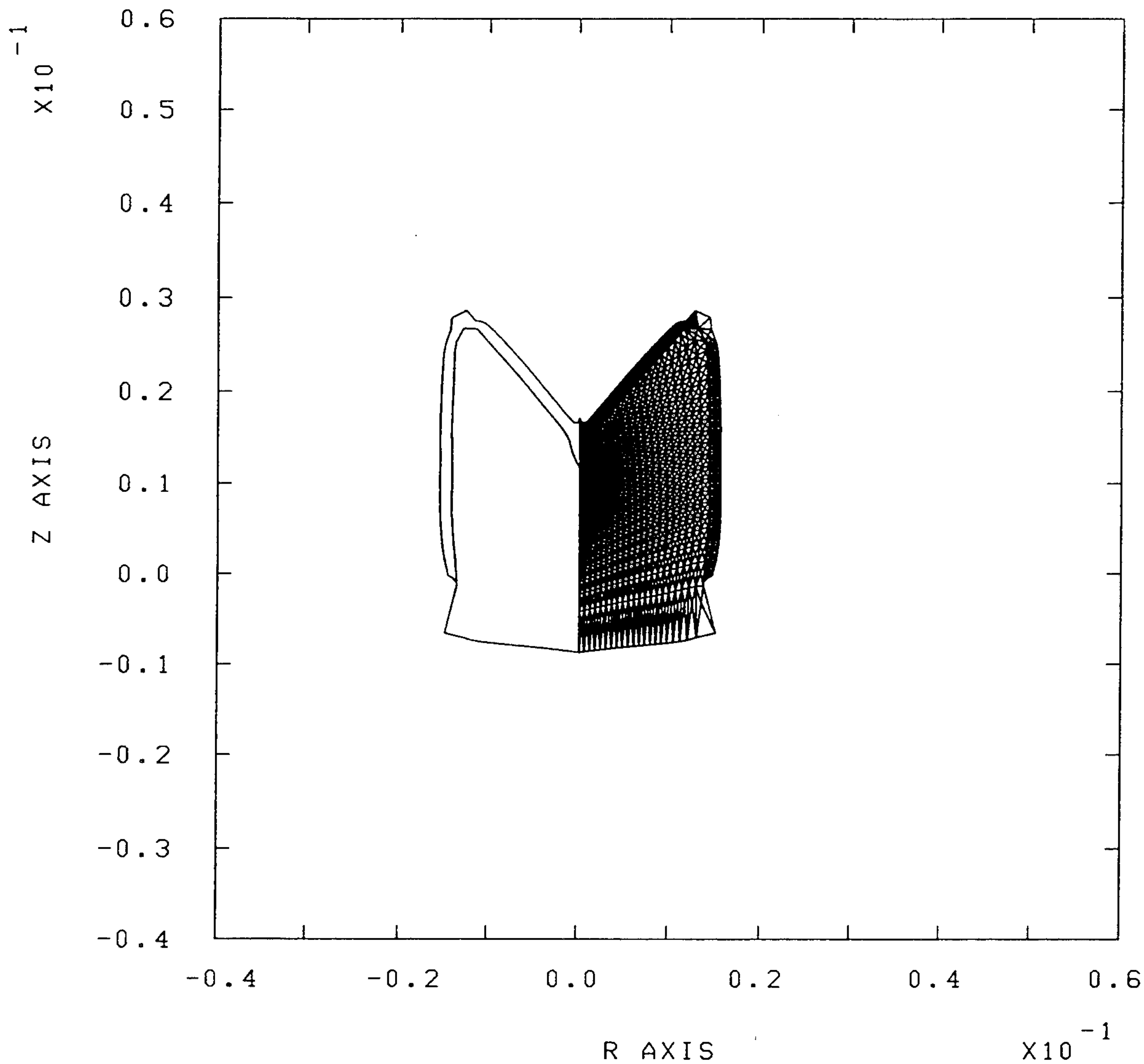

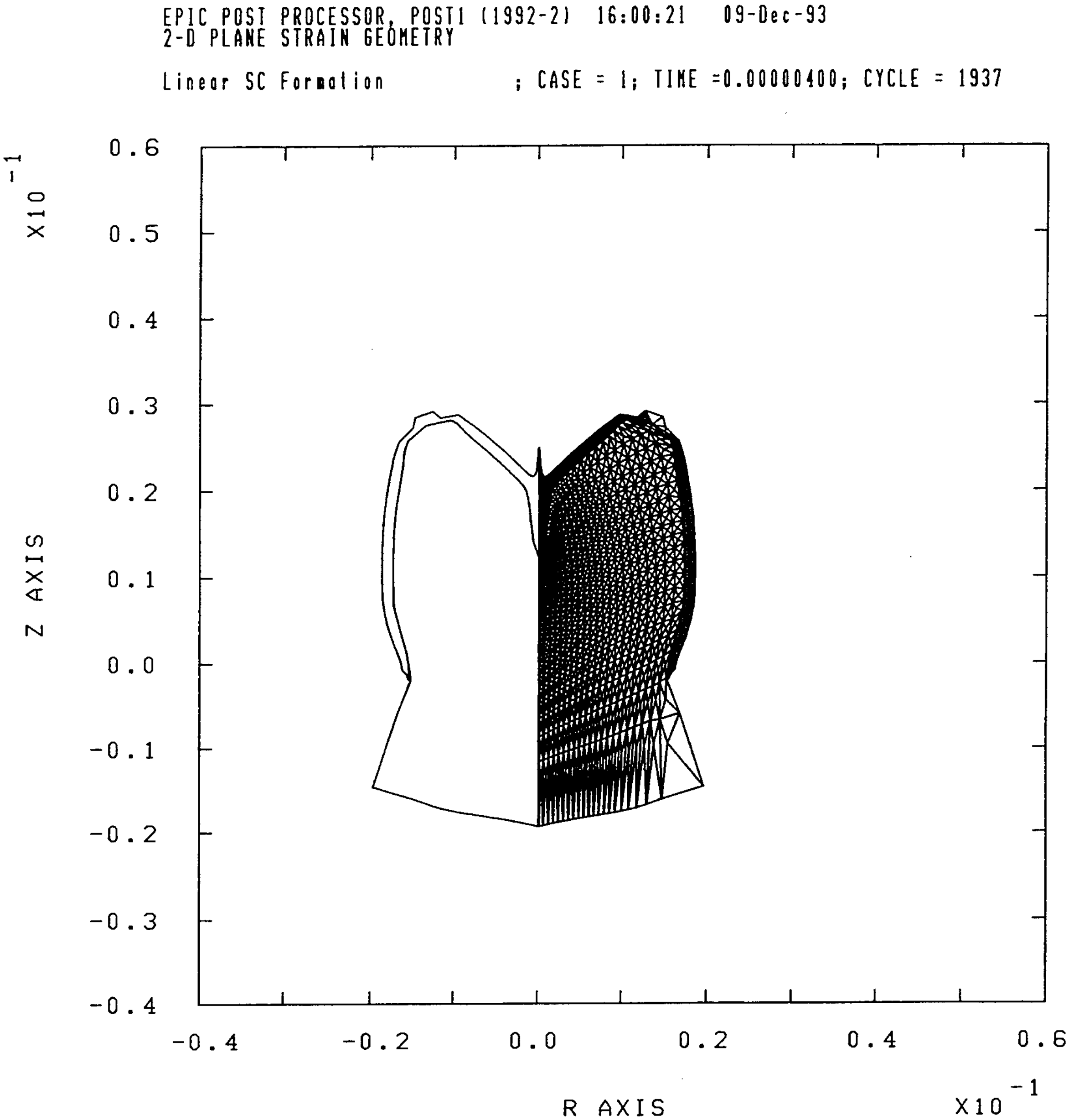
EPIC POST PROCESSOR, POST1 (1992-2) 16:00:21 09-Dec-93
2-D PLANE STRAIN GEOMETRY
Linear SC Formation ; CASE = 1; TIME =0.00000400; CYCLE = 1937
Z AXIS
X10 -1
0.6
0.5
0.4
0.3
0.2
0.1
0.0
-0.1
-0.2
-0.3
-0.4
-0.4
-0.2
0.0
0.2
0.4
0.6
R AXIS
X10 -1

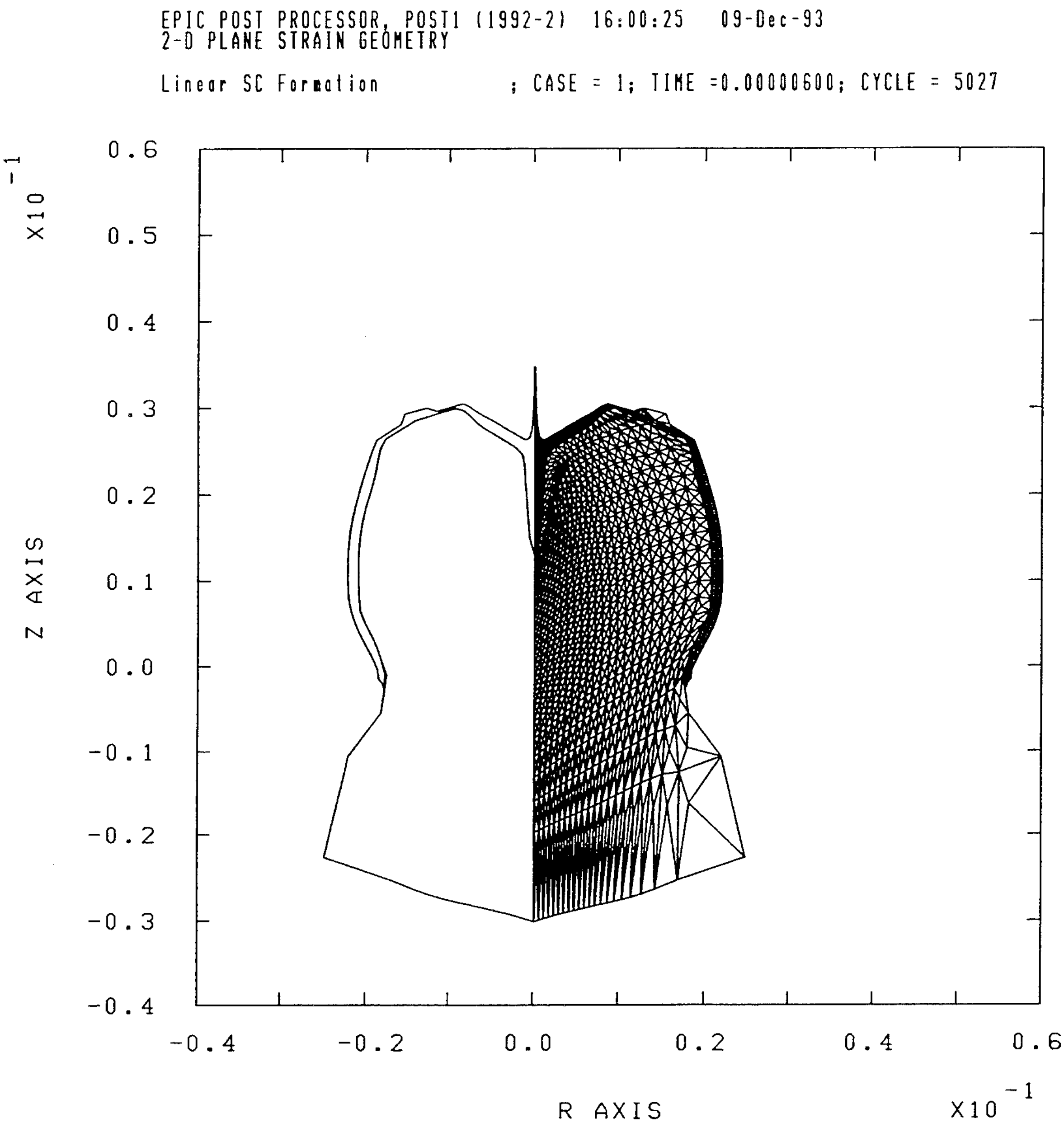
EPIC POST PROCESSOR, POST1 (1992-2) 16:00:25 09-Dec-93
2-D PLANE STRAIN GEOMETRY
Linear SC Formation ; CASE = 1; TIME =0.00000600; CYCLE = 5027
0.6
0.5
0.4
0.3
0.2
0.1
0.0
-0.1
-0.2
-0.3
-0.4
Z AXIS
X10 -1
-0.4
-0.2
0.0
0.2
0.4
0.6
R AXIS
X10 -1

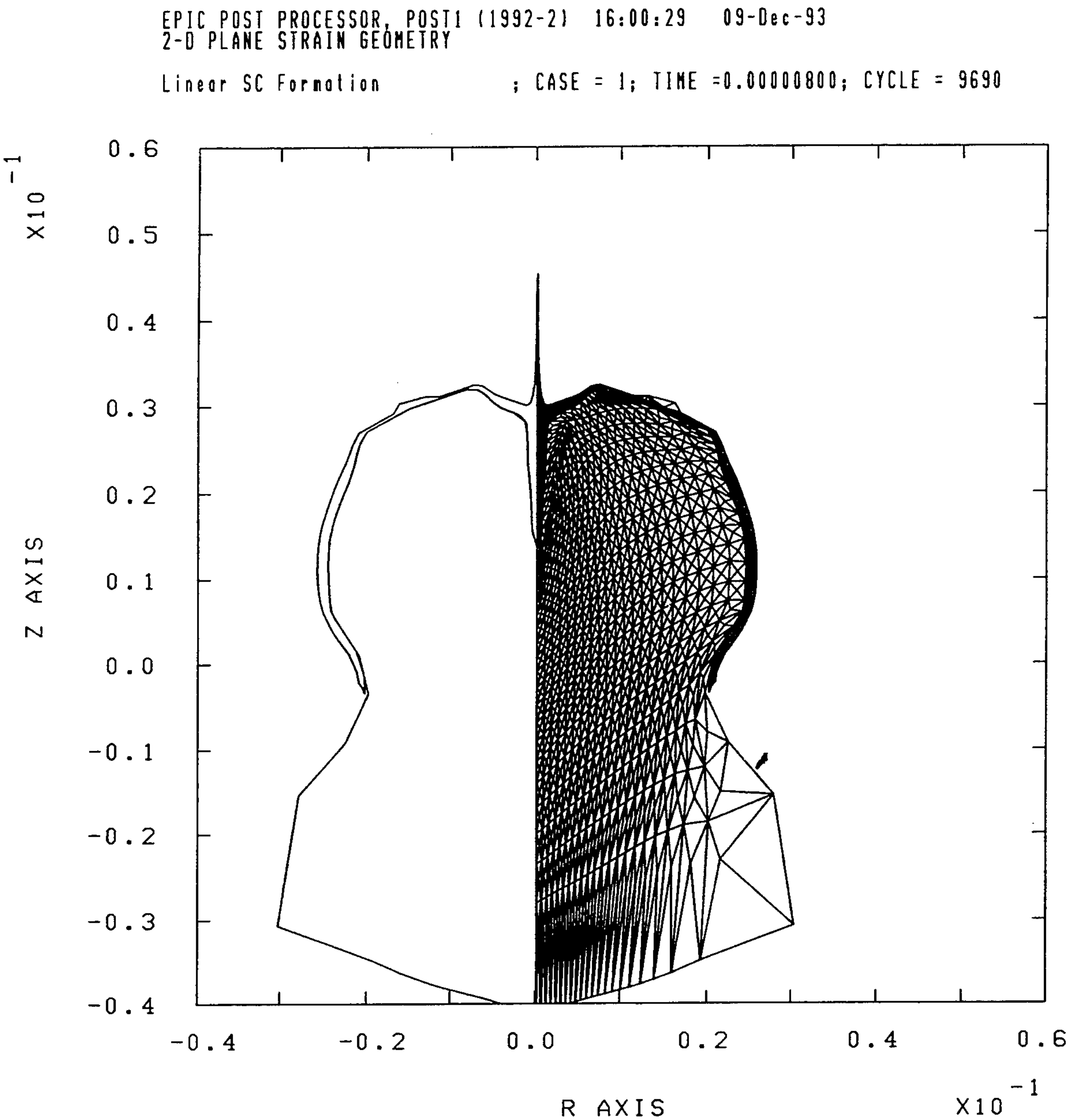
EPIC POST PROCESSOR, POST1 (1992-2) 16:00:29 09-Dec-93
2-D PLANE STRAIN GEOMETRY
Linear SC Formation ; CASE = 1; TIME =0.00000800; CYCLE = 9690
Z AXIS
X10 -1
0.6
0.5
0.4
0.3
0.2
0.1
0.0
-0.1
-0.2
-0.3
-0.4
-0.4
-0.2
0.0
0.2
0.4
0.6
R AXIS
X10 -1

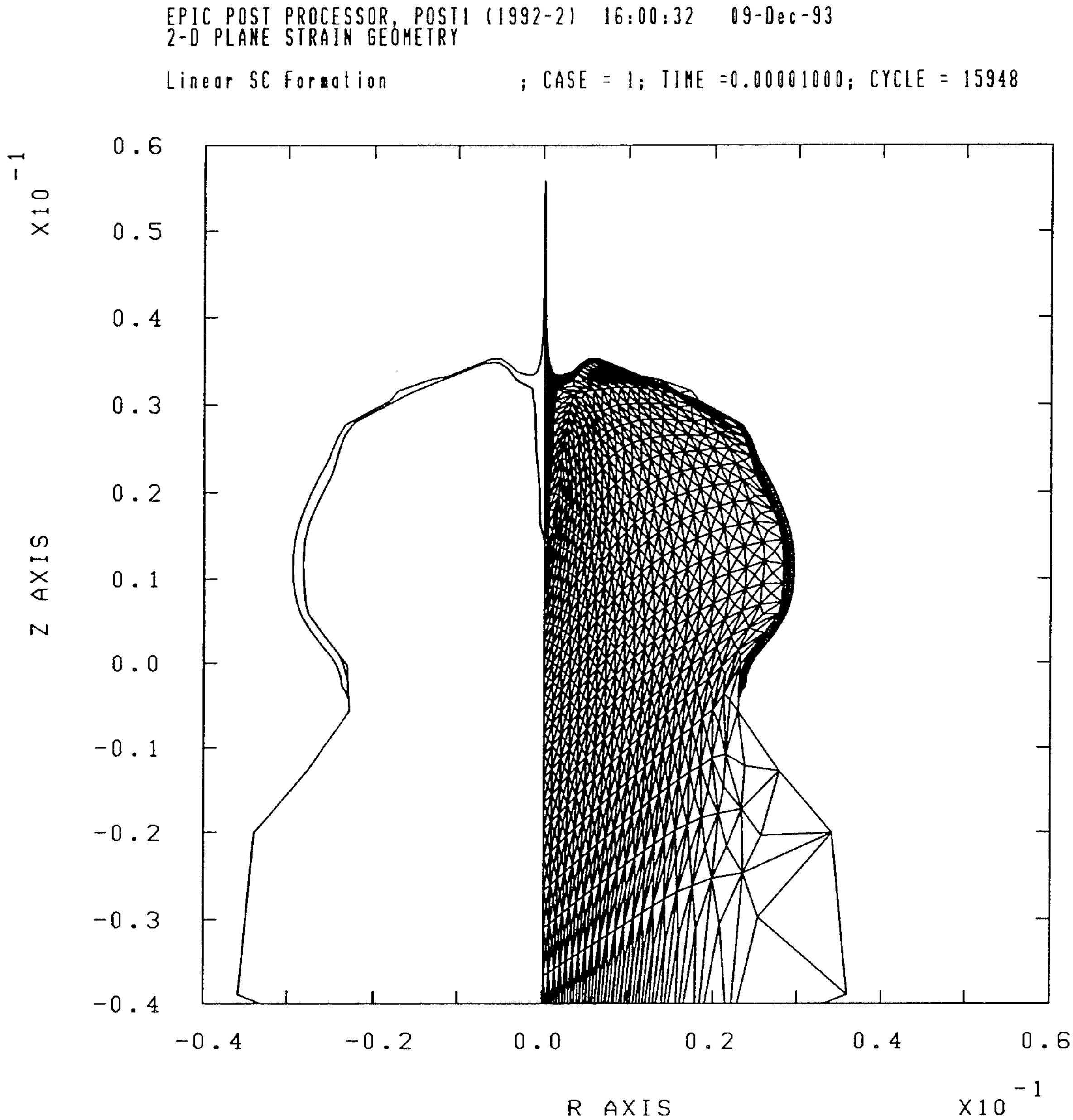
EPIC POST PROCESSOR, POST1 (1992-2) 16:00:32 09-Dec-93
2-D PLANE STRAIN GEOMETRY
Linear SC Formation ; CASE = 1; TIME =0.00001000; CYCLE = 15948
Z AXIS
X10 -1
R AXIS
X10 -1
0.6
0.5
0.4
0.3
0.2
0.1
0.0
-0.1
-0.2
-0.3
-0.4
-0.4
-0.2
0.0
0.2
0.4
0.6

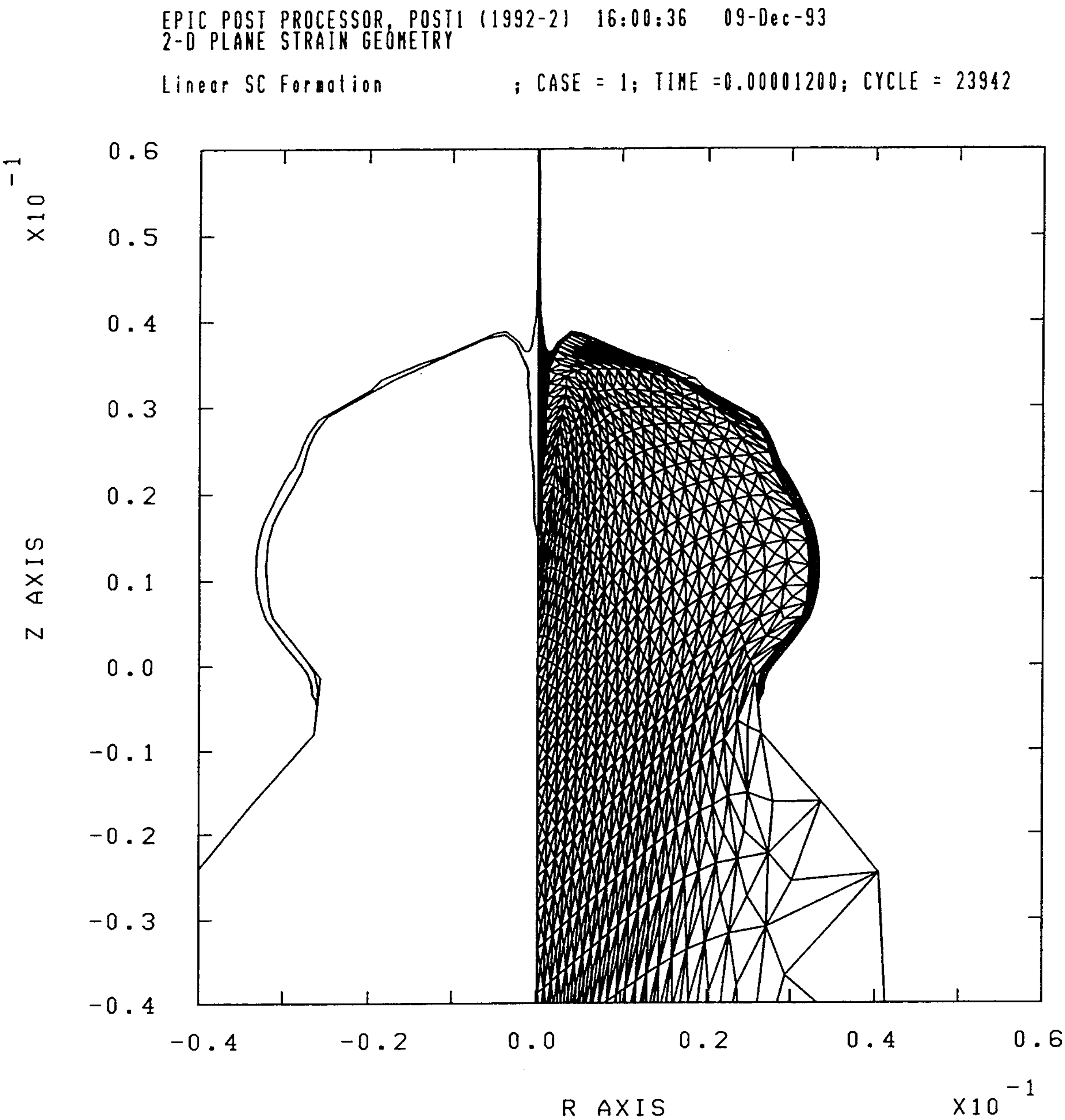

EPIC POST PROCESSOR, POST1 (1992-2) 16:00:36 09-Dec-93
2-D PLANE STRAIN GEOMETRY
Linear SC Formation ; CASE = 1; TIME =0.00001200; CYCLE = 23942
0.6
0.5
0.4
0.3
0.2
0.1
0.0
-0.1
-0.2
-0.3
-0.4
X10^-1
Z AXIS
-0.4
-0.2
0.0
0.2
0.4
0.6
R AXIS
X10^-1

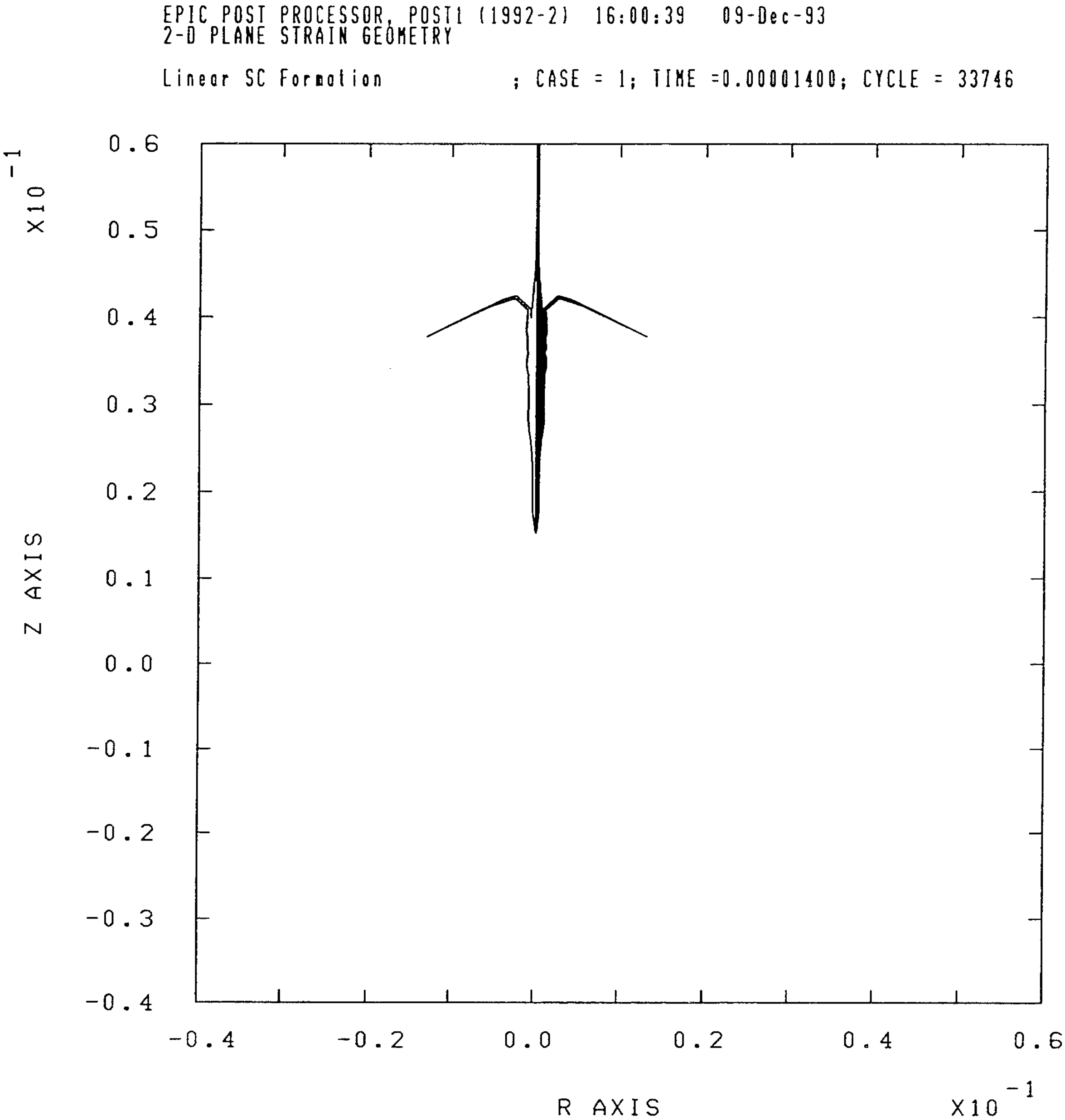
EPIC POST PROCESSOR, POST1 (1992-2) 16:00:39 09-Dec-93
2-D PLANE STRAIN GEOMETRY
Linear SC Formation ; CASE = 1; TIME =0.00001400; CYCLE = 33746
Z AXIS
X10 -1
R AXIS
X10 -1
0.6
0.5
0.4
0.3
0.2
0.1
0.0
-0.1
-0.2
-0.3
-0.4
-0.4
-0.2
0.0
0.2
0.4
0.6

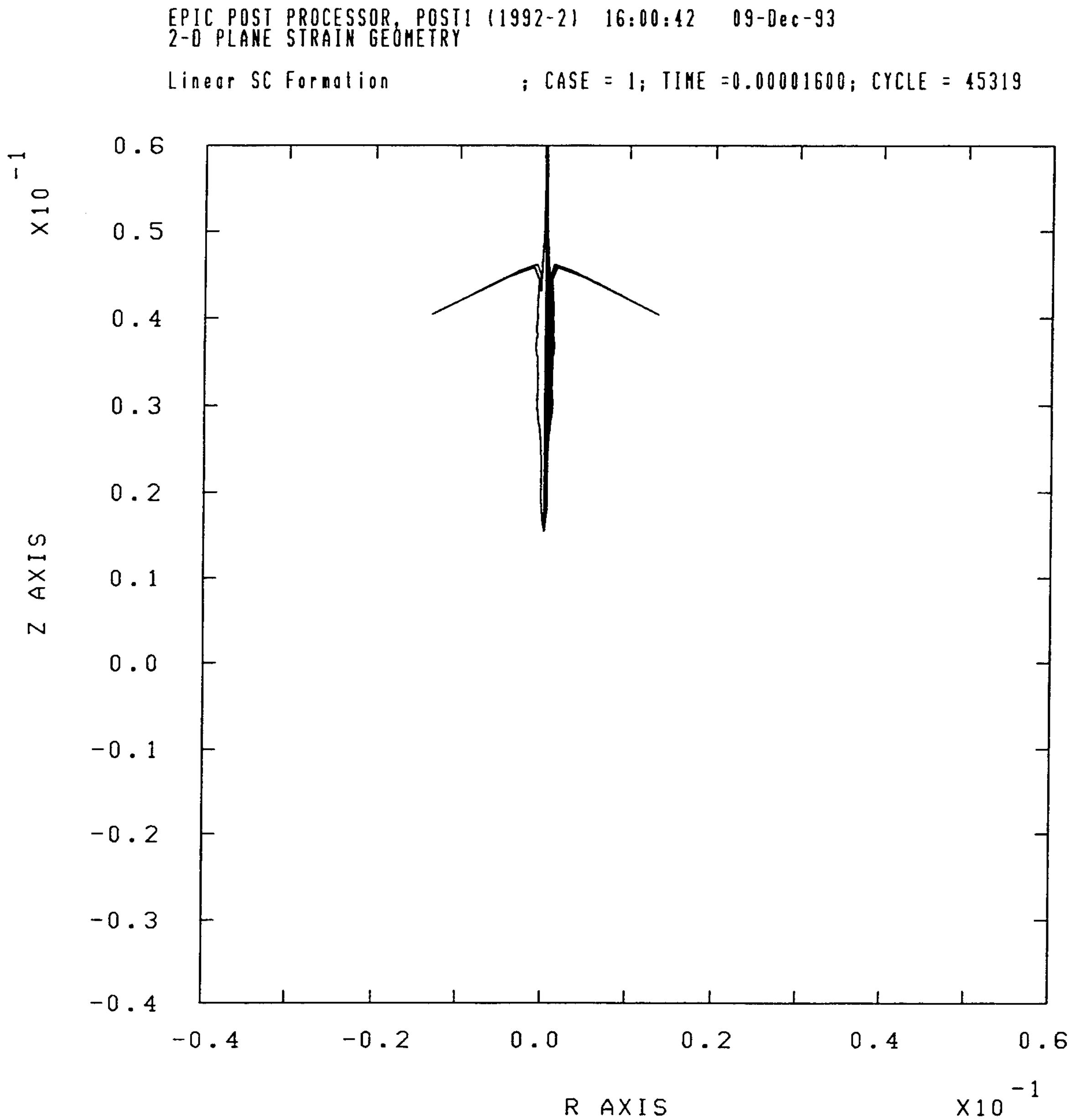
EPIC POST PROCESSOR, POST1 (1992-2) 16:00:42 09-Dec-93
2-D PLANE STRAIN GEOMETRY
Linear SC Formation ; CASE = 1; TIME =0.00001600; CYCLE = 45319
Z AXIS
X10 -1
R AXIS
X10 -1
0.6
0.5
0.4
0.3
0.2
0.1
0.0
-0.1
-0.2
-0.3
-0.4
-0.4
-0.2
0.0
0.2
0.4
0.6

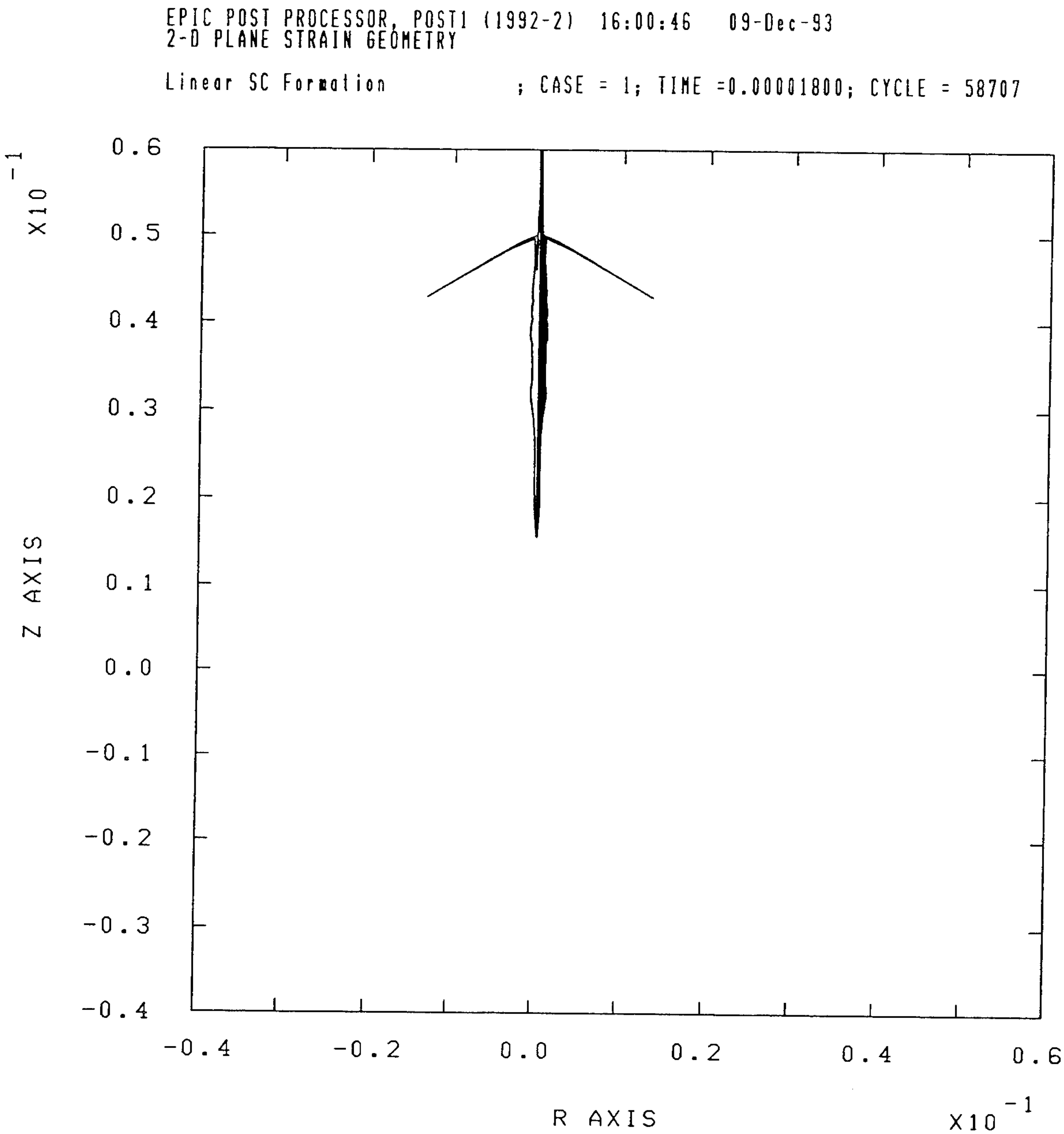
EPIC POST PROCESSOR, POST1 (1992-2) 16:00:46 09-Dec-93
2-D PLANE STRAIN GEOMETRY
Linear SC Formation ; CASE = 1; TIME =0.00001800; CYCLE = 58707
Z AXIS
X10 -1
0.6
0.5
0.4
0.3
0.2
0.1
0.0
-0.1
-0.2
-0.3
-0.4
-0.4
-0.2
0.0
0.2
0.4
0.6
R AXIS
X10 -1

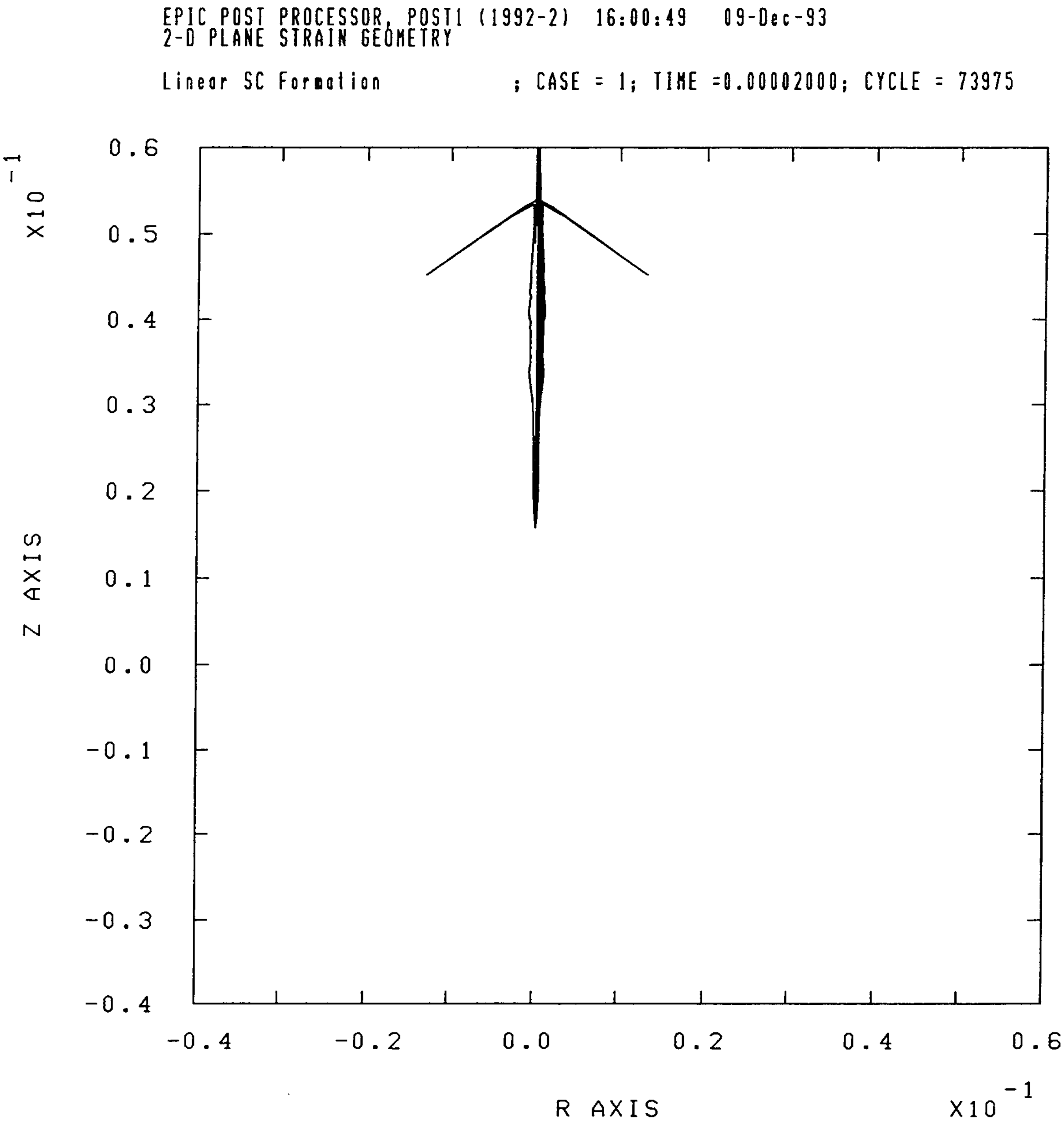
EPIC POST PROCESSOR, POST1 (1992-2) 16:00:49 09-Dec-93
2-D PLANE STRAIN GEOMETRY
Linear SC Formation ; CASE = 1; TIME =0.00002000; CYCLE = 73975
X10 -1
0.6
0.5
0.4
0.3
0.2
0.1
0.0
-0.1
-0.2
-0.3
-0.4
Z AXIS
-0.4
-0.2
0.0
0.2
0.4
0.6
R AXIS
X10 -1

INTENTIONALLY LEFT BLANK.

APPENDIX B:

SHAPED CHARGE JET PENETRATION INPUT DECK AND COMPUTATIONAL RESULTS

INTENTIONALLY LEFT BLANK.

```
$$ preprocessor data  ***********************************************************
$       Target is: UNCLASSIFIED, Linear Shaped Charge Detonation
$       Mk-7 is:
$                - Mild Steel Liner ASTM-A569
$                - Explosive C-4
$
$type.case...........problem description......................................]
    1     1 NEOD TARGET - S. Segletes & George Gazonas - MAY 1994
$geom.prnt.save.nsld.nmas.nrst.nrig.nchk.load.nzonPCrtz.splt..dp3.unit/////..per
    5    0    3    2    0    2    0    0    0    0 1100    0    0    1         0
$ material data
$ solids from library
$matl....0..dam.fail.dfrc.efal.SOLIDS FROM LIBRARY
    6    0    1    0       999. 1006 Steel (Mild Steel Simulant)
    9    0    1    0       999. 4340 Steel (RHA Simulant)
         $ end of material
$//\\//\\//\\//\\//\\//\\//\\//\\//\\//\\//\\//\\//\\//\\//\\//\\//\\//\\//\\//
$ projectile nodes (Rod)
$.x/rscale....yscale....zscale..x/rshift....zshift....rotate.....slant.x/r0...z0
    1.0000    1.0000    1.0000   0.00019   0.00000     -90.0       0.0    0    0
$ Rod nodes
$...2..nor..nir.npln..rad...ax.cros.join...n1.ntop......ztop......zbot....expand
    2  311    1    4    2    2    1    0 0001    0   0.00000    0.0000        1.
$RAD=2.RT1.......RT2.......RT3.......RT4.......RT5.......RT6.......RT7.......RT8
 2.841E-02 2.845E-02 2.849E-02 2.853E-02 2.857E-02 2.861E-02 2.865E-02 2.869E-02
 2.873E-02 2.877E-02 2.881E-02 2.885E-02 2.889E-02 2.893E-02 2.897E-02 2.901E-02
 2.905E-02 2.909E-02 2.913E-02 2.917E-02 2.921E-02 2.925E-02 2.929E-02 2.933E-02
 2.937E-02 2.941E-02 2.945E-02 2.949E-02 2.953E-02 2.957E-02 2.961E-02 2.965E-02
 2.969E-02 2.973E-02 2.977E-02 2.981E-02 2.985E-02 2.989E-02 2.993E-02 2.997E-02
 3.001E-02 3.005E-02 3.009E-02 3.013E-02 3.017E-02 3.021E-02 3.025E-02 3.029E-02
 3.033E-02 3.037E-02 3.041E-02 3.045E-02 3.049E-02 3.053E-02 3.057E-02 3.061E-02
 3.065E-02 3.069E-02 3.073E-02 3.077E-02 3.081E-02 3.085E-02 3.089E-02 3.093E-02
 3.097E-02 3.101E-02 3.105E-02 3.109E-02 3.113E-02 3.117E-02 3.121E-02 3.125E-02
 3.129E-02 3.133E-02 3.137E-02 3.141E-02 3.145E-02 3.149E-02 3.153E-02 3.157E-02
 3.161E-02 3.165E-02 3.169E-02 3.173E-02 3.177E-02 3.181E-02 3.185E-02 3.189E-02
 3.193E-02 3.197E-02 3.201E-02 3.205E-02 3.209E-02 3.213E-02 3.217E-02 3.221E-02
 3.225E-02 3.229E-02 3.233E-02 3.237E-02 3.241E-02 3.245E-02 3.249E-02 3.253E-02
 3.257E-02 3.261E-02 3.265E-02 3.269E-02 3.273E-02 3.277E-02 3.281E-02 3.285E-02
 3.289E-02 3.293E-02 3.297E-02 3.301E-02 3.305E-02 3.309E-02 3.313E-02 3.317E-02
 3.321E-02 3.325E-02 3.329E-02 3.333E-02 3.337E-02 3.341E-02 3.345E-02 3.349E-02
 3.353E-02 3.357E-02 3.361E-02 3.365E-02 3.369E-02 3.373E-02 3.377E-02 3.381E-02
 3.385E-02 3.389E-02 3.393E-02 3.397E-02 3.401E-02 3.405E-02 3.409E-02 3.413E-02
 3.417E-02 3.421E-02 3.425E-02 3.429E-02 3.433E-02 3.437E-02 3.441E-02 3.445E-02
 3.449E-02 3.453E-02 3.457E-02 3.461E-02 3.465E-02 3.469E-02 3.473E-02 3.477E-02
 3.481E-02 3.485E-02 3.489E-02 3.493E-02 3.497E-02 3.501E-02 3.505E-02 3.509E-02
 3.513E-02 3.517E-02 3.521E-02 3.525E-02 3.529E-02 3.533E-02 3.537E-02 3.541E-02
 3.545E-02 3.549E-02 3.553E-02 3.557E-02 3.561E-02 3.565E-02 3.569E-02 3.573E-02
 3.577E-02 3.581E-02 3.585E-02 3.589E-02 3.593E-02 3.597E-02 3.601E-02 3.605E-02
 3.609E-02 3.613E-02 3.617E-02 3.621E-02 3.625E-02 3.629E-02 3.633E-02 3.637E-02
 3.641E-02 3.645E-02 3.649E-02 3.653E-02 3.657E-02 3.661E-02 3.665E-02 3.669E-02
 3.673E-02 3.677E-02 3.681E-02 3.685E-02 3.689E-02 3.693E-02 3.697E-02 3.701E-02
 3.705E-02 3.709E-02 3.713E-02 3.717E-02 3.721E-02 3.725E-02 3.729E-02 3.733E-02
 3.737E-02 3.741E-02 3.745E-02 3.749E-02 3.753E-02 3.757E-02 3.761E-02 3.765E-02
 3.769E-02 3.773E-02 3.777E-02 3.781E-02 3.785E-02 3.789E-02 3.793E-02 3.797E-02
 3.801E-02 3.805E-02 3.809E-02 3.813E-02 3.817E-02 3.821E-02 3.825E-02 3.829E-02
```

```
 3.833E-02 3.837E-02 3.841E-02 3.845E-02 3.849E-02 3.853E-02 3.857E-02 3.861E-02
 3.865E-02 3.869E-02 3.873E-02 3.877E-02 3.881E-02 3.885E-02 3.889E-02 3.893E-02
 3.897E-02 3.901E-02 3.905E-02 3.909E-02 3.913E-02 3.917E-02 3.921E-02 3.925E-02
 3.929E-02 3.933E-02 3.937E-02 3.941E-02 3.945E-02 3.949E-02 3.953E-02 3.957E-02
 3.961E-02 3.965E-02 3.969E-02 3.973E-02 3.977E-02 3.981E-02 3.985E-02 3.989E-02
 3.993E-02 3.997E-02 4.001E-02 4.005E-02 4.009E-02 4.013E-02 4.017E-02 4.021E-02
 4.025E-02 4.029E-02 4.033E-02 4.037E-02 4.041E-02 4.045E-02 4.049E-02 4.053E-02
 4.057E-02 4.061E-02 4.065E-02 4.069E-02 4.073E-02 4.077E-02 4.081E-02
$RAD=2.RB1.......RB2.......RB3.......RB4.......RB5.......RB6.......RB7.......RB8
 2.841E-02 2.845E-02 2.849E-02 2.853E-02 2.857E-02 2.861E-02 2.865E-02 2.869E-02
 2.873E-02 2.877E-02 2.881E-02 2.885E-02 2.889E-02 2.893E-02 2.897E-02 2.901E-02
 2.905E-02 2.909E-02 2.913E-02 2.917E-02 2.921E-02 2.925E-02 2.929E-02 2.933E-02
 2.937E-02 2.941E-02 2.945E-02 2.949E-02 2.953E-02 2.957E-02 2.961E-02 2.965E-02
 2.969E-02 2.973E-02 2.977E-02 2.981E-02 2.985E-02 2.989E-02 2.993E-02 2.997E-02
 3.001E-02 3.005E-02 3.009E-02 3.013E-02 3.017E-02 3.021E-02 3.025E-02 3.029E-02
 3.033E-02 3.037E-02 3.041E-02 3.045E-02 3.049E-02 3.053E-02 3.057E-02 3.061E-02
 3.065E-02 3.069E-02 3.073E-02 3.077E-02 3.081E-02 3.085E-02 3.089E-02 3.093E-02
 3.097E-02 3.101E-02 3.105E-02 3.109E-02 3.113E-02 3.117E-02 3.121E-02 3.125E-02
 3.129E-02 3.133E-02 3.137E-02 3.141E-02 3.145E-02 3.149E-02 3.153E-02 3.157E-02
 3.161E-02 3.165E-02 3.169E-02 3.173E-02 3.177E-02 3.181E-02 3.185E-02 3.189E-02
 3.193E-02 3.197E-02 3.201E-02 3.205E-02 3.209E-02 3.213E-02 3.217E-02 3.221E-02
 3.225E-02 3.229E-02 3.233E-02 3.237E-02 3.241E-02 3.245E-02 3.249E-02 3.253E-02
 3.257E-02 3.261E-02 3.265E-02 3.269E-02 3.273E-02 3.277E-02 3.281E-02 3.285E-02
 3.289E-02 3.293E-02 3.297E-02 3.301E-02 3.305E-02 3.309E-02 3.313E-02 3.317E-02
 3.321E-02 3.325E-02 3.329E-02 3.333E-02 3.337E-02 3.341E-02 3.345E-02 3.349E-02
 3.353E-02 3.357E-02 3.361E-02 3.365E-02 3.369E-02 3.373E-02 3.377E-02 3.381E-02
 3.385E-02 3.389E-02 3.393E-02 3.397E-02 3.401E-02 3.405E-02 3.409E-02 3.413E-02
 3.417E-02 3.421E-02 3.425E-02 3.429E-02 3.433E-02 3.437E-02 3.441E-02 3.445E-02
 3.449E-02 3.453E-02 3.457E-02 3.461E-02 3.465E-02 3.469E-02 3.473E-02 3.477E-02
 3.481E-02 3.485E-02 3.489E-02 3.493E-02 3.497E-02 3.501E-02 3.505E-02 3.509E-02
 3.513E-02 3.517E-02 3.521E-02 3.525E-02 3.529E-02 3.533E-02 3.537E-02 3.541E-02
 3.545E-02 3.549E-02 3.553E-02 3.557E-02 3.561E-02 3.565E-02 3.569E-02 3.573E-02
 3.577E-02 3.581E-02 3.585E-02 3.589E-02 3.593E-02 3.597E-02 3.601E-02 3.605E-02
 3.609E-02 3.613E-02 3.617E-02 3.621E-02 3.625E-02 3.629E-02 3.633E-02 3.637E-02
 3.641E-02 3.645E-02 3.649E-02 3.653E-02 3.657E-02 3.661E-02 3.665E-02 3.669E-02
 3.673E-02 3.677E-02 3.681E-02 3.685E-02 3.689E-02 3.693E-02 3.697E-02 3.701E-02
 3.705E-02 3.709E-02 3.713E-02 3.717E-02 3.721E-02 3.725E-02 3.729E-02 3.733E-02
 3.737E-02 3.741E-02 3.745E-02 3.749E-02 3.753E-02 3.757E-02 3.761E-02 3.765E-02
 3.769E-02 3.773E-02 3.777E-02 3.781E-02 3.785E-02 3.789E-02 3.793E-02 3.797E-02
 3.801E-02 3.805E-02 3.809E-02 3.813E-02 3.817E-02 3.821E-02 3.825E-02 3.829E-02
 3.833E-02 3.837E-02 3.841E-02 3.845E-02 3.849E-02 3.853E-02 3.857E-02 3.861E-02
 3.865E-02 3.869E-02 3.873E-02 3.877E-02 3.881E-02 3.885E-02 3.889E-02 3.893E-02
 3.897E-02 3.901E-02 3.905E-02 3.909E-02 3.913E-02 3.917E-02 3.921E-02 3.925E-02
 3.929E-02 3.933E-02 3.937E-02 3.941E-02 3.945E-02 3.949E-02 3.953E-02 3.957E-02
 3.961E-02 3.965E-02 3.969E-02 3.973E-02 3.977E-02 3.981E-02 3.985E-02 3.989E-02
 3.993E-02 3.997E-02 4.001E-02 4.005E-02 4.009E-02 4.013E-02 4.017E-02 4.021E-02
 4.025E-02 4.029E-02 4.033E-02 4.037E-02 4.041E-02 4.045E-02 4.049E-02 4.053E-02
 4.057E-02 4.061E-02 4.065E-02 4.069E-02 4.073E-02 4.077E-02 4.081E-02
$AX=2..ZT1.......ZT2.......ZT3.......ZT4.......ZT5.......ZT6.......ZT7.......ZT8
        0.        0.        0.        0.        0.        0.        0.        0.
        0.        0.        0.        0.        0.        0.        0.        0.
        0.        0.        0.        0.        0.        0.        0.        0.
        0.        0.        0.        0.        0.        0.        0.        0.
        0.        0.        0.        0.        0.        0.        0.        0.
        0.        0.        0.        0.        0.        0.        0.        0.
        0.        0.        0.        0.        0.        0.        0.        0.
        0.        0.        0.        0.        0.        0.        0.        0.
```

```
      0.        0.        0.        0.        0.        0.        0.        0.
      0.        0.        0.        0.        0.        0.        0.        0.
      0.        0.        0.        0.        0.        0.        0.        0.
      0.        0.        0.        0.        0.        0.        0.        0.
      0.        0.        0.        0.        0.        0.        0.        0.
      0.        0.        0.        0.        0.        0.        0.        0.
      0.        0.        0.        0.        0.        0.        0.        0.
      0.        0.        0.        0.        0.        0.        0.        0.
      0.        0.        0.        0.        0.        0.        0.        0.
      0.        0.        0.        0.        0.        0.        0.        0.
      0.        0.        0.        0.        0.        0.        0.        0.
      0.        0.        0.        0.        0.        0.        0.        0.
      0.        0.        0.        0.        0.        0.        0.        0.
      0.        0.        0.        0.        0.        0.        0.        0.
      0.        0.        0.        0.        0.        0.        0.        0.
      0.        0.        0.        0.        0.        0.        0.        0.
      0.        0.        0.        0.        0.        0.        0.        0.
      0.        0.        0.        0.        0.        0.        0.        0.
      0.        0.        0.        0.        0.        0.        0.        0.
      0.        0.        0.        0.        0.        0.        0.        0.
      0.        0.        0.        0.        0.        0.        0.        0.
      0.        0.        0.        0.        0.        0.        0.        0.
      0.        0.        0.        0.        0.        0.        0.        0.
      0.        0.        0.        0.        0.        0.        0.        0.
      0.        0.        0.        0.        0.        0.        0.        0.
      0.        0.        0.        0.        0.        0.        0.        0.
      0.        0.        0.        0.        0.        0.        0.        0.
      0.        0.        0.        0.        0.        0.        0.        0.
      0.        0.        0.        0.        0.        0.        0.        0.
      0.        0.        0.        0.        0.        0.        0.        0.
      0.        0.        0.        0.        0.        0.        0.
$AX=2..ZB1.......ZB2.......ZB3.......ZB4.......ZB5.......ZB6.......ZB7.......ZB8
-1.037E-03-9.828E-04-9.359E-04-8.947E-04-8.581E-04-8.254E-04-7.958E-04-7.689E-04
-7.442E-04-7.214E-04-7.003E-04-6.807E-04-6.624E-04-6.453E-04-6.291E-04-6.139E-04
-5.996E-04-5.860E-04-5.730E-04-5.607E-04-5.490E-04-5.378E-04-5.270E-04-5.168E-04
-5.069E-04-4.975E-04-4.883E-04-4.796E-04-4.711E-04-4.630E-04-4.551E-04-4.475E-04
-4.401E-04-4.329E-04-4.260E-04-4.193E-04-4.128E-04-4.065E-04-4.003E-04-3.943E-04
-3.885E-04-3.828E-04-3.773E-04-3.719E-04-3.667E-04-3.616E-04-3.566E-04-3.517E-04
-3.469E-04-3.423E-04-3.378E-04-3.333E-04-3.290E-04-3.247E-04-3.205E-04-3.165E-04
-3.125E-04-3.086E-04-3.047E-04-3.010E-04-2.973E-04-2.937E-04-2.901E-04-2.867E-04
-2.832E-04-2.799E-04-2.766E-04-2.734E-04-2.702E-04-2.671E-04-2.640E-04-2.610E-04
-2.581E-04-2.552E-04-2.523E-04-2.495E-04-2.467E-04-2.440E-04-2.413E-04-2.387E-04
-2.361E-04-2.336E-04-2.310E-04-2.286E-04-2.261E-04-2.237E-04-2.214E-04-2.191E-04
-2.168E-04-2.145E-04-2.123E-04-2.101E-04-2.079E-04-2.058E-04-2.037E-04-2.016E-04
-1.996E-04-1.976E-04-1.956E-04-1.936E-04-1.917E-04-1.898E-04-1.879E-04-1.861E-04
-1.842E-04-1.824E-04-1.806E-04-1.789E-04-1.772E-04-1.754E-04-1.738E-04-1.721E-04
-1.704E-04-1.688E-04-1.672E-04-1.656E-04-1.641E-04-1.625E-04-1.610E-04-1.595E-04
-1.580E-04-1.565E-04-1.551E-04-1.536E-04-1.522E-04-1.508E-04-1.494E-04-1.481E-04
-1.467E-04-1.454E-04-1.441E-04-1.428E-04-1.415E-04-1.402E-04-1.389E-04-1.377E-04
-1.365E-04-1.353E-04-1.341E-04-1.329E-04-1.317E-04-1.305E-04-1.294E-04-1.283E-04
-1.271E-04-1.260E-04-1.249E-04-1.239E-04-1.228E-04-1.217E-04-1.207E-04-1.197E-04
-1.186E-04-1.176E-04-1.166E-04-1.157E-04-1.147E-04-1.137E-04-1.128E-04-1.118E-04
-1.109E-04-1.100E-04-1.091E-04-1.082E-04-1.073E-04-1.064E-04-1.055E-04-1.047E-04
-1.038E-04-1.030E-04-1.021E-04-1.013E-04-1.005E-04-9.976E-05-9.897E-05-9.819E-05
-9.742E-05-9.666E-05-9.590E-05-9.516E-05-9.442E-05-9.369E-05-9.298E-05-9.227E-05
-9.157E-05-9.088E-05-9.020E-05-8.952E-05-8.886E-05-8.820E-05-8.756E-05-8.692E-05
-8.629E-05-8.567E-05-8.506E-05-8.446E-05-8.386E-05-8.328E-05-8.270E-05-8.214E-05
```

```
-8.158E-05-8.103E-05-8.050E-05-7.997E-05-7.945E-05-7.894E-05-7.844E-05-7.795E-05
-7.747E-05-7.700E-05-7.655E-05-7.610E-05-7.566E-05-7.524E-05-7.483E-05-7.443E-05
-7.404E-05-7.367E-05-7.331E-05-7.296E-05-7.263E-05-7.232E-05-7.202E-05-7.174E-05
-7.148E-05-7.124E-05-7.102E-05-7.082E-05-7.065E-05-7.050E-05-7.038E-05-7.030E-05
-7.024E-05-7.023E-05-7.026E-05-7.033E-05-7.046E-05-7.065E-05-7.090E-05-7.090E-05
-7.090E-05-7.090E-05-7.090E-05-7.090E-05-7.090E-05-7.090E-05-7.090E-05-7.090E-05
-7.090E-05-7.090E-05-7.090E-05-7.090E-05-7.090E-05-7.090E-05-7.090E-05-7.090E-05
-7.090E-05-7.090E-05-7.090E-05-7.090E-05-7.090E-05-7.090E-05-7.090E-05-7.090E-05
-7.090E-05-7.090E-05-7.090E-05-7.090E-05-7.090E-05-7.090E-05-7.090E-05-7.090E-05
-7.090E-05-7.090E-05-7.090E-05-7.090E-05-7.090E-05-7.090E-05-7.090E-05-7.090E-05
-7.090E-05-7.090E-05-7.090E-05-7.090E-05-7.090E-05-7.090E-05-7.090E-05-7.090E-05
-7.090E-05-7.090E-05-7.090E-05-7.090E-05-7.090E-05-7.090E-05-7.090E-05-7.090E-05
-7.090E-05-7.090E-05-7.090E-05-7.090E-05-7.090E-05-7.090E-05-7.090E-05-7.090E-05
-7.090E-05-7.090E-05-7.090E-05-7.090E-05-7.090E-05-7.090E-05-7.090E-05
         $ end of projectile nodes
$ target nodes (RHA Plate)
$.x/rscale....yscale....zscale..x/rshift....zshift....rotate.....slant.x/r0...z0
    1.0000    1.0000    1.0000   0.00000   0.00000     000.0       0.0    0    0
$ Plate nodes
$...4.type..nxr...ny...nz..fix.cros.join...n1..inc..x.expand..y.expand..z.expand
    4    1   20      350    1    1    0 2501   49      1.15                  1.0
$nrnd.nznd.rprt.zprt.....rmax.....rmin.....zmax.....zmin
   20    0  1.0  0.0    0.0018    0.000    0.0664    0.041
$...4.type..nxr...ny...nz..fix.cros.join...n1..inc..x.expand..y.expand..z.expand
    4    1    6      350    1    1    2 2520   49      1.80                  1.0
$nrnd.nznd.rprt.zprt.....rmax.....rmin.....zmax.....zmin
    6    0  1.0  0.0    0.0200   0.0018    0.0664    0.041
         $ end of target nodes
$//\\//\\//\\//\\//\\//\\//\\//\\//\\//\\//\\//\\//\\//\\//\\//\\//\\//\\//\\//
$ projectile element data (Jet)
$...2.matl...n1.diag.noer.nier.nlay.....shel.plac//////////.....thick
    2    6 0001    5  311    2    3         0    0
         $ end of projectile elements
$ target element data (RHA Plate)
$ plate elements
$...2.matl...n1.diag.type.nlxr..nly..nlz.shel.plac//////////.....thick
    4    9 2501    5    1   24      349    0    0
         $ end of target elements
$//\\//\\//\\//\\//\\//\\//\\//\\//\\//\\//\\//\\//\\//\\//\\//\\//\\//\\//\\//
$ begin slide line data
$
$ slide #1
$ master: target plate
$ slave : projectile (jet)
$.nmg..nmn..nsg..nsn..nsr.type.mbot..isr..it1..it2...ref vel.....erode..friction
    1    0    1    0    0    1 0000    0    1    0                   2.0
$.m1g..mng..inc
1962619602   -1            $ target plate front surface
$.s1g..sng..inc
    1 2174    1            $ All of jet
$
$ slide #2
$ master: projectile (jet)
$ slave : target plate
$.nmg..nmn..nsg..nsn..nsr.type.mbot..isr..it1..it2...ref vel.....erode..friction
    3    0    1    0    0    1 0000    0    1    0                   2.0
$.m1g..mng..inc
```

```
  311 1553  621               $ jet tip
$.m1g..mng..inc
 2174 1864   -1               $ jet side
$.m1g..mng..inc
 1243    1 -621               $ jet tail
$.s1g..sng..inc
1962619602   -1               $ target plate front surface
$
$//\\//\\//\\//\\//\\//\\//\\//\\//\\//\\//\\//\\//\\//\\//\\//\\//\\//\\//\\//
$ Restraints
$ Tie liner nodes to axis of symmetry
  311    1  100                $ 311 nodes, 1 set, R-constraint
 0001 0311    1                $ First=1, Last=311, Increment=1
$ Restrain Target Outer Nodes in R
  350    1  100                $ 350 nodes, 1 set, R-constraint
 252519626   49                $ First=2525, Last=19626, Increment=49
$ detonation
$...x/rdet......ydet......zdet.....tburn.shad.npnt
      0.0       0.0       0.0       0.0
$ initial velocity data
$..px/rdot...py/tdot.....pzdot...tx/rdot...ty/tdot.....tzdot.......dt1.vfld/////
   -000.00       0.0       0.0       0.0       0.0       0.0                -1
$                                                                        ^^^^^
$ NOTE: SPECIAL SUBROUTINE USED TO INPUT VELOCITY FIELD, TRIGGERED BY VFLD=-1




$$ Main Processor data  *******************************************************
$
$type.case...........problem description......................................]
    3    1 NEOD Linear Shaped Charge Penetration - S. Segletes JUN 1994
$
$$ main run data   ************************************************************
$
$cycl.ncpu......time.....dtmax.....dtmin.......ssf......tmax.....cpmax......emax
    0    0 0000.0e-6       1.0    1.e-11      0.80   15.0e-6  00000.00
$tplt.drop..add.pres.push..hrg....vfract.....vnref...nabfact...sphdist//////////
    1    0    0    0    0    0
$.sys.nplt.lplt.dplt.....dtsys......tsys....dtnode.....tnode.....dtdyn......tdyn
    1    0               1.0e-6       0.0   0.25e-6       0.0
$.....time....echeck....ncheck.....rdamp.save.burn.yprt.ndat.slpr.proj..pat.rzne
  00.4E-06    1001.0       999       0.0    3    0    1  500    0    0    0    0
  00.8E-06    1001.0       999       0.0    3    0    1  500    0    0    0    0
  01.2E-06    1001.0       999       0.0    3    0    1  500    0    0    0    0
  01.6E-06    1001.0       999       0.0    3    0    1  500    0    0    0    0
  02.0E-06    1001.0       999       0.0    3    0    1  500    0    0    0    0
  04.0E-06    1001.0       999       0.0    3    0    1  500    0    0    0    0
  06.0E-06    1001.0       999       0.0    3    0    1  500    0    0    0    0
  08.0E-06    1001.0       999       0.0    3    0    1  500    0    0    0    0
  10.0E-06    1001.0       999       0.0    3    0    1  500    0    0    0    0
  15.1E-06    1001.0       999       0.0    3    0    1  500    0    0    0    0


$$ Main Processor data  *******************************************************
$
$type.case...........problem description......................................]
```

```
   3    1 NEOD Linear Shaped Charge Penetration - S. Segletes JUN 1994
$
$$ main run data    *************************************************************
$
$cycl.ncpu......time.....dtmax.....dtmin.......ssf......tmax.....cpmax......emax
   0    0 0015.0e-6       1.0     1.e-11      0.80   30.0e-6  00000.00
$tplt.drop..add.pres.push..hrg....vfract.....vnref...nabfact...sphdist//////////
   1    0    0    0    0    0
$.sys.nplt.lplt.dplt.....dtsys......tsys....dtnode.....tnode.....dtdyn......tdyn
   1    0             1.0e-6       0.0    0.25e-6       0.0
$.....time....echeck....ncheck.....rdamp.save.burn.yprt.ndat.slpr.proj..pat.rzne
  20.0E-06     1001.0       999       0.0    3    0    1  500    0    0    0    0
  25.0E-06     1001.0       999       0.0    3    0    1  500    0    0    0    0
  30.1E-06     1001.0       999       0.0    3    0    1  500    0    0    0    0
```

```
      subroutine myvfld(nvfld)
C
C     USES MY DATA FOR NODAL VELOCITIES;
C     REQUIRES FOLLOWING MODIFICATION TO epic5.f:
C
C:cmy     9 FORMAT(/5X,'NVFLD MUST BE POSITIVE, NVFLD = ',I6)               DELMY
C:
C:...[Code Omitted]...
C:
C:        ELSEIF(NVFLD.LT.0)THEN
C:          WRITE(IOUT,9)NVFLD
C:      9   format (' Invoking specially tailored V-Field...')              ADDMY
C:          call myvfld (nvfld)                                             ADDMY
C:cmy          STOP                                                         DELMY
C:        ENDIF

C
      include 'NODE'
      real field(311), f1(100), f2(100), f3(100), f4(11)
      equivalence (field(1),f1(1)),    (field(101),f2(1)),
     &            (field(201),f3(1)), (field(301),f4(1))
      data f1 (1:100)/
     &   5259.999, 5259.999, 5259.999, 5259.999, 5259.999,
     &   5259.999, 5259.999, 5259.999, 5259.999, 5259.999,
     &   5259.999, 5259.999, 5259.999, 5259.999, 5259.999,
     &   5259.999, 5259.999, 5259.999, 5259.999, 5259.999,
     &   5259.999, 5259.999, 5259.999, 5259.999, 5259.999,
     &   5259.999, 5259.999, 5259.999, 5259.999, 5259.999,
     &   5259.999, 5259.999, 5259.999, 5259.999, 5259.999,
     &   5259.999, 5259.999, 5259.999, 5259.999, 5259.999,
     &   5259.999, 5259.999, 5259.999, 5259.999, 5259.999,
     &   5259.999, 5259.999, 5259.999, 5259.999, 5259.999,
     &   5259.999, 5259.999, 5259.999, 5259.999, 5259.999,
     &   5259.999, 5259.999, 5259.999, 5259.999, 5259.999,
     &   5259.999, 5259.999, 5259.999, 5259.999, 5259.999,
     &   5259.999, 5259.999, 5259.999, 5259.999, 5259.999,
     &   5259.999, 5259.999, 5259.999, 5241.896, 5224.222,
     &   5206.958, 5190.071, 5173.526, 5157.299, 5141.371,
     &   5125.724, 5110.336, 5095.195, 5080.280, 5065.590,
```

```
     &    5051.104, 5036.811, 5022.705, 5008.770, 4995.006,
     &    4981.402, 4967.948, 4954.640, 4941.470, 4928.432,
     &    4915.522, 4902.730, 4890.058, 4877.499, 4865.044/
      data f2 (101:200)/
     &    4852.695, 4840.443, 4828.293, 4816.229, 4804.255,
     &    4792.370, 4780.569, 4768.847, 4757.201, 4745.629,
     &    4734.132, 4722.703, 4711.340, 4700.047, 4688.817,
     &    4677.646, 4666.537, 4655.483, 4644.486, 4633.543,
     &    4622.653, 4611.813, 4601.025, 4590.284, 4579.589,
     &    4568.938, 4558.335, 4547.771, 4537.249, 4526.767,
     &    4516.324, 4505.918, 4495.553, 4485.220, 4474.923,
     &    4464.657, 4454.425, 4444.227, 4434.060, 4423.919,
     &    4413.810, 4403.728, 4393.673, 4383.646, 4373.641,
     &    4363.665, 4353.709, 4343.778, 4333.874, 4323.984,
     &    4314.120, 4304.275, 4294.449, 4284.642, 4274.856,
     &    4265.087, 4255.335, 4245.596, 4235.875, 4226.173,
     &    4216.479, 4206.805, 4197.142, 4187.492, 4177.854,
     &    4168.226, 4158.610, 4149.006, 4139.414, 4129.829,
     &    4120.253, 4110.687, 4101.126, 4091.576, 4082.031,
     &    4072.493, 4062.959, 4053.431, 4043.913, 4034.394,
     &    4024.881, 4015.372, 4005.866, 3996.359, 3986.856,
     &    3977.356, 3967.855, 3958.356, 3948.855, 3939.354,
     &    3929.855, 3920.353, 3910.849, 3901.341, 3891.831,
     &    3882.318, 3872.799, 3863.280, 3853.754, 3844.221/
      data f3 (201:300)/
     &    3834.684, 3825.138, 3815.587, 3806.028, 3796.463,
     &    3786.886, 3777.305, 3767.709, 3758.105, 3748.493,
     &    3738.867, 3729.229, 3719.582, 3709.917, 3700.242,
     &    3690.552, 3680.849, 3671.128, 3661.395, 3651.639,
     &    3641.872, 3632.084, 3622.281, 3612.458, 3602.614,
     &    3592.750, 3582.864, 3572.957, 3563.029, 3553.076,
     &    3543.100, 3533.097, 3523.072, 3513.018, 3502.937,
     &    3492.827, 3482.693, 3472.525, 3462.327, 3452.100,
     &    3441.836, 3431.540, 3421.210, 3410.843, 3400.439,
     &    3389.999, 3379.520, 3369.000, 3358.439, 3347.835,
     &    3337.187, 3326.496, 3315.757, 3304.969, 3294.135,
     &    3283.246, 3272.307, 3261.312, 3250.263, 3239.155,
     &    3227.989, 3216.759, 3205.468, 3194.111, 3182.687,
     &    3171.193, 3159.625, 3147.983, 3136.264, 3124.465,
     &    3112.583, 3100.617, 3088.560, 3076.413, 3064.168,
     &    3051.824, 3039.376, 3026.822, 3014.156, 3001.373,
     &    2988.468, 2975.438, 2962.275, 2948.973, 2935.527,
     &    2921.930, 2908.173, 2894.251, 2880.155, 2865.874,
     &    2851.396, 2836.715, 2821.818, 2806.689, 2791.314,
     &    2775.681, 2759.770, 2743.559, 2727.032, 2710.160/
      data f4 (301:311)/
     &    2692.922, 2675.279, 2657.195, 2638.635, 2619.551,
     &    2599.880, 2579.562, 2558.512, 2536.633, 2513.806,
     &    2489.873/
c
      write (*,100) field
  100 format (5f10.3)
      mjdelt = 311
      idelt  = 621
c     DO FOR NODES IN JET ONLY
      do 10 n = 1, 2174
        index = mod(n-1,idelt) + 1
```

```
c         print *, 'index=',index
        if (index .le. mjdelt) then
          i2 = mjdelt + 1 - index
c           print *, 'i2=',i2
          zdot(n) = field(i2)
        else
          i1 = index - mjdelt
          i2 = mjdelt + 1 - i1
c           print *,'i1,i2=',i1,i2
          zdot(n) = (field(i2) + field(i2-1)) * 0.5
        end if
   10 continue
      return
      end
```

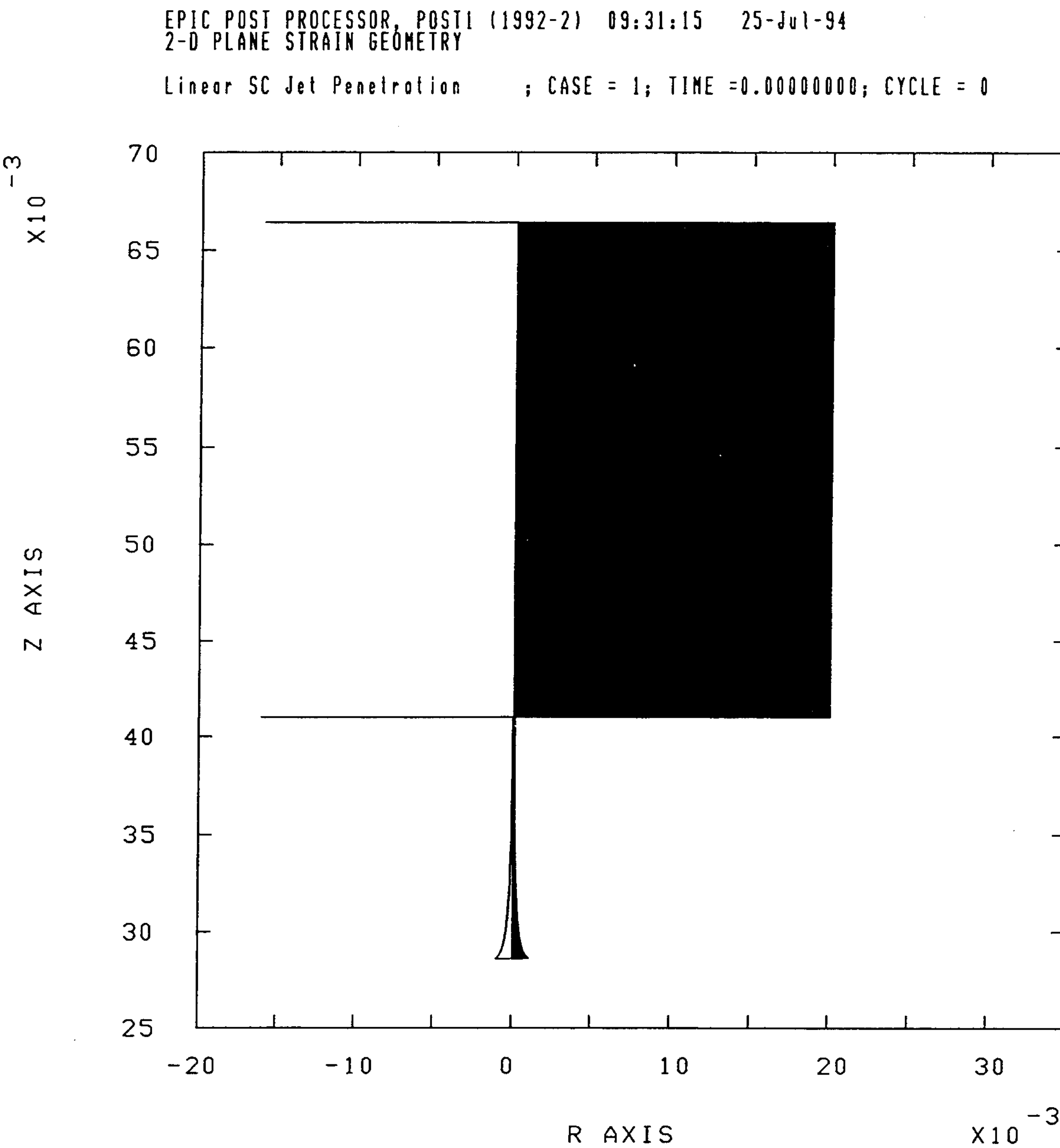
EPIC POST PROCESSOR, POST1 (1992-2) 09:31:15 25-Jul-94
2-D PLANE STRAIN GEOMETRY
Linear SC Jet Penetration ; CASE = 1; TIME =0.00000000; CYCLE = 0
Z AXIS
X10 -3
70
65
60
55
50
45
40
35
30
25
-20
-10
0
10
20
30
R AXIS
X10 -3

EPIC POST PROCESSOR, POST1 (1992-2) 09:31:57 25-Jul-94
2-D PLANE STRAIN GEOMETRY

Linear SC Jet Penetration ; CASE = 1; TIME =0.00000040; CYCLE = 809

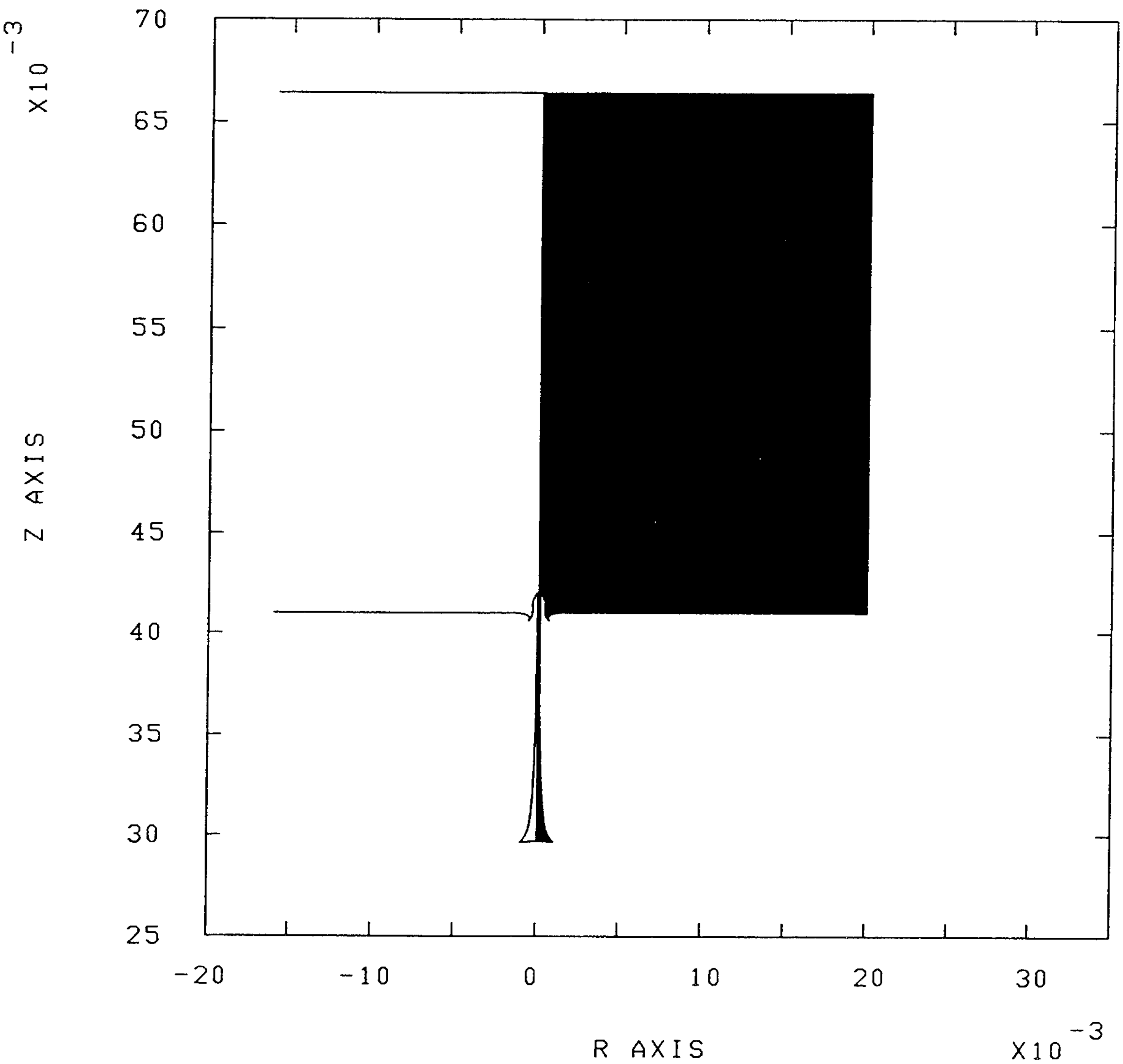

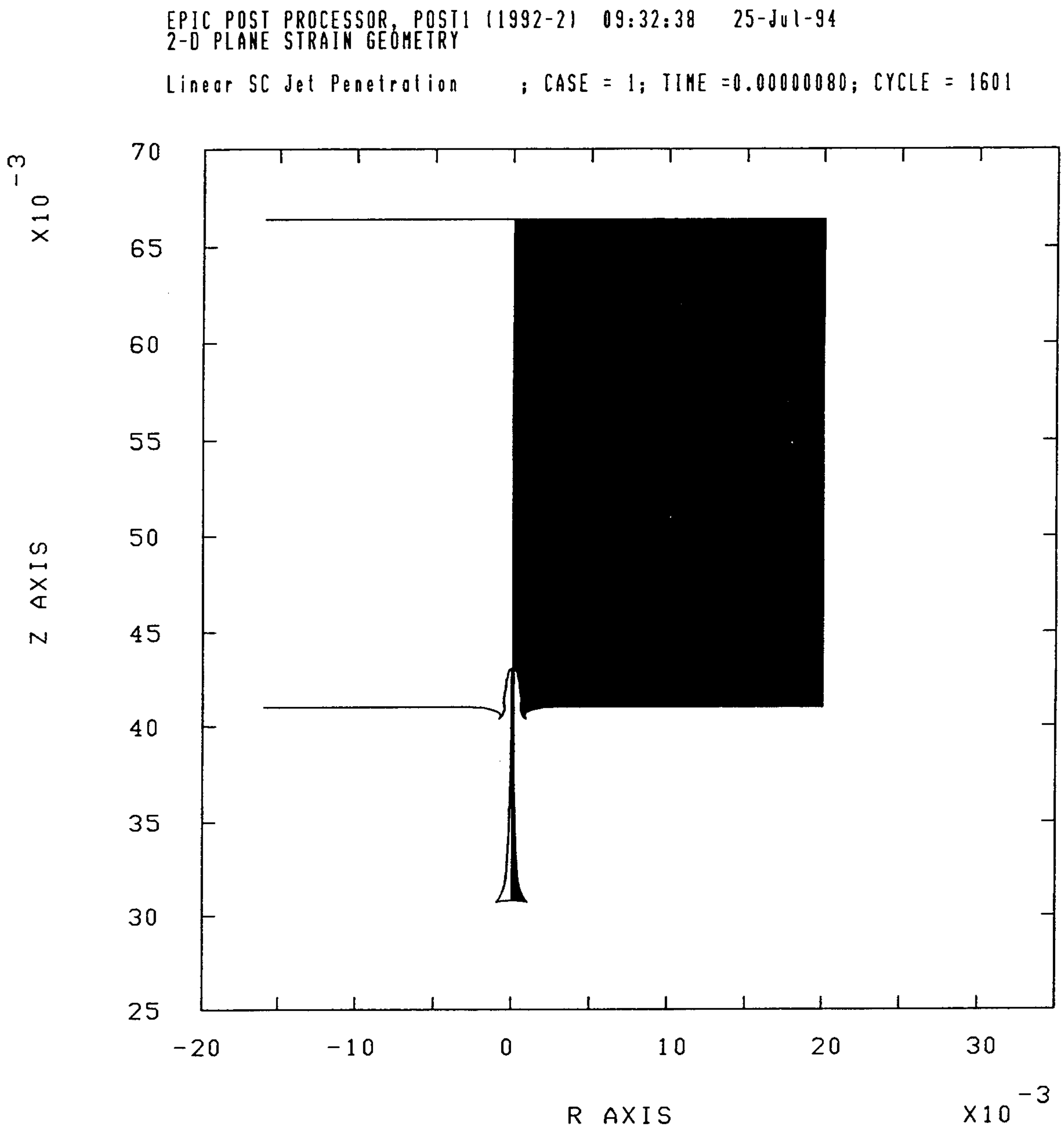

EPIC POST PROCESSOR, POST1 (1992-2) 09:32:38 25-Jul-94
2-D PLANE STRAIN GEOMETRY
Linear SC Jet Penetration ; CASE = 1; TIME =0.00000080; CYCLE = 1601
70
65
60
55
50
45
40
35
30
25
Z AXIS
X10 -3
-20
-10
0
10
20
30
R AXIS
X10 -3

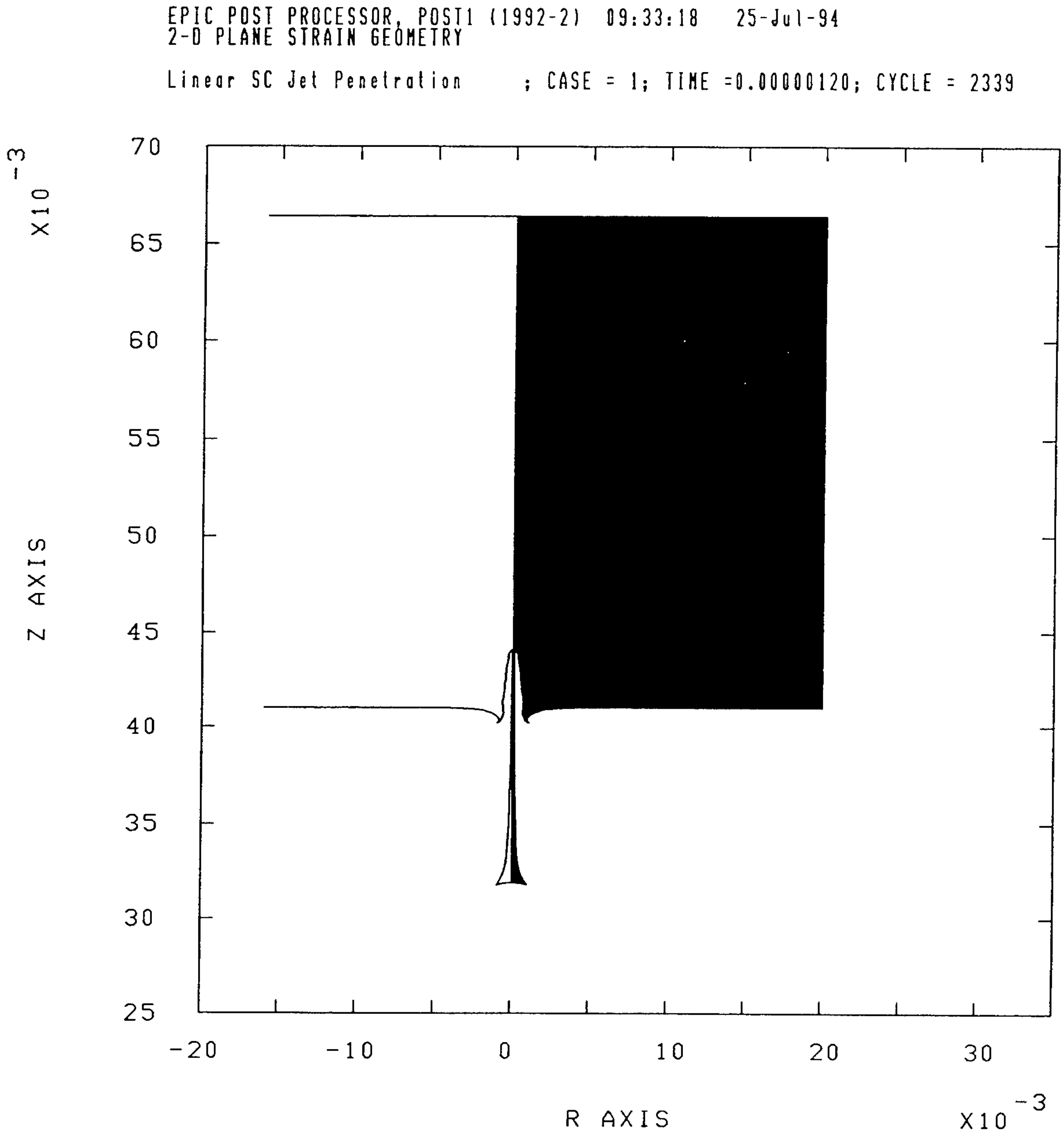
EPIC POST PROCESSOR, POST1 (1992-2) 09:33:18 25-Jul-94
2-D PLANE STRAIN GEOMETRY
Linear SC Jet Penetration ; CASE = 1; TIME =0.00000120; CYCLE = 2339
70
65
60
55
50
45
40
35
30
25
Z AXIS
X10 -3
-20
-10
0
10
20
30
R AXIS
X10 -3

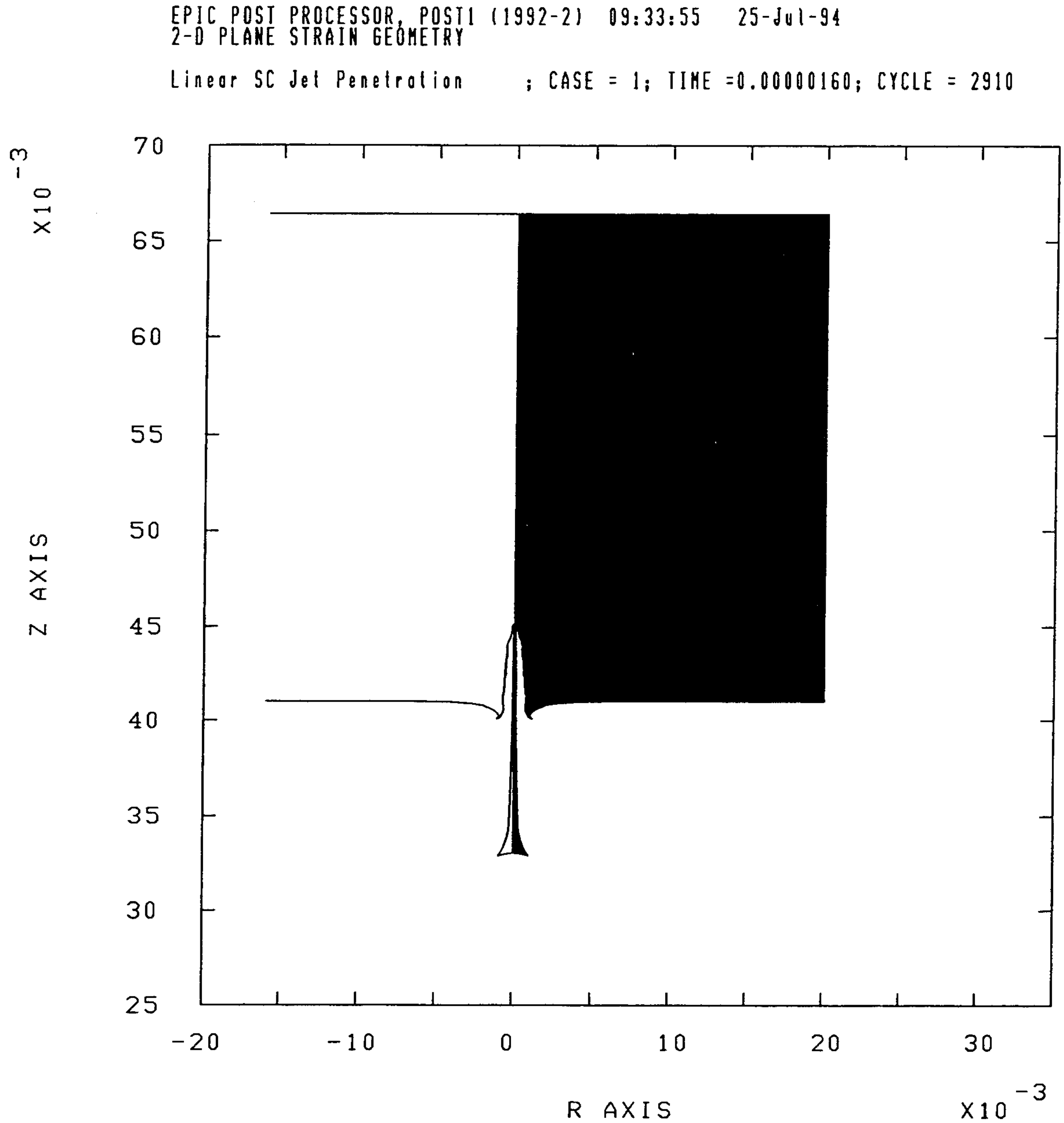
EPIC POST PROCESSOR, POST1 (1992-2) 09:33:55 25-Jul-94
2-D PLANE STRAIN GEOMETRY
Linear SC Jet Penetration ; CASE = 1; TIME =0.00000160; CYCLE = 2910
Z AXIS
X10 -3
70
65
60
55
50
45
40
35
30
25
-20
-10
0
10
20
30
R AXIS
X10 -3

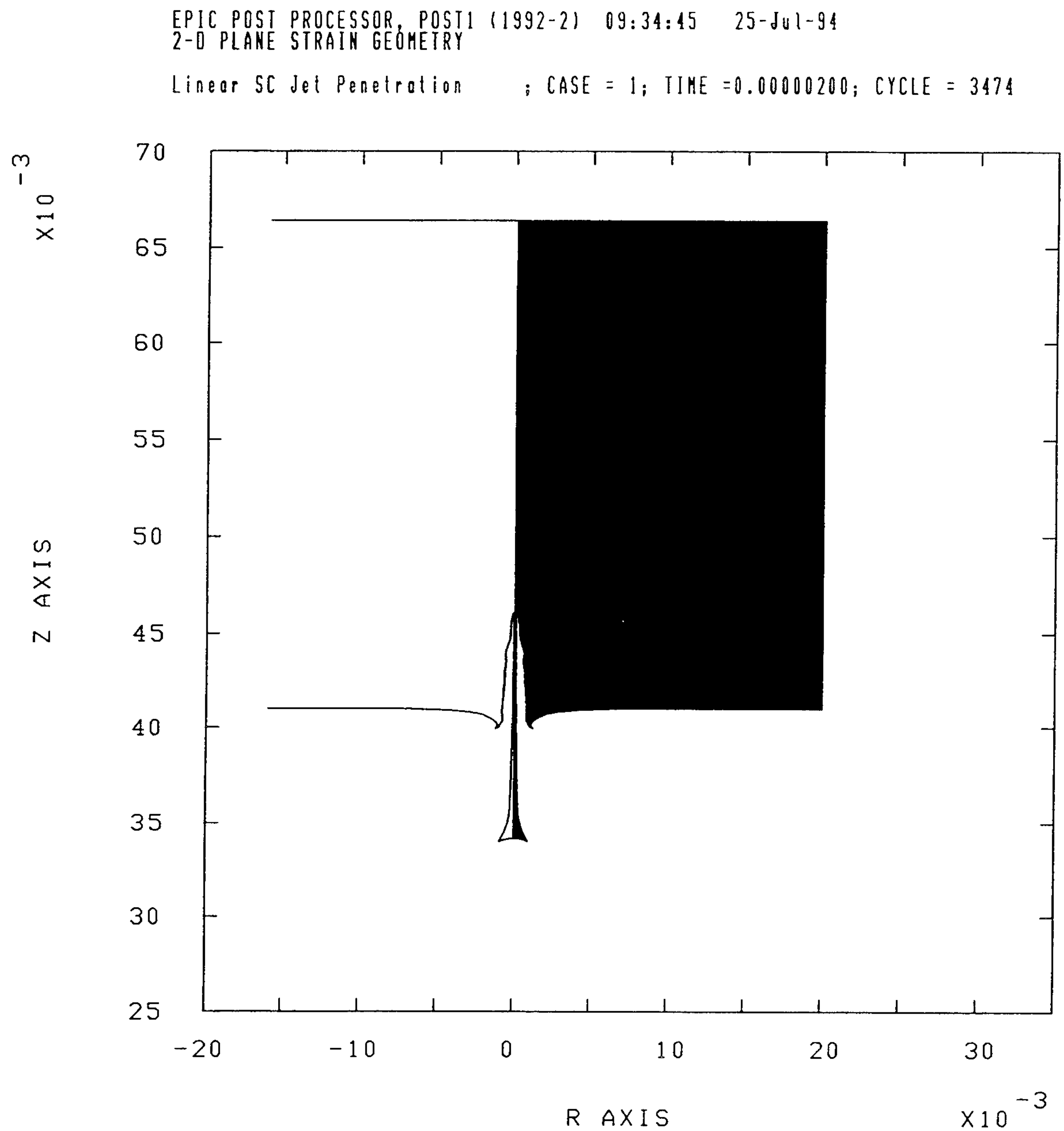
EPIC POST PROCESSOR, POST1 (1992-2) 09:34:45 25-Jul-94
2-D PLANE STRAIN GEOMETRY
Linear SC Jet Penetration ; CASE = 1; TIME =0.00000200; CYCLE = 3474
Z AXIS
X10 -3
70
65
60
55
50
45
40
35
30
25
-20
-10
0
10
20
30
R AXIS
X10 -3

EPIC POST PROCESSOR, POST1 (1992-2) 09:35:29 25-Jul-94
2-D PLANE STRAIN GEOMETRY

Linear SC Jet Penetration ; CASE = 1; TIME =0.00000400; CYCLE = 6111

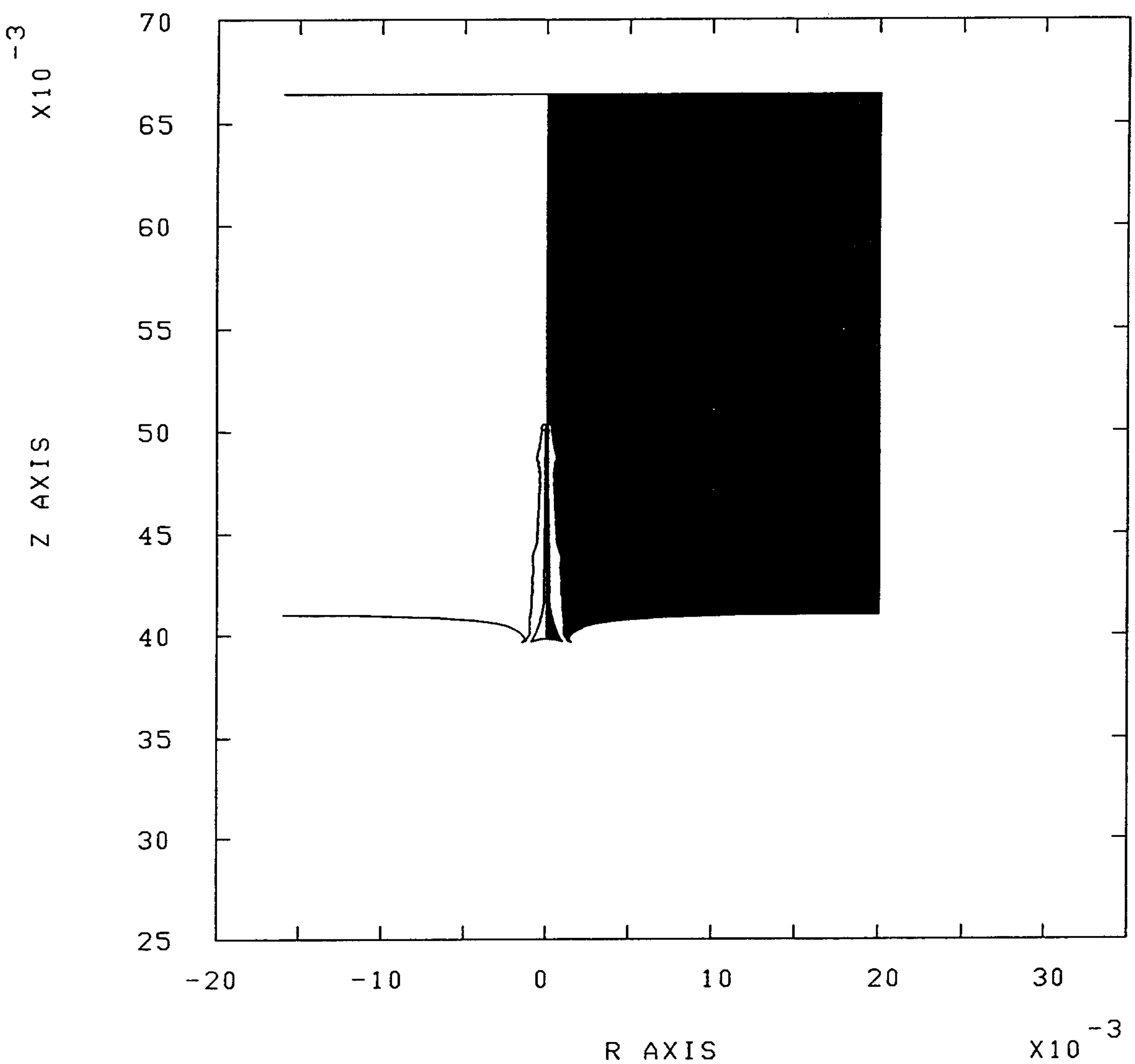

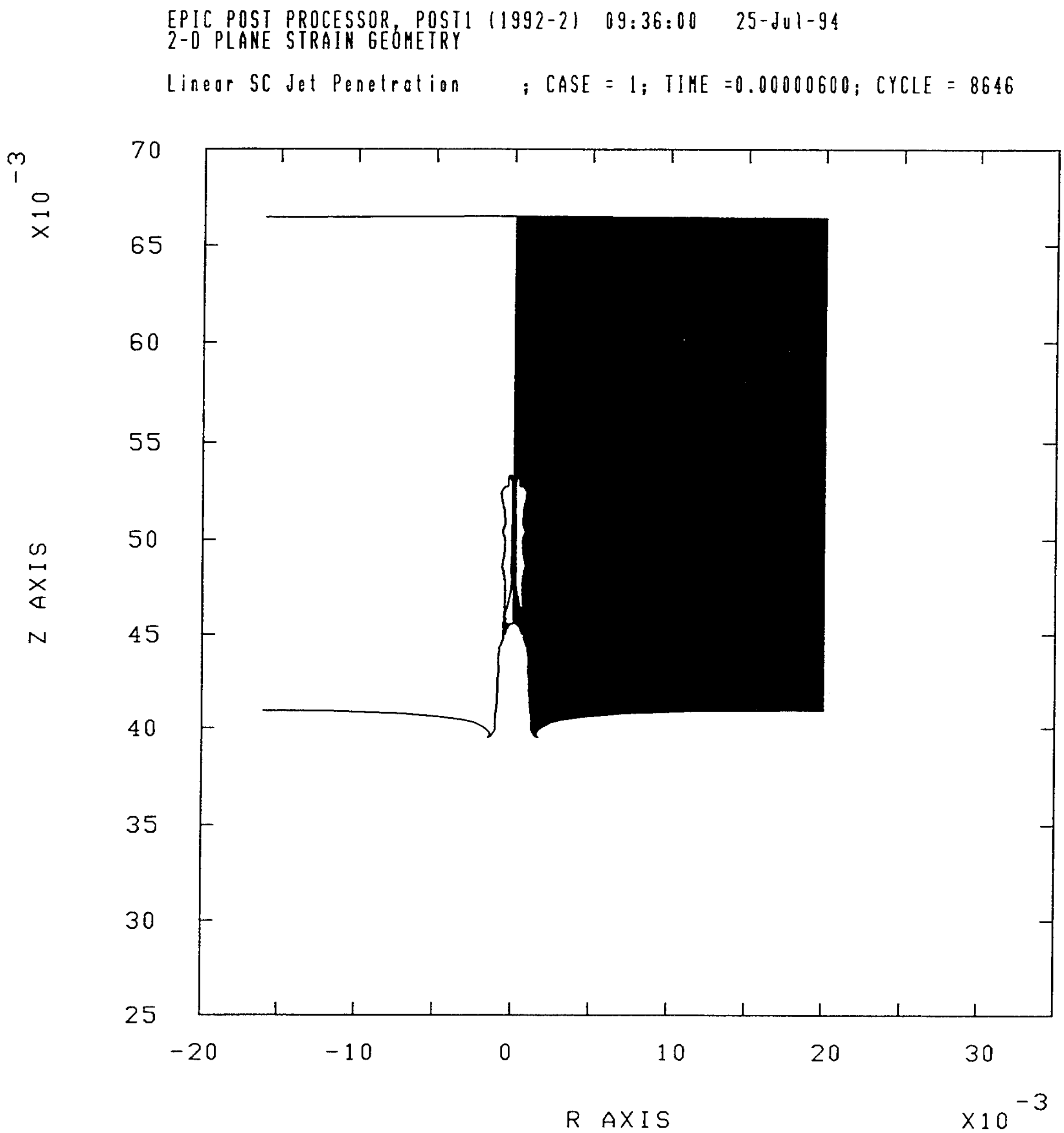
EPIC POST PROCESSOR, POST1 (1992-2) 09:36:00 25-Jul-94
2-D PLANE STRAIN GEOMETRY
Linear SC Jet Penetration ; CASE = 1; TIME =0.00000600; CYCLE = 8646
70
65
60
55
50
45
40
35
30
25
X10 -3
Z AXIS
-20
-10
0
10
20
30
R AXIS
X10 -3

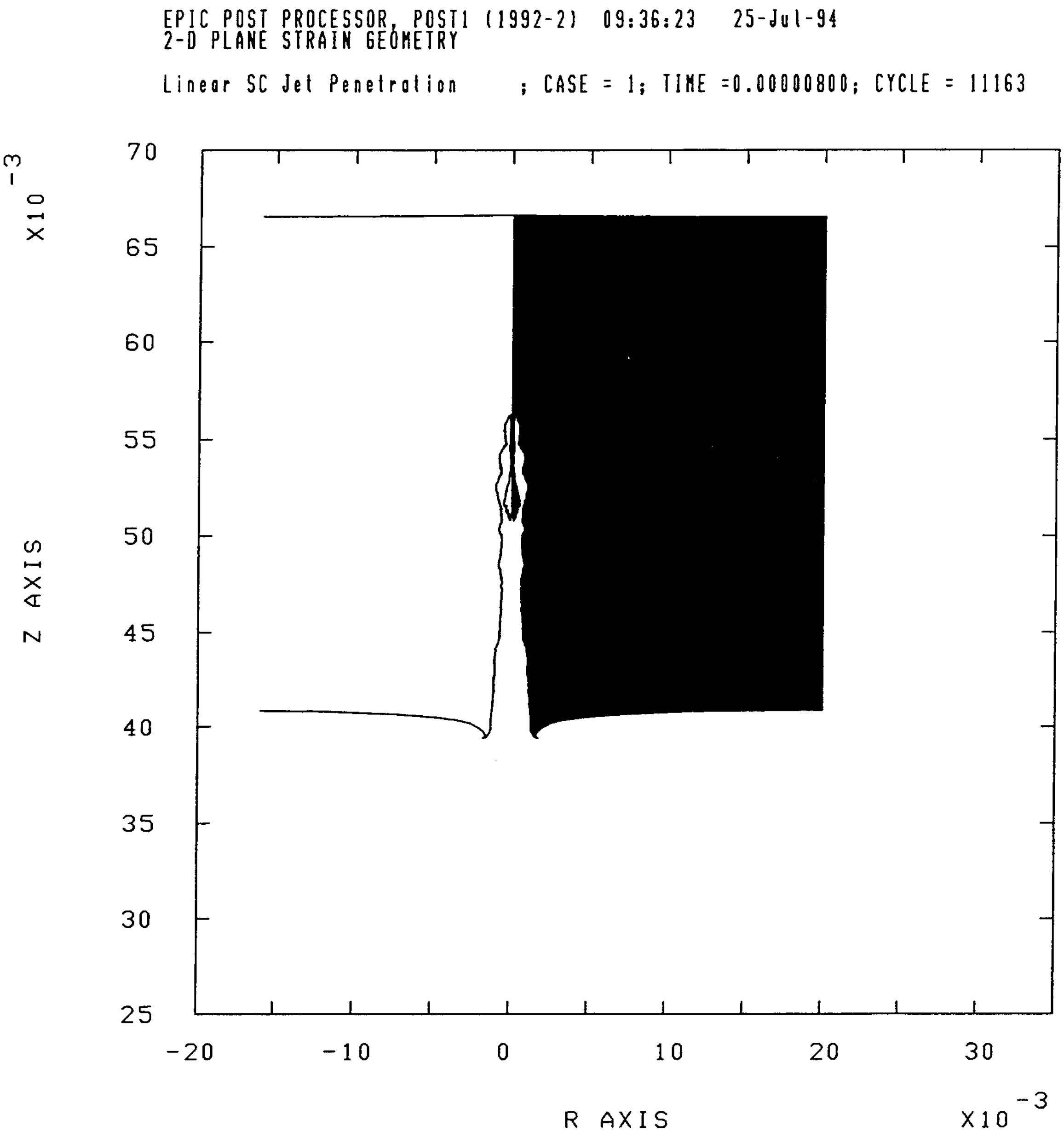
EPIC POST PROCESSOR, POST1 (1992-2) 09:36:23 25-Jul-94
2-D PLANE STRAIN GEOMETRY
Linear SC Jet Penetration ; CASE = 1; TIME =0.00000800; CYCLE = 11163
70
65
60
55
50
45
40
35
30
25
Z AXIS
X10 -3
-20
-10
0
10
20
30
R AXIS
X10 -3

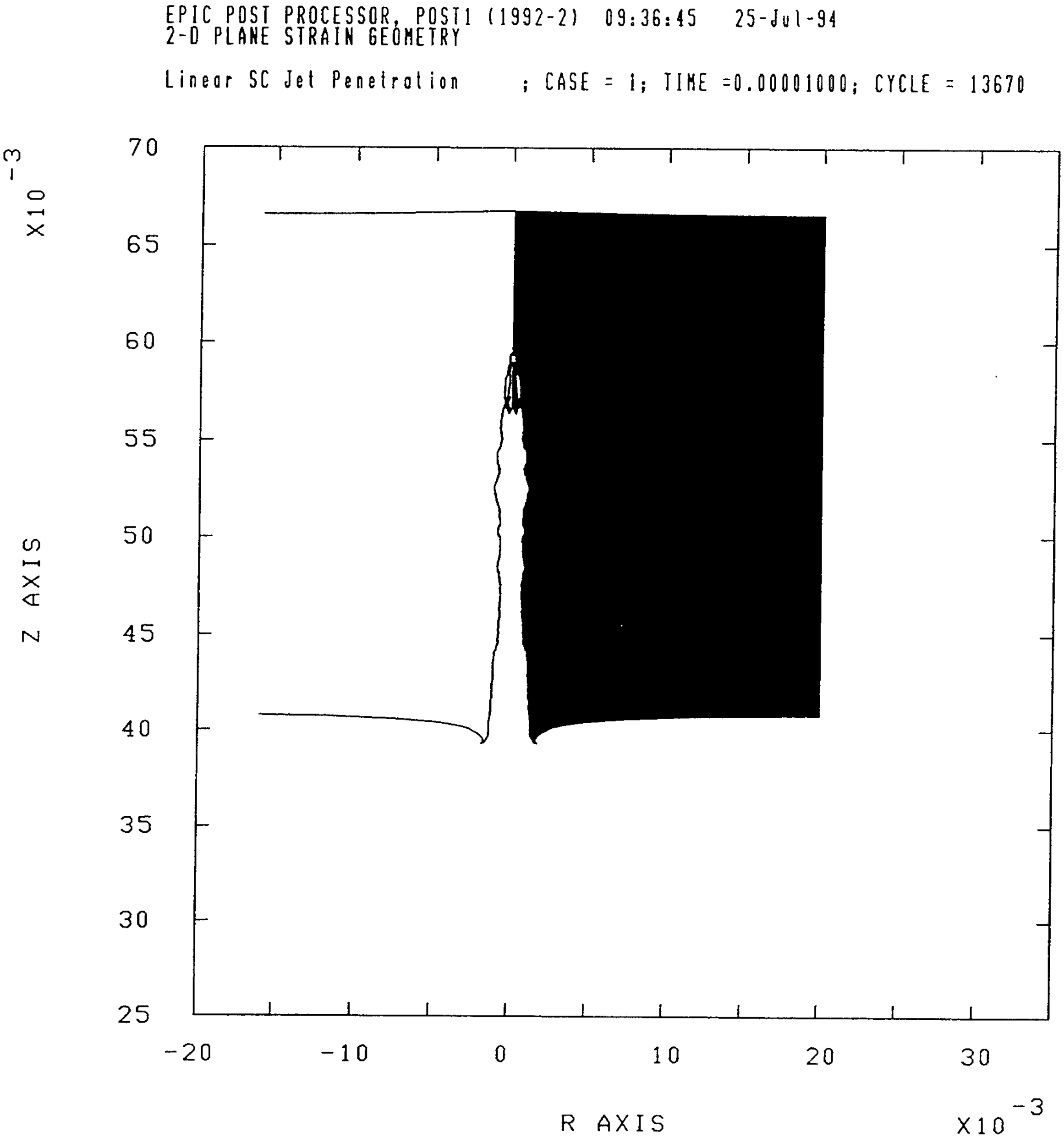
EPIC POST PROCESSOR, POST1 (1992-2) 09:36:45 25-Jul-94
2-D PLANE STRAIN GEOMETRY
Linear SC Jet Penetration ; CASE = 1; TIME =0.00001000; CYCLE = 13670
70
65
60
55
50
45
40
35
30
25
X10 -3
Z AXIS
-20
-10
0
10
20
30
R AXIS
X10 -3

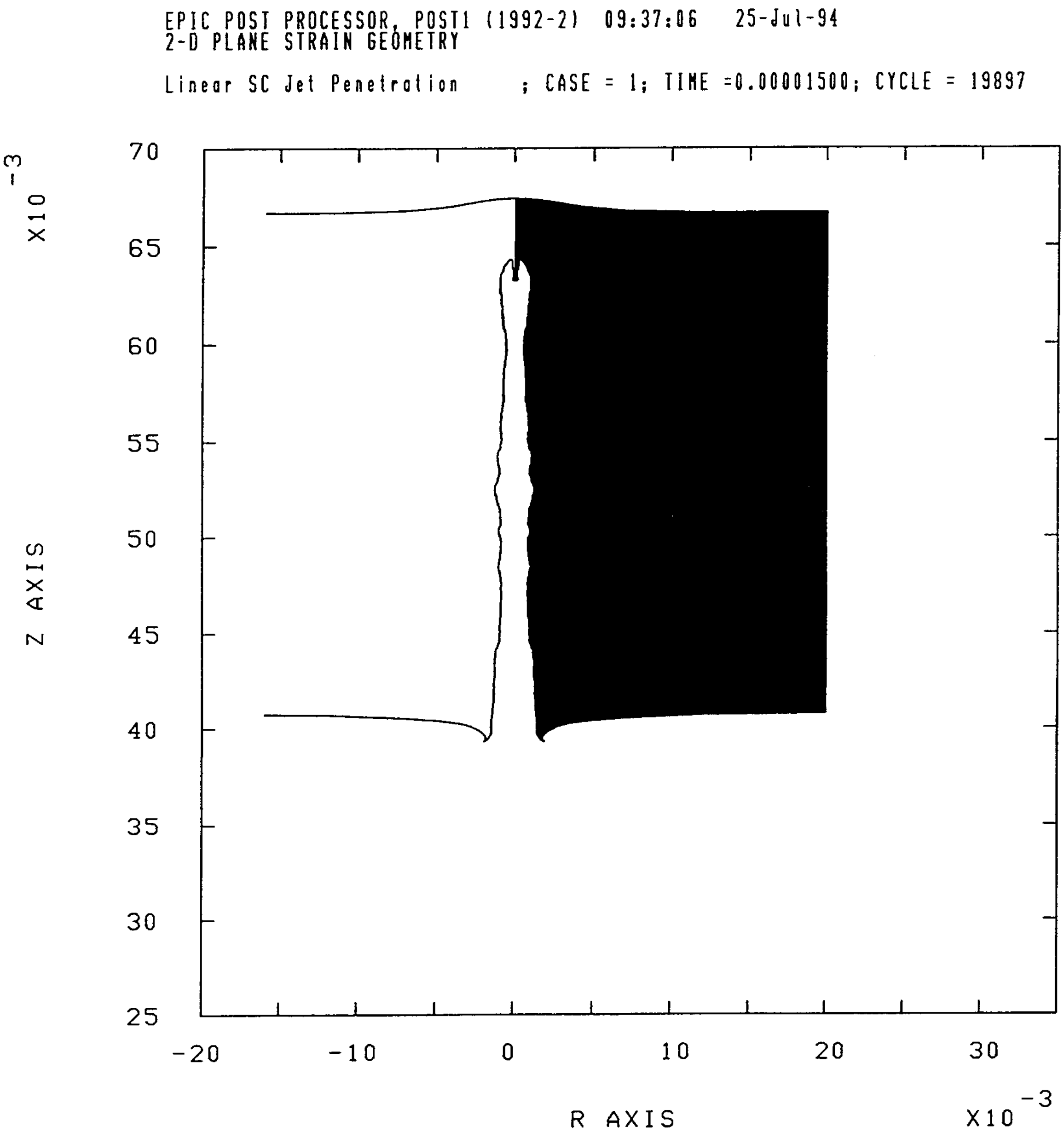

EPIC POST PROCESSOR, POST1 (1992-2) 09:37:06 25-Jul-94
2-D PLANE STRAIN GEOMETRY
Linear SC Jet Penetration ; CASE = 1; TIME =0.00001500; CYCLE = 19897
70
65
60
55
50
45
40
35
30
25
Z AXIS
X10 -3
-20
-10
0
10
20
30
R AXIS
X10 -3

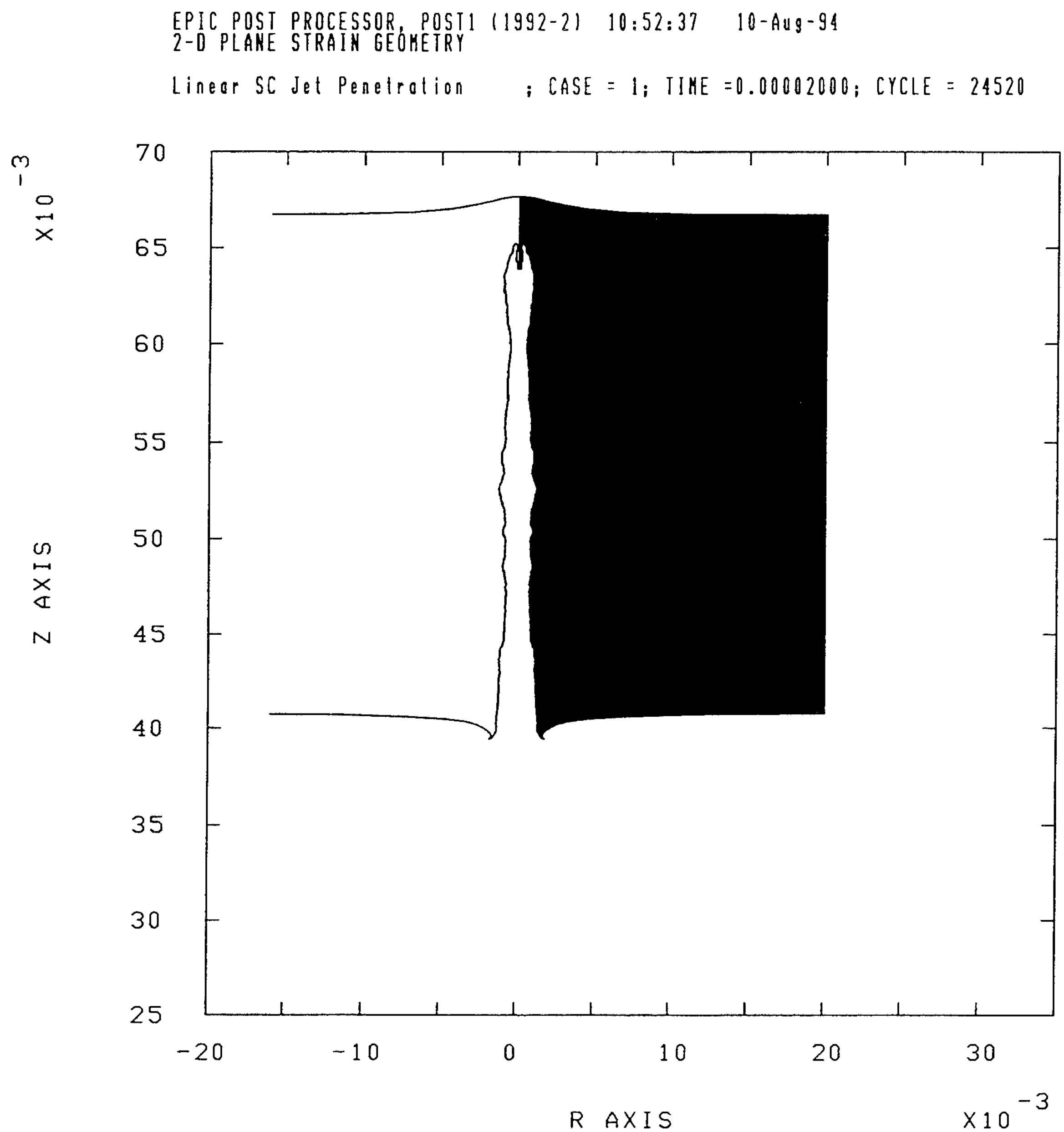
EPIC POST PROCESSOR, POST1 (1992-2) 10:52:37 10-Aug-94
2-D PLANE STRAIN GEOMETRY
Linear SC Jet Penetration ; CASE = 1; TIME =0.00002000; CYCLE = 24520
Z AXIS
X10 -3
70
65
60
55
50
45
40
35
30
25
-20
-10
0
10
20
30
R AXIS
X10 -3

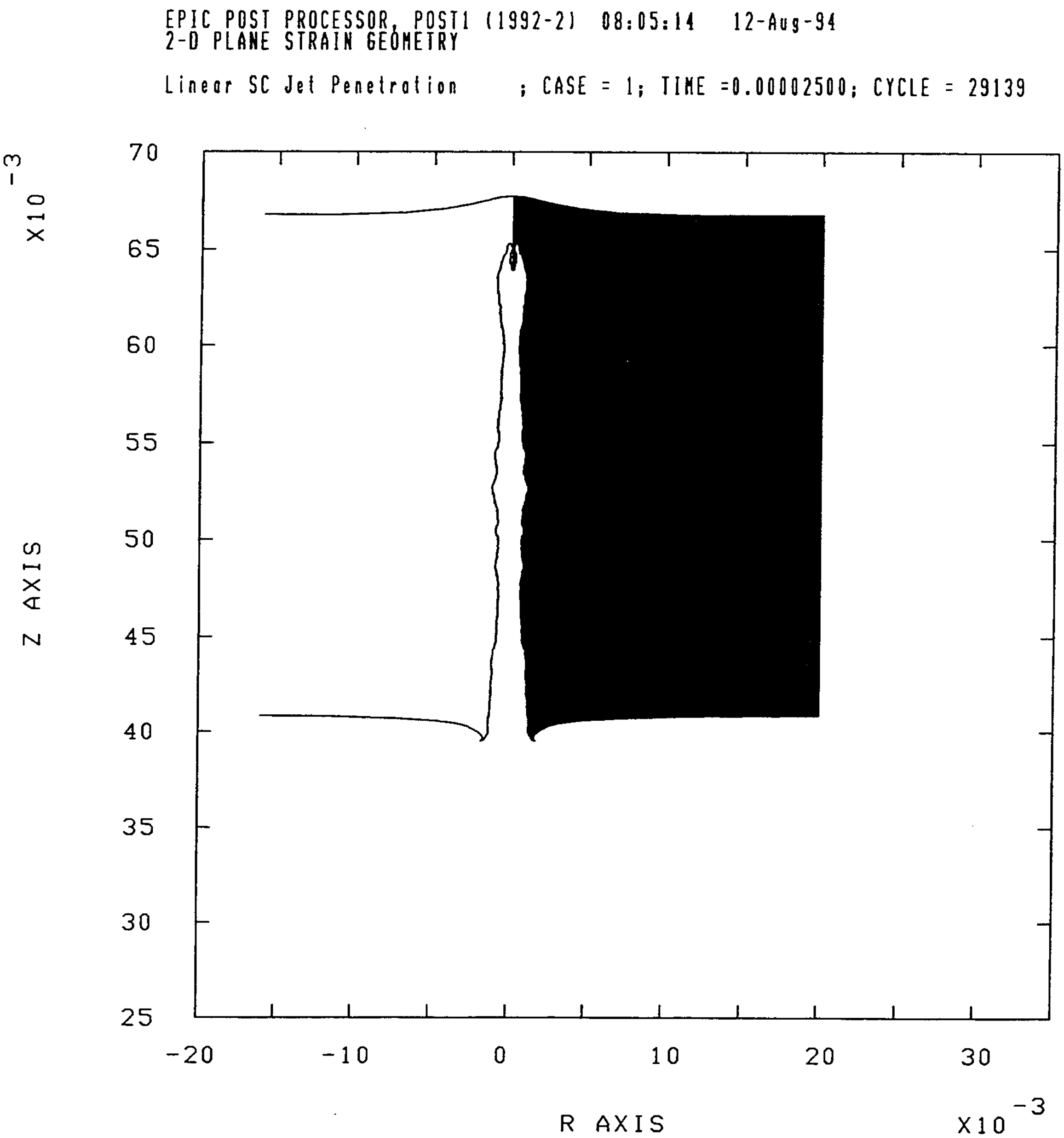
EPIC POST PROCESSOR, POST1 (1992-2) 08:05:14 12-Aug-94
2-D PLANE STRAIN GEOMETRY
Linear SC Jet Penetration ; CASE = 1; TIME =0.00002500; CYCLE = 29139
Z AXIS
X10 -3
70
65
60
55
50
45
40
35
30
25
-20
-10
0
10
20
30
R AXIS
X10 -3

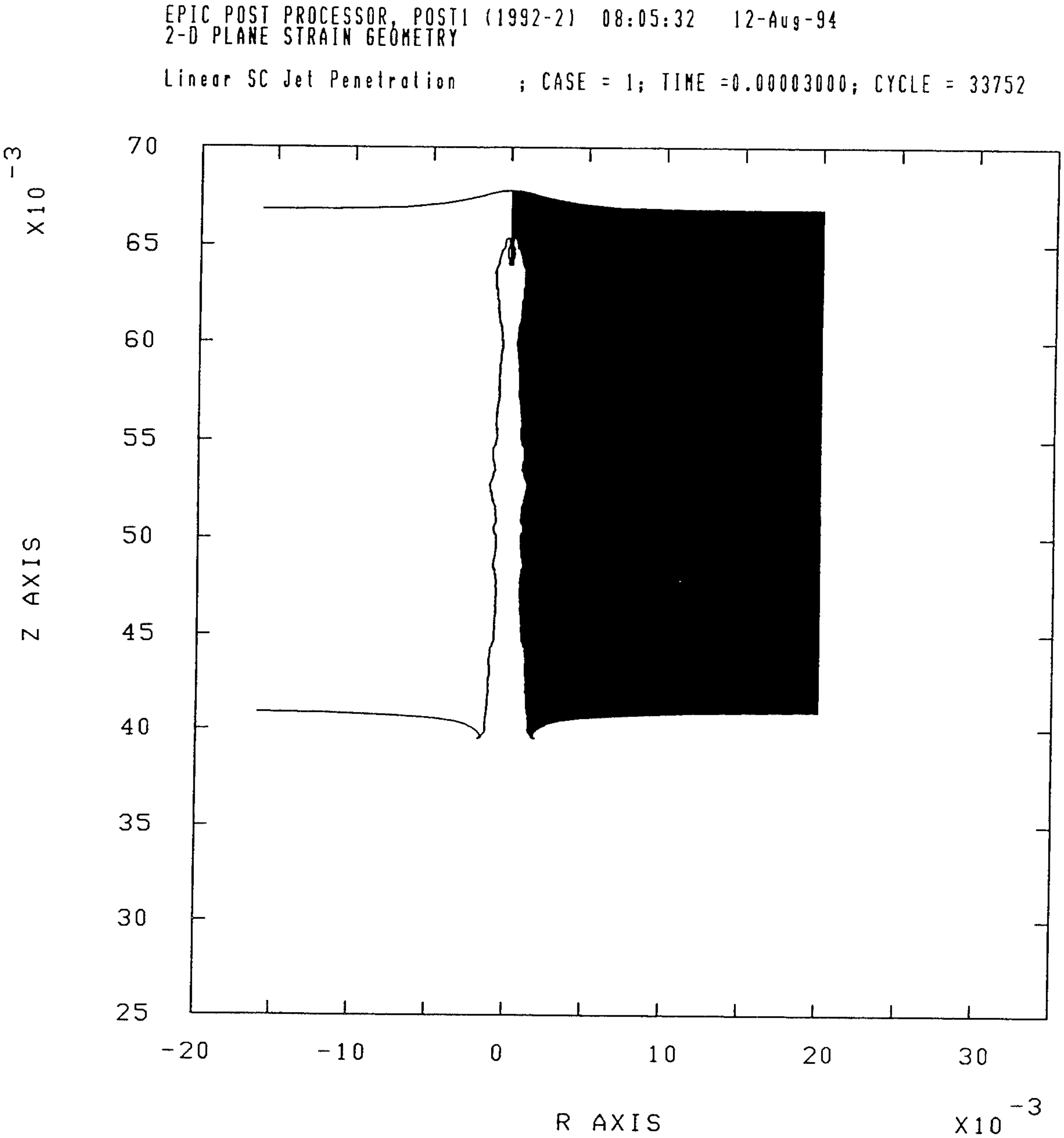
EPIC POST PROCESSOR, POST1 (1992-2) 08:05:32 12-Aug-94
2-D PLANE STRAIN GEOMETRY
Linear SC Jet Penetration ; CASE = 1; TIME =0.00003000; CYCLE = 33752
Z AXIS
X10 -3
70
65
60
55
50
45
40
35
30
25
-20
-10
0
10
20
30
R AXIS
X10 -3

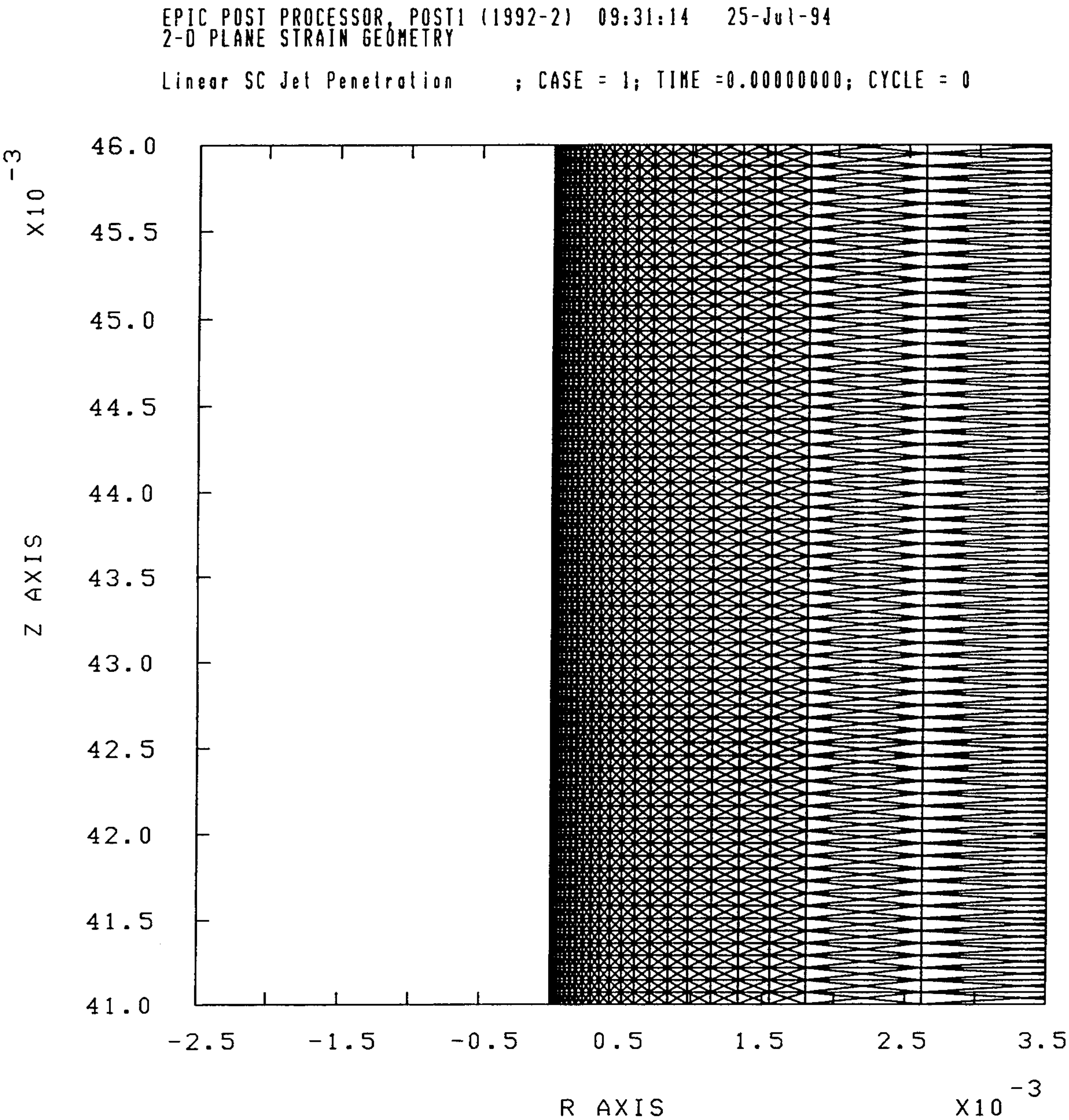
EPIC POST PROCESSOR, POST1 (1992-2) 09:31:14 25-Jul-94
2-D PLANE STRAIN GEOMETRY
Linear SC Jet Penetration ; CASE = 1; TIME =0.00000000; CYCLE = 0
46.0
45.5
45.0
44.5
44.0
43.5
43.0
42.5
42.0
41.5
41.0
Z AXIS
X10 -3
-2.5
-1.5
-0.5
0.5
1.5
2.5
3.5
R AXIS
X10 -3

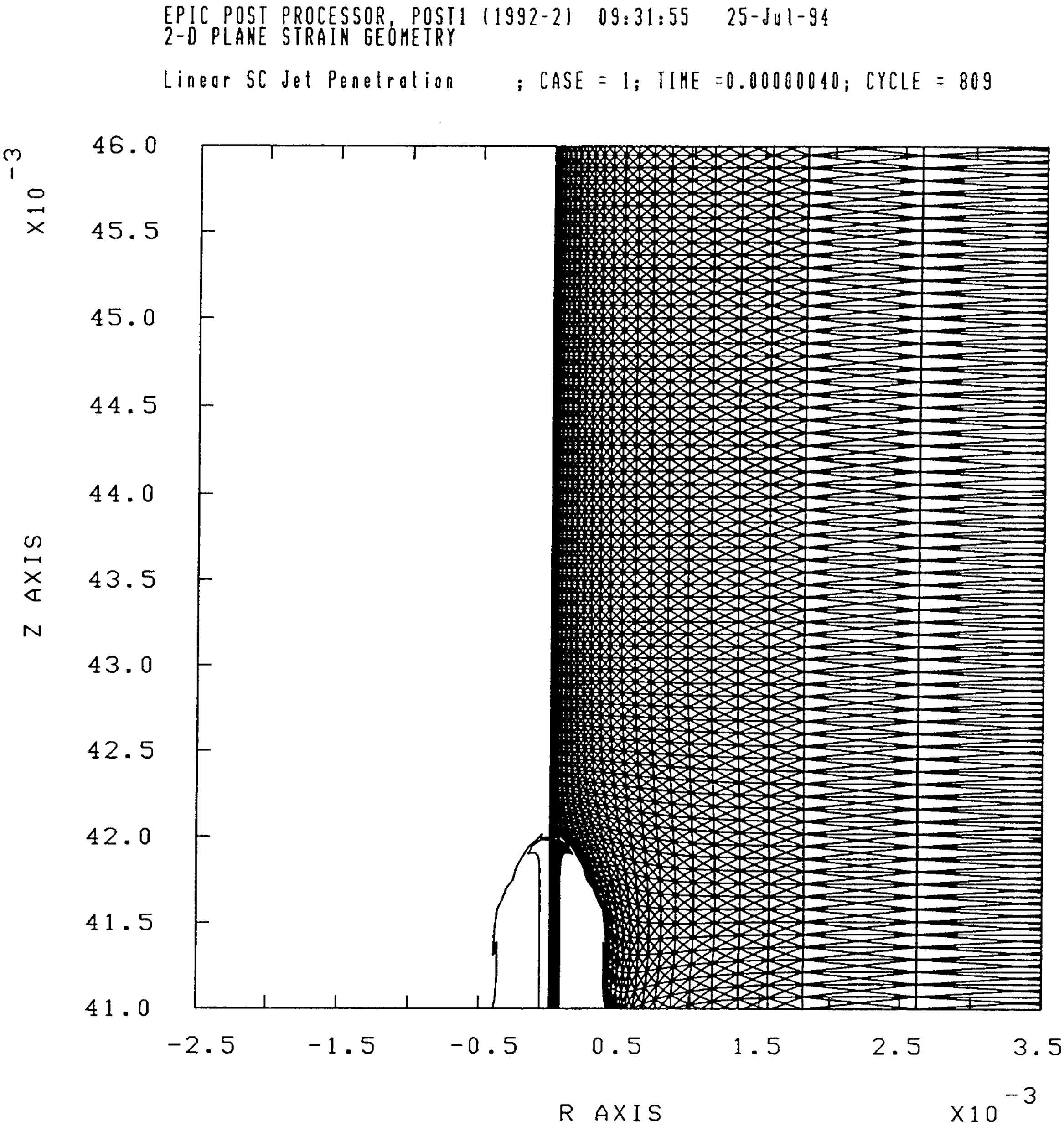
EPIC POST PROCESSOR, POST1 (1992-2) 09:31:55 25-Jul-94
2-D PLANE STRAIN GEOMETRY
Linear SC Jet Penetration ; CASE = 1; TIME =0.00000040; CYCLE = 809
46.0
45.5
45.0
44.5
44.0
43.5
43.0
42.5
42.0
41.5
41.0
X10 -3
Z AXIS
-2.5
-1.5
-0.5
0.5
1.5
2.5
3.5
R AXIS
X10 -3

EPIC POST PROCESSOR, POST1 (1992-2) 09:32:36 25-Jul-94
2-D PLANE STRAIN GEOMETRY

Linear SC Jet Penetration ; CASE = 1; TIME =0.00000080; CYCLE = 1601

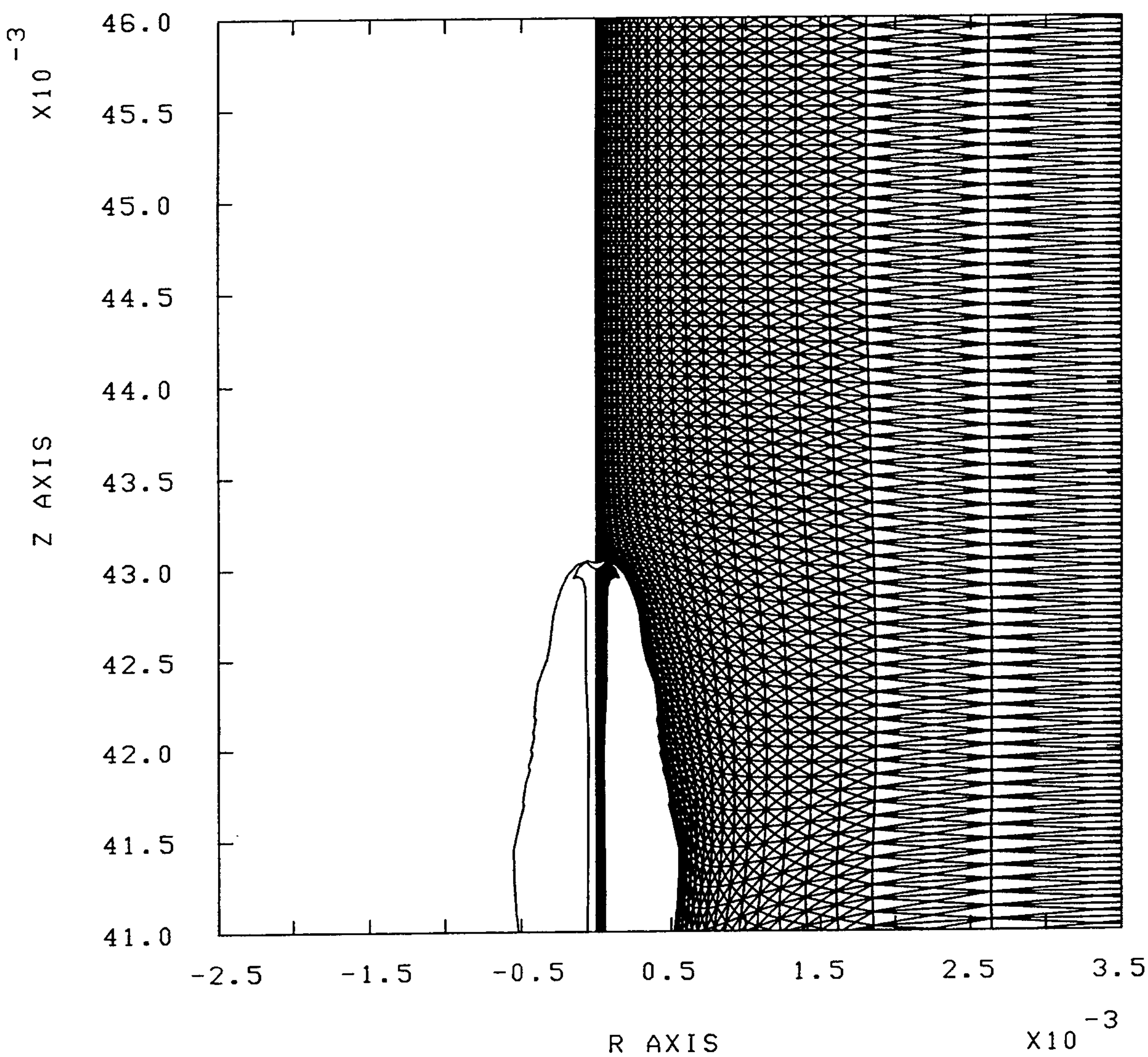

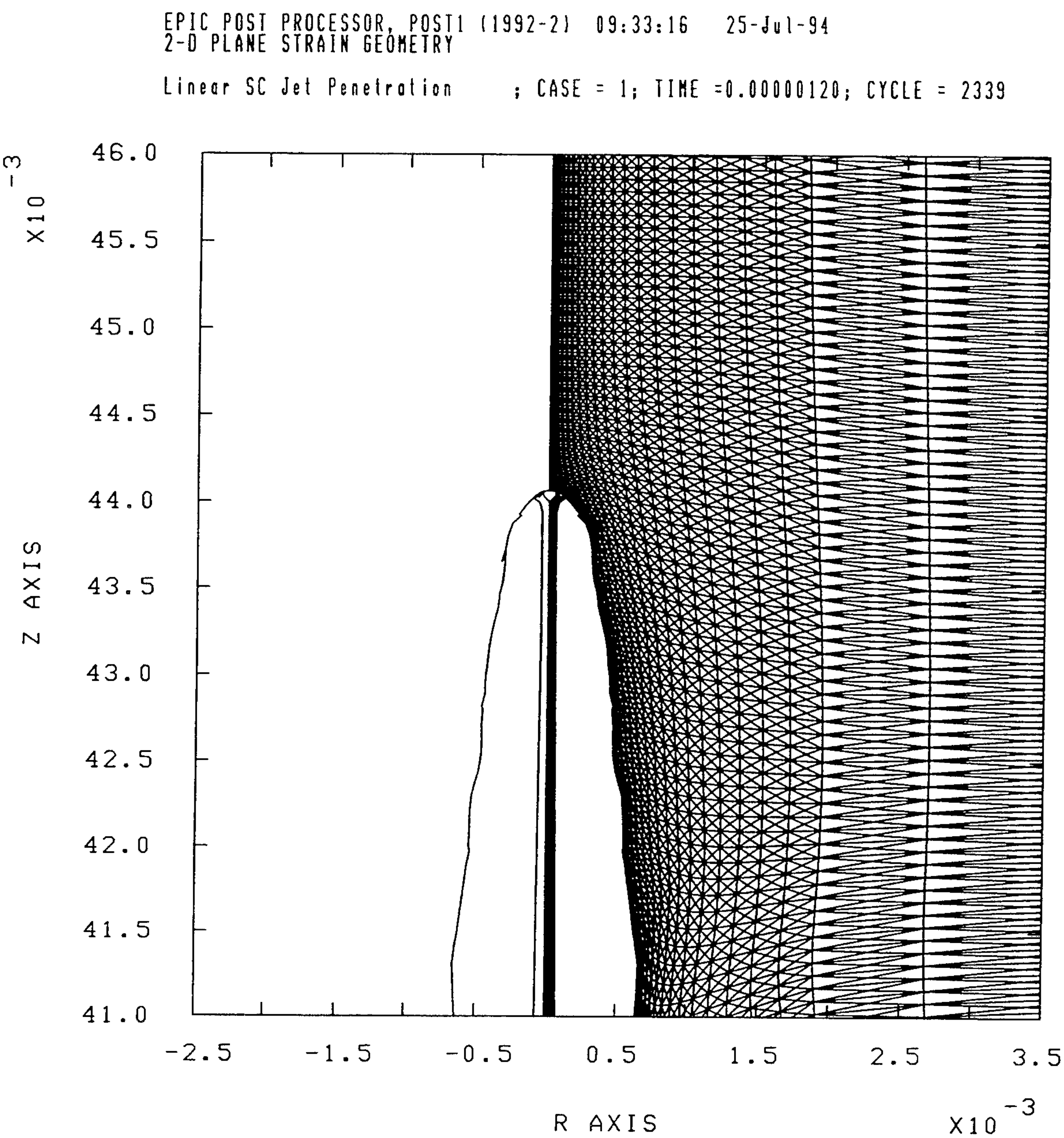
EPIC POST PROCESSOR, POST1 (1992-2) 09:33:16 25-Jul-94
2-D PLANE STRAIN GEOMETRY
Linear SC Jet Penetration ; CASE = 1; TIME =0.00000120; CYCLE = 2339
Z AXIS
X10 -3
46.0
45.5
45.0
44.5
44.0
43.5
43.0
42.5
42.0
41.5
41.0
-2.5
-1.5
-0.5
0.5
1.5
2.5
3.5
R AXIS
X10 -3

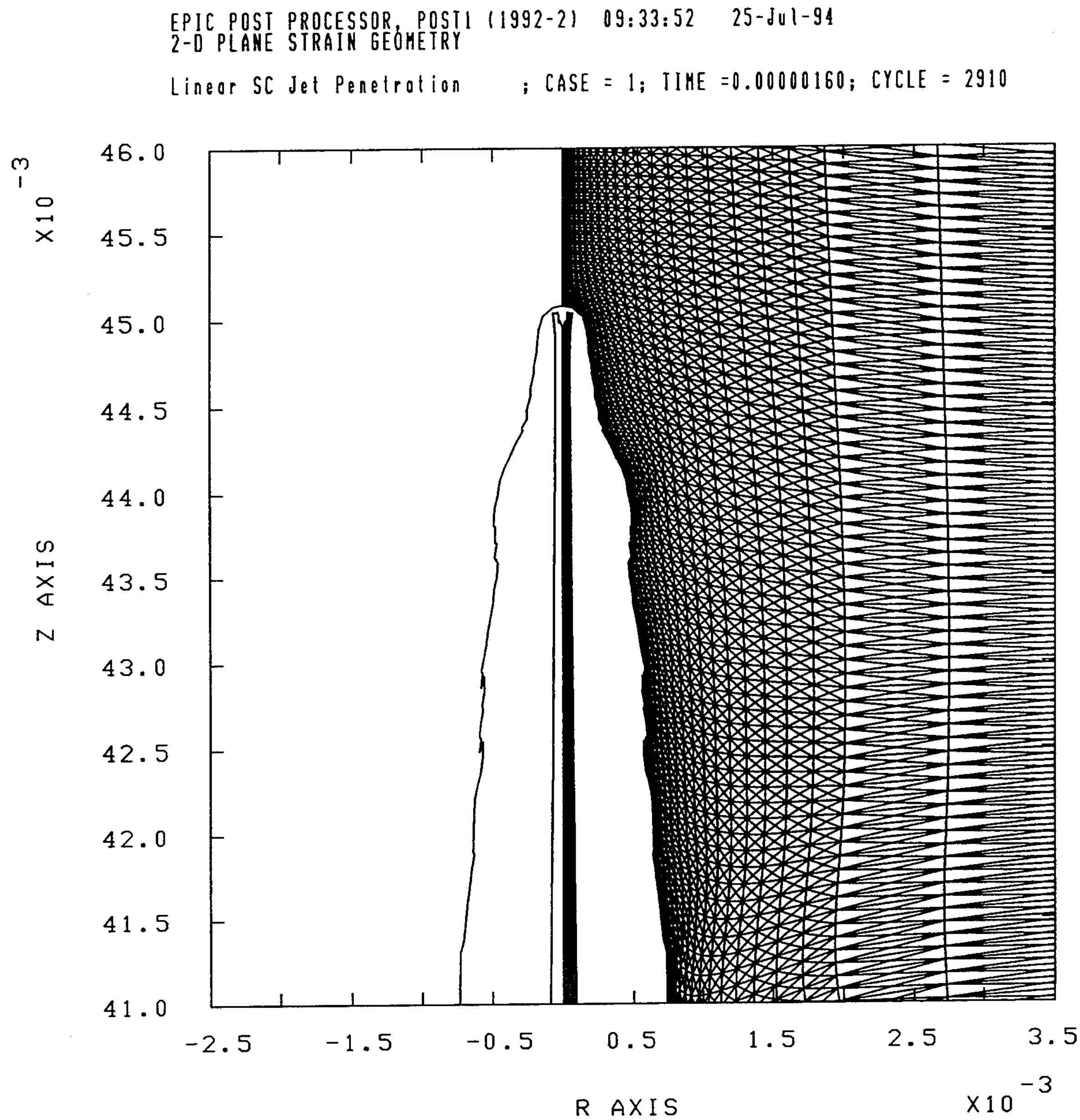
EPIC POST PROCESSOR, POSTI (1992-2) 09:33:52 25-Jul-94
2-D PLANE STRAIN GEOMETRY
Linear SC Jet Penetration ; CASE = 1; TIME =0.00000160; CYCLE = 2910
Z AXIS
X10 -3
46.0
45.5
45.0
44.5
44.0
43.5
43.0
42.5
42.0
41.5
41.0
-2.5
-1.5
-0.5
0.5
1.5
2.5
3.5
R AXIS
X10 -3

EPIC POST PROCESSOR, POST1 (1992-2) 09:34:40 25-Jul-94
2-D PLANE STRAIN GEOMETRY

Linear SC Jet Penetration ; CASE = 1; TIME =0.00000200; CYCLE = 3474

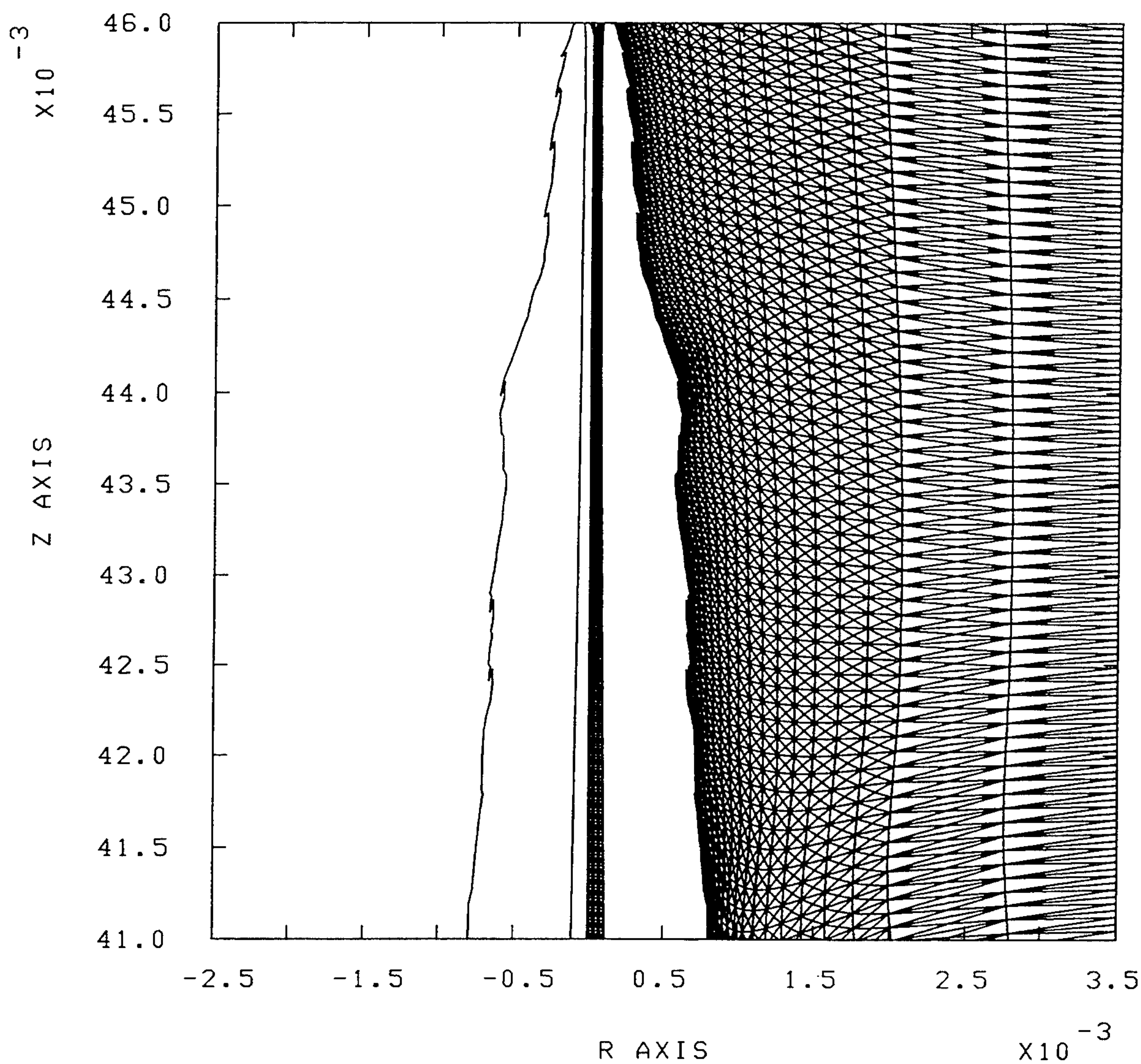

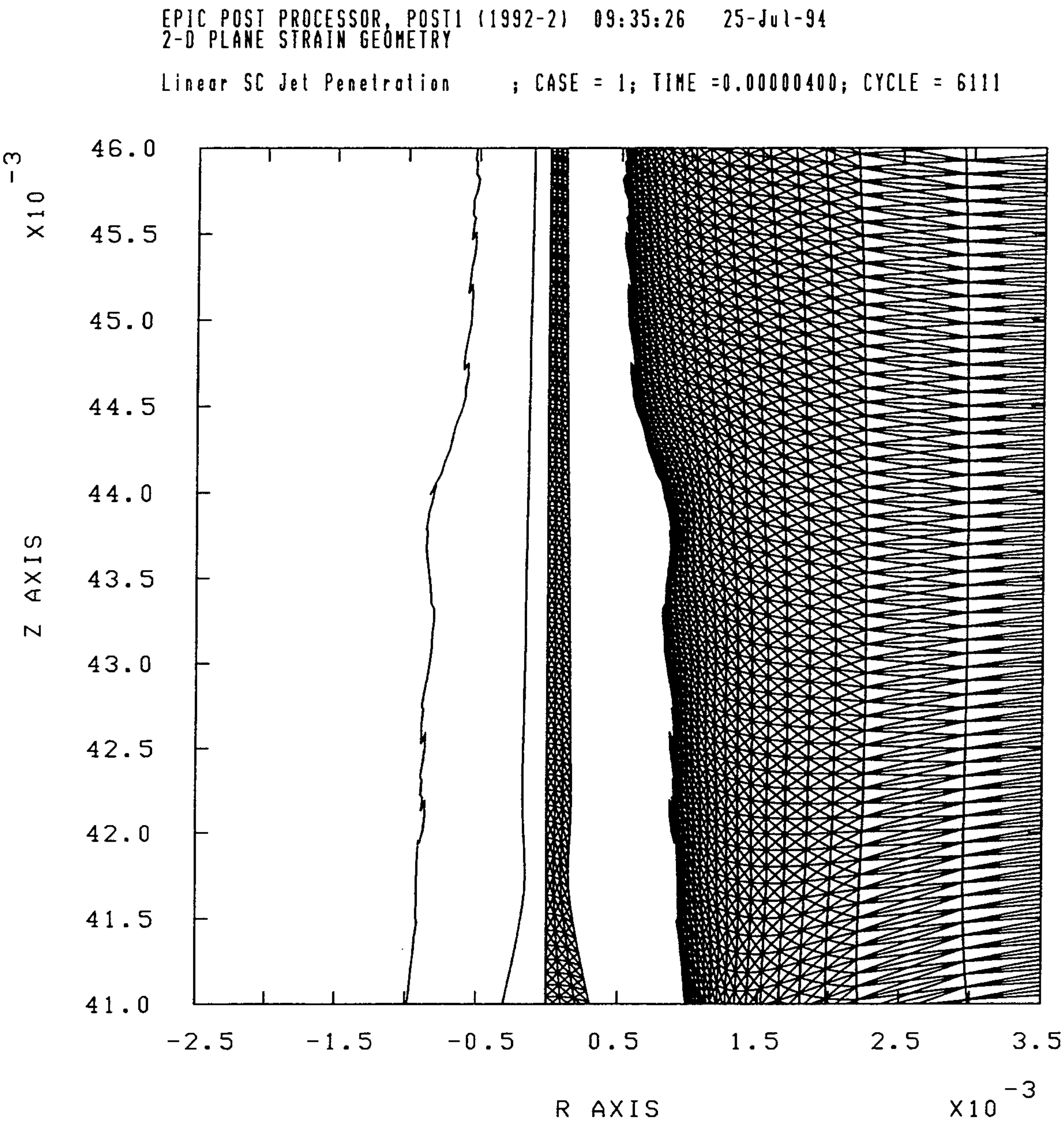
EPIC POST PROCESSOR, POST1 (1992-2) 09:35:26 25-Jul-94
2-D PLANE STRAIN GEOMETRY
Linear SC Jet Penetration ; CASE = 1; TIME =0.00000400; CYCLE = 6111
Z AXIS
X10 -3
46.0
45.5
45.0
44.5
44.0
43.5
43.0
42.5
42.0
41.5
41.0
-2.5
-1.5
-0.5
0.5
1.5
2.5
3.5
R AXIS
X10 -3

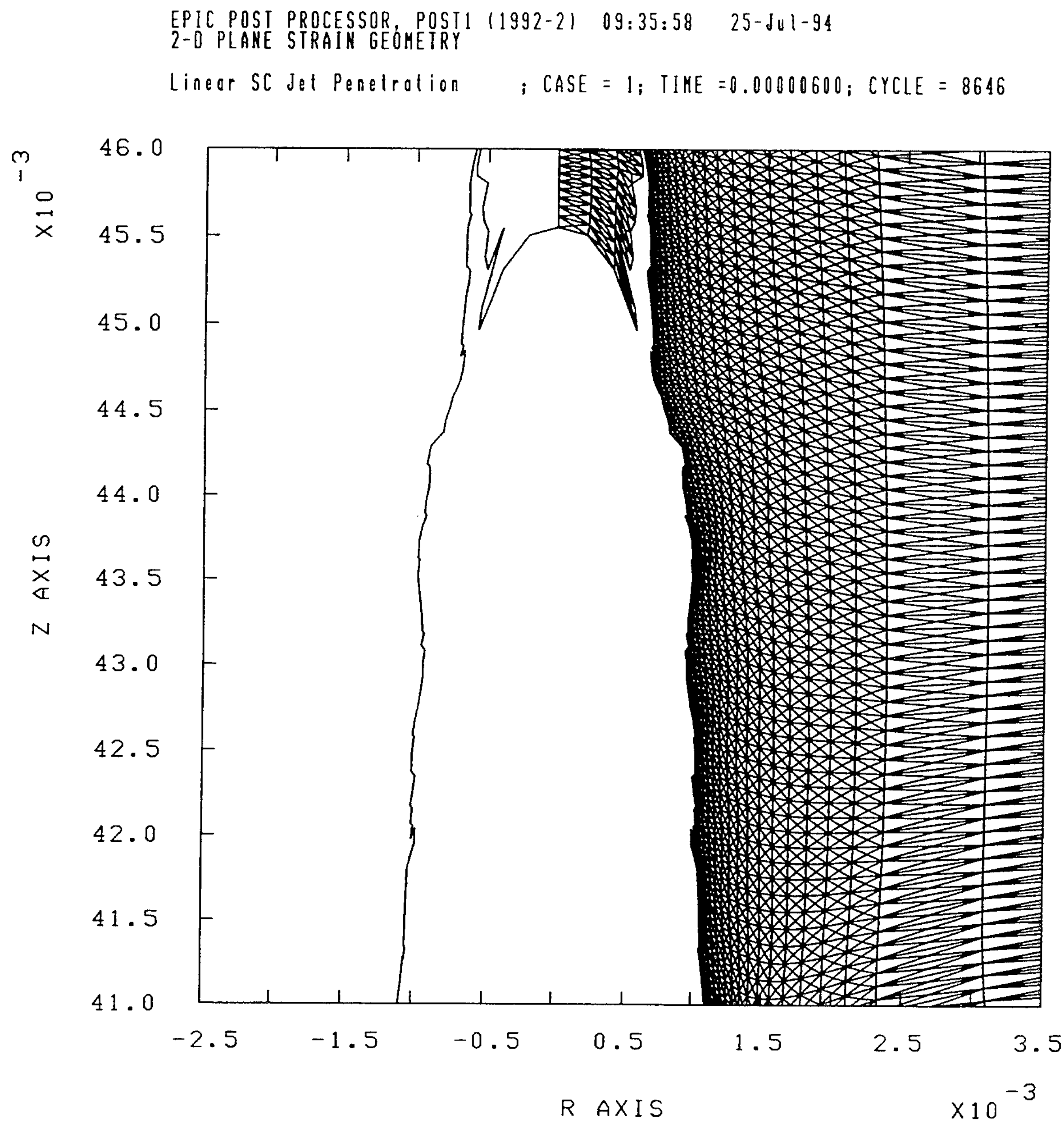

EPIC POST PROCESSOR, POST1 (1992-2) 09:35:58 25-Jul-94
2-D PLANE STRAIN GEOMETRY
Linear SC Jet Penetration ; CASE = 1; TIME =0.00000600; CYCLE = 8646
Z AXIS
X10 -3
46.0
45.5
45.0
44.5
44.0
43.5
43.0
42.5
42.0
41.5
41.0
-2.5
-1.5
-0.5
0.5
1.5
2.5
3.5
R AXIS
X10 -3

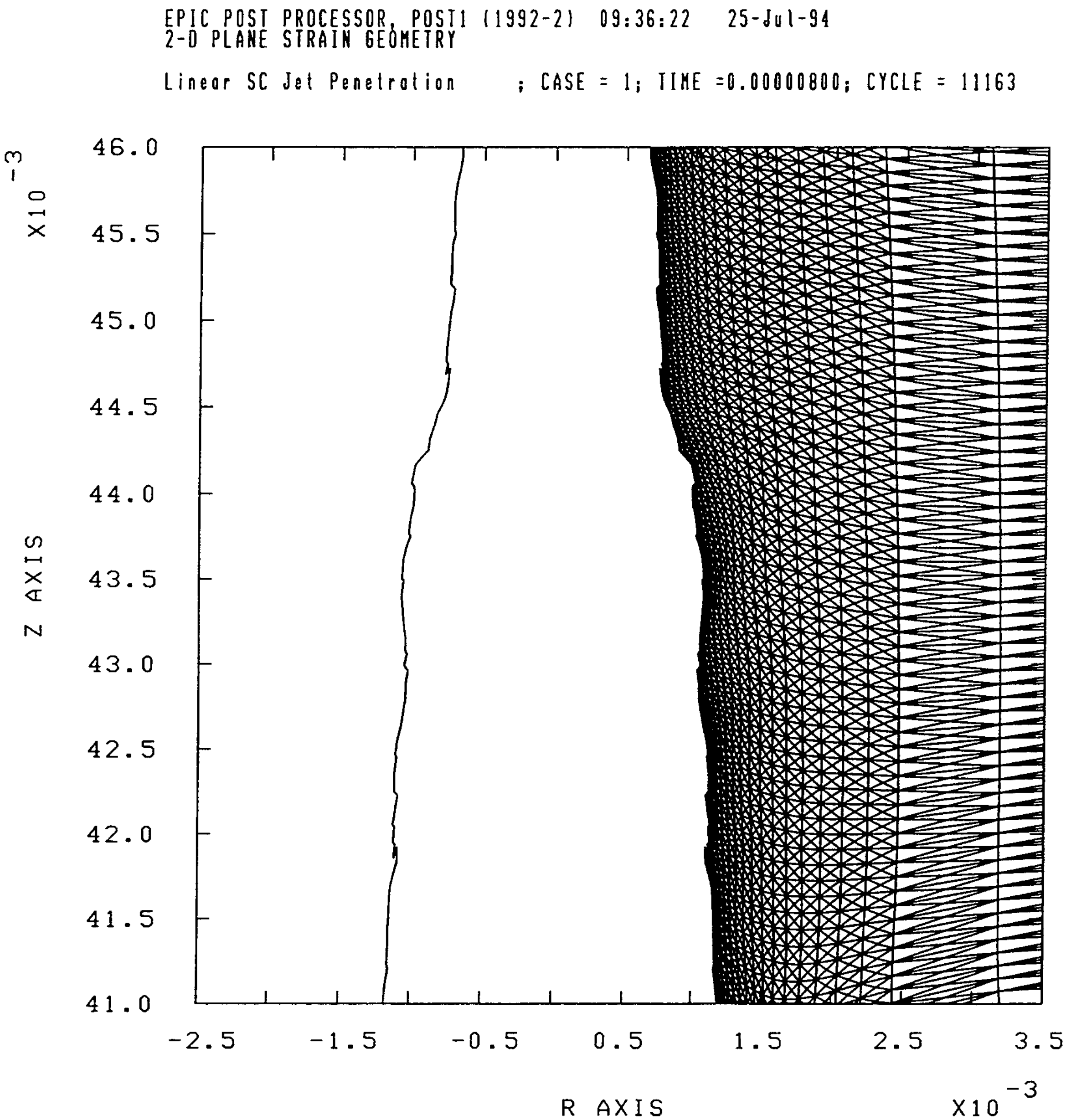
EPIC POST PROCESSOR, POST1 (1992-2) 09:36:22 25-Jul-94
2-D PLANE STRAIN GEOMETRY
Linear SC Jet Penetration ; CASE = 1; TIME =0.00000800; CYCLE = 11163
46.0
45.5
45.0
44.5
44.0
43.5
43.0
42.5
42.0
41.5
41.0
Z AXIS
X10 -3
-2.5
-1.5
-0.5
0.5
1.5
2.5
3.5
R AXIS
X10 -3

INTENTIONALLY LEFT BLANK.

NO. OF COPIES	ORGANIZATION
2	ADMINISTRATOR ATTN DTIC DDA DEFENSE TECHNICAL INFO CTR CAMERON STATION ALEXANDRIA VA 22304-6145
1	DIRECTOR ATTN AMSRL OP SD TA US ARMY RESEARCH LAB 2800 POWDER MILL RD ADELPHI MD 20783-1145
3	DIRECTOR ATTN AMSRL OP SD TL US ARMY RESEARCH LAB 2800 POWDER MILL RD ADELPHI MD 20783-1145
1	DIRECTOR ATTN AMSRL OP SD TP US ARMY RESEARCH LAB 2800 POWDER MILL RD ADELPHI MD 20783-1145
	<u>ABERDEEN PROVING GROUND</u>
5	DIR USARL ATTN AMSRL OP AP L (305)

NO. OF COPIES	ORGANIZATION
1	HEADQUARTERS ATTN SARD TT DR F MILTON PENTAGON WASHINGTON DC 20310-0103
1	HEADQUARTERS ATTN SARD TT MR J APPEL PENTAGON WASHINGTON DC 20310-0103
1	HEADQUARTERS ATTN SARD TT MS C NASH PENTAGON WASHINGTON DC 20310-0103
1	HEADQUARTERS ATTN SARD TR DR R CHAIT PENTAGON WASHINGTON DC 20310-0103
1	HEADQUARTERS ATTN SARD TR MS K KOMINOS PENTAGON WASHINGTON DC 20310-0103
1	DIRECTOR ATTN AMSRL CP CA D SNIDER US ARMY RESEARCH LAB 2800 POWDER MILL ROAD ADELPHI MD 20783-1145
8	DIRECTOR ATTN AMSRL MA P L JOHNSON B HALPIN T CHOU C WHITE J MCLAUGHLIN AMSRL MA PA D GRANVILLE W HASKELL AMSRL MA MA G HAGNAUER US ARMY RESEARCH LAB WATERTOWN MA 02172-0001

NO. OF COPIES	ORGANIZATION
4	COMMANDER ATTN SMCAR FSE T GORA E ANDRICOPOULOS B KNUTELSKY A GRAF US ARMY ARDEC PCTNY ARSNL NJ 07806-5000
3	COMMANDER ATTN SMCAR TD R PRICE V LINDER T DAVIDSON US ARMY ARDEC PCTNY ARSNL NJ 07806-5000
1	COMMANDER ATTN F MCLAUGHLIN US ARMY ARDEC PCTNY ARSNL NJ 07806-5000
5	COMMANDER ATTN SMCAR CCH T S MUSALLI P CHRISTIAN K FEHSAL N KRASNOW R CARR US ARMY ARDEC PCTNY ARSNL NJ 07806-5000
1	COMMANDER ATTN SMCAR CCH V E FENNELL US ARMY ARDEC PCTNY ARSNL NJ 07806-5000
1	COMMANDER ATTN SMCAR CCH J DELORENZO US ARMY ARDEC PCTNY ARSNL NJ 07806-5000
2	COMMANDER ATTN SMCAR CC J HEDDERICH COL SINCLAIR US ARMY ARDEC PCTNY ARSNL NJ 07806-5000

NO. OF COPIES	ORGANIZATION
1	COMMANDER ATTN SMCAR CCH P J LUTZ US ARMY ARDEC PCTNY ARSNL NJ 07806-5000
2	COMMANDER ATTN SMCAR FSA M D DEMELLA F DIORIO US ARMY ARDEC PCTNY ARSNL NJ 07806-5000
1	COMMANDER ATTN SMCAR FSA C SPINELLI US ARMY ARDEC PCTNY ARSNL NJ 07806-5000
11	DIRECTOR ATTN SMCAR CCB C KITCHENS J KEANE J SANTINI J VASILAKIS G FRIAR R FISCELLA V MONTVORI J WRZOCHALSKI J BATTAGLIA R HASENBEIN SMCAR CCB R S SOPOK BENET LABORATORIES WATERVLIET NY 12189-4050
1	COMMANDER ATTN SMCWV QAE Q C HOWD BLDG 44 WATERVLIET ARSENAL WATERVLIET NY 12189-4050
1	COMMANDER ATTN SMCWV SPM T MCCLOSKEY BLDG 25 3 WATERVLIET ARSENAL WATERVLIET NY 12189-4050
1	COMMANDER ATTN SMCWV QA QS K INSCO WATERVLIET ARSENAL WATERVLIET NY 12189-4050

NO. OF COPIES	ORGANIZATION
1	COMMANDER ATTN AMSMC PBM K US ARMY ARDEC PCTNY ARSNL NJ 07806-5000
1	DIRECTOR ATTN P DUTTA US ARMY CRREL 72 LYME ROAD HANOVER NH 03755
1	DIRECTOR ATTN AMSRL WT L D WOODBURY US ARMY RESEARCH LABORATORY 2800 POWDER MILL ROAD ADELPHI MD 20783-1145
4	COMMANDER ATTN AMSMI RD W MCCORKLE AMSMI RD ST P DOYLE AMSMI RD ST CN T VANDIVER AMSMI RD ST WF M COLE US ARMY MISSILE COMMAND REDSTONE ARSNL AL 35898-5247
2	DIRECTOR ATTN A CROWSON J CHANDRA US ARMY RESEARCH OFFICE MATH & COMPUTER SCIENCES DIV PO BOX 12211 RSRCH TRI PK NC 27709-2211
2	DIRECTOR ATTN G ANDERSON R SINGLETON US ARMY RESEARCH OFFICE ENGINEERING SCIENCES DIVISION PO BOX 12211 RSRCH TRI PK NC 27709-2211
2	PROJECT MANAGER SADARM PCTNY ARSNL NJ 07806-5000
2	PM TMAS ATTN SFAE AR TMA COL BREGARD C KIMKER PCTNY ARSNL NJ 07806-5000

NO. OF COPIES	ORGANIZATION
3	PM TMAS ATTN SFAE AR TMA MD H YUEN J MCGREEN R KOWALSKI PCTNY ARSNL NJ 07806-5000
2	PM TMAS ATTN SFAE AR TMA MS R JOINSON D GUZIEWICZ PCTNY ARSNL NJ 07806-5000
1	PM TMAS ATTN SFAE AR TMA MP W LANG PCTNY ARSNL NJ 07806-5000
2	PEO ARMAMENTS ATTN SFAE AR PM D ADAMS T MCWILLIAMS PCTNY ARSNL NJ 07806-5000
1	PEO FIELD ARTILLERY SYSTEMS ATTN SFAE FAS PM H GOLDMAN PCTNY ARSNL NJ 07806-5000
4	PM AFAS ATTN LTC D ELLIS G DELCOCO J SHIELDS B MACHAK PCTNY ARSNL NJ 07806 5000
2	COMMANDER ATTN WL FIV A MAYER WL MLBM S DONALDSON WRIGHT PATTERSON AFB DAYTON OH 45433
2	NASA LANGLEY RSRCH CTR ATTN AMSRL VS W ELBER AMSRL VS S F BARTLETT JR MAIL STOP 266 HAMPTON VA 23681-0001
2	NAVAL SURFACE WARFARE CTR CODE G33 DAHLGREN VA 22448

NO. OF COPIES	ORGANIZATION
1	OFFICE OF NAVAL RESEARCH ATTN YAPA RAJAPAKSE MECH DIV CODE 1132SM ARLINGTON VA 22217
1	NAVAL ORDNANCE STATION ATTN D HOLMES CODE 2011 ADVANCED SYSTEMS TECHNOLOGY BR LOUISVILLE KY 40214-5245
1	DAVID TAYLOR RESEARCH CTR SHIP STRUCTURES AND PROT DEPT ATTN J CORRADO CODE 1702 BETHESDA MD 20084
2	DAVID TAYLOR RESEARCH CTR ATTN R ROCKWELL W PHYILLAIER BETHESDA MD 20054-5000
5	DIRECTOR ATTN R CHRISTENSEN S DETERESA W FENG F MAGNESS M FINGER LAWRENCE LIVERMORE NATL LAB PO BOX 808 LIVERMORE CA 94550
1	DIRECTOR ATTN D RABERN MEE 13 MAIL STOP J 576 LOS ALAMOS NATL LAB PO BOX 1633 LOS ALAMOS NM 87545
2	NAVAL EOD TECH CTR ATTN CODE 6012A A PATEL R GOLD INDIAN HEAD MD 20640-5070
1	OAK RIDGE NATIONAL LAB ATTN R M DAVIS PO BOX 2008 OAK RIDGE TN 37831-6195

NO. OF COPIES	ORGANIZATION
2	BATTELLE PNL ATTN M SMITH M C C BAMPTON PO BOX 999 RICHLAND WA 99352
6	DIRECTOR ATTN C ROBINSON G BENEDETTI W KAWAHARA K PERANO D DAWSON P NIELAN SANDIA NATL LABS PO BOX 969 LIVERMORE CA 94550-0096
1	PENNSYLVANIA STATE UNIV ATTN RICHARD MCNITT 227 HAMMOND BLDG UNIVERSITY PARK PA 16802
1	SOUTHWEST RSRCH INSTITUTE ATTN C ANDERSON 6220 CULEBRA RD SAN ANTONIO TX 78284
1	UCLA MANE DEPT ENGRG IV ATTN H THOMAS HAHN LOS ANGELES CA 90024 1597
2	UNIV OF DAYTON RESEARCH INST ATTN RAN Y KIM AJIT K ROY 300 COLLEGE PARK AVENUE DAYTON OH 45469-0168
2	UNIV OF DELAWARE ATTN J GILLESPE M SANTARE CTR FOR COMPOSITE MATERIALS 201 SPENCER LABORATORY NEWARK DE 19716
1	UNIV OF TEXAS AT AUSTIN ATTN J PRICE CTR FOR ELECTROMECHANICS 10100 BURNET ROAD AUSTIN TX 78758-4497

NO. OF COPIES	ORGANIZATION
1	AAI CORPORATION ATTN TECH LIBRARY PO BOX 126 HUNT VALLEY MD 21030-0126
1	ARMTEC DEFENSE PRODUCTS ATTN STEVE DYER PO BOX 848 COACHELLA CA 92236
3	ALLIANT TECHSYSTEMS INC ATTN J BODE C CANDLAND K WARD 5901 LINCOLN DR MINNEAPOLIS MN 55346-1674
2	ALLIANT TECHSYSTEMS INC ATTN TIM HOLMQUIST G R JOHNSON 600 SECOND STREET NE HOPKINS MN 55343
1	BALLISTIC IMPACT DYNAMICS ATTN RODNEY RECHT 3650 S CHEROKEE 2 ENGLEWOOD CO 80110
1	CALIFORNIA RSRCH & TECH ATTN DENNIS ORPHAL 5117 JOHNSON DRIVE PLEASANTON CA 94566
1	CHAMBERLAIN MFG CORP R&D DIV ATTN M TOWNSEND PO BOX 2545 WATERLOO IA 50704
1	COMPUTNL MECHANICS ASSOC ATTN JONAS A ZUKAS PO BOX 11314 BALTIMORE MD 21239-0314
1	CUSTOM ANALYTICAL ENGRNG SYS INC ATTN A ALEXANDER STAR ROUTE BOX 4A FLINTSTONE MD 21530

NO. OF COPIES	ORGANIZATION
1	GEN DYNAMICS LAND SYS DIV ATTN D BARTLE PO BOX 1901 WARREN MI 48090
1	IAP RESEARCH INC ATTN A CHALLITA 2763 CULVER AVENUE DAYTON OHIO 45429
3	IINSTITUTE FOR ADV TECHNOLOGY ATTN T KIEHNE H FAIR P SULLIVAN S BLESS R SUBRAMANIAN 4030 2 W BRAKER LANE AUSTIN TX 78759
1	INTERFEROMETRICS INC ATTN R LARRIVA VP 8150 LESSBURG PIKE VIENNA VA 22100
2	KAMAN SCIENCES CORP ATTN D ELDER T HAYDEN N ARI PO BOX 7463 COLORADO SPRINGS CO 80933
1	DR KENNEDY & ASSOCIATES INC ATTN D KENNEDY PO BOX 4003 MOUNTAIN VIEW CA 94040
1	LIVERMORE SOFTWARE TECH CORP ATTN J O HALLQUIST 2876 WAVERLY WAY LIVERMORE CA 94550
2	LORAL VOUGHT SYSTEMS CORP ATTN G JACKSON K COOK 1701 W MARSHALL DR GRAND PRAIRIE TX 75051
1	LORAL VOUGHT SYS CORP ATTN K HAVENS MS EM 36 PO BOX 650003 DALLAS TX 75265-0003

NO. OF COPIES	ORGANIZATION
2	MARTIN MARIETTA CORP ATTN P DEWAR L SPONAR 230 EAST GODDARD BLVD KING OF PRUSSIA PA 19406
2	OLIN CORP FLINCHBAUGH DIV ATTN E STEINER B STEWART PO BOX 127 RED LION PA 17356
1	OLIN CORP ATTN L WHITMORE 10101 9TH ST NORTH ST PETERSBURG FL 33702
2	UNIV OF MINNESOTA AHPCRC ATTN G SELL D AUSTIN 1100 WASHINGTON AVE S MINNEAPOLIS MN 55415
	ABERDEEN PROVING GROUND
21	DIR USARL ATTN AMSRL CI C MERMEGAN 394 AMSRL CI C W STUREK 1121 AMSRL CI CB R KASTE 394 AMSRL CI S A MARK 309 AMSRL SL B P DIETZ 328 AMSRL SL BA J WALBERT 1065 AMSRL SL BL D BELY 328 AMSRL SL I D HASKILL 1065 AMSRL WT P A HORST 390A AMSRL WT PA T MINOR 390 C LEVERITT 390 D KOOKER 390A AMSRL WT PB E SCHMIDT 120 P PLOSTINS 120 AMSRL WT PC R FIFER 390A AMSRL WT PD B BURNS 390 W DRYSDALE 390 K BANNISTER 390 T BOGETTI 390 J BENDER 390 R MURRAY 390

NO. OF COPIES	ORGANIZATION
	ABERDEEN PROVING GROUND (CONT.)
51	DIR USARL ATTN AMSRL WT PD R KIRKENDALL 390 T ERLINE 390 D HOPKINS 390 S WILKERSON 390 C MCCALL 390 D HENRY 390 R KASTE 390 L BURTON 390 J TZENG 390 R LIEB 390 G GAZONAS 390 5 CP M LEADORE 390 AMSRL WT PD ALC A ABRAHAMIAN K BARNES M BERMAN H DAVISON A FRYDMAN T LI W MCINTOSH E SZYMANSKI AMSRL WT T W MORRISON 309 T WRIGHT 309 AMSRL WT TA W GILLICH 390 W BRUCHEY 390 J DEHN 390 AMSRL WT TB K BENJAMIN 309 T DORSEY 309 R FREY 309 F GREGORY 309 W HILLSTROM 309 W LAWRENCE 309 O LYMAN 1185 J STARKENBERG 309 L VANDE KIEFT 309 J WATSON 309 V BOYLE 309 S STEGALL 1185 5 CP AMSRL WT TC K KIMSEY 309 R COATES 309 W DE ROSSET 309 F GRACE 309 M LAMPSON 309 D SCHEFFLER 309

NO. OF COPIES	ORGANIZATION
38	DIR USARL ATTN AMSRL WT TC B SORENSEN 309 R SUMMERS 309 E WALKER 309 W WALTERS 309 AMSRL WT TD D DIETRICH 309 G RANDERS PEHRSON 309 J HUFFINGTON 309 A DAS GUPTA 309 J SANTIAGO 309 K FRANK J HARRISON M SCHEIDLER S SEGLETES 5 CP J WALTER C PAXTON 5 CP AMSRL WT NC R LOTTERO 309 R PEARSON 309 S SCHRAML 309 AMSRL WT W C MURPHY 120 AMSRL WT WA H ROGERS 394 B MOORE 394 A BARAN 394 AMSRL WT WB F BRANDON 120 W D'AMICO 120 AMSRL WT WC J ROCCHIO 120 AMSRL WT WD A ZIELINSKI 120 J POWELL 120 A PRAKASH 120 AMSRL WT WE J TEMPERLEY 120 J THOMAS 394

INTENTIONALLY LEFT BLANK.

USER EVALUATION SHEET/CHANGE OF ADDRESS

This Laboratory undertakes a continuing effort to improve the quality of the reports it publishes. Your comments/answers to the items/questions below will aid us in our efforts.

1. ARL Report Number ARL-TR-788 Date of Report July 1995

2. Date Report Received ____________________

3. Does this report satisfy a need? (Comment on purpose, related project, or other area of interest for which the report will be used.) ____________________

4. Specifically, how is the report being used? (Information source, design data, procedure, source of ideas, etc.)

5. Has the information in this report led to any quantitative savings as far as man-hours or dollars saved, operating costs avoided, or efficiencies achieved, etc? If so, please elaborate. ____________________

6. General Comments. What do you think should be changed to improve future reports? (Indicate changes to organization, technical content, format, etc.) ____________________

CURRENT ADDRESS

Organization

Name

Street or P.O. Box No.

City, State, Zip Code

7. If indicating a Change of Address or Address Correction, please provide the Current or Correct address above and the Old or Incorrect address below.

OLD ADDRESS

Organization

Name

Street or P.O. Box No.

City, State, Zip Code

(Remove this sheet, fold as indicated, tape closed, and mail.)
(DO NOT STAPLE)